

2.6. Conclusion	38
CHAPTER 3	40
EXPERIMENTAL FACILITIES AND TEST PROCEDURES	40
3.1. Introduction.....	41
3.2. Test facilities.....	42
3.2.1. High-voltage equipment.....	42
3.2.2. Climate Chamber	43
3.2.3. Physical Objects.....	45
3.2.4. Current and voltage measurement devices	46
3.2.5. High-speed camera.....	46
3.3. Test Procedures.....	47
3.3.1. Ice test preparation prior to flashover	49
3.3.2. Evaluation sequence.....	53
3.3.3. Water film conductivity and volume flow rate measurement procedure.....	54
3.4. Conclusion	55
CHAPTER 4	56
EXPERIMENTAL RESULTS AND DISCUSSIONS	56
4.1. Introduction.....	57
4.2. Withstand voltage measurement of a string of five standard insulator units under icing conditions.....	57
4.3. Withstand voltage measurement of post insulator units under icing conditions	61
4.3.1. Experimental results and discussion under DC Voltage.....	63
4.3.2. Experimental results and discussion under AC Voltage.....	69
4.4. Arc propagation on the ice surface	73
4.4.1. Arc propagation velocity on the ice surface	77
4.5. Volume flow rate and water film conductivity.....	79
4.6. Discussions	82
4.6.1. Effect of voltage polarity on minimum flashover voltage	82
4.6.2. Effect of water film conductivity on arc velocity	84
4.6.3. Effect of freezing water conductivity and dry arc distance on maximum withstand voltage.....	84
4.7. Flashover results presentation using Icing Stress Product (ISP)	85
4.7.1. Comparison of flashover results from different laboratories under icing conditions	88
4.8. Conclusion	90
CHAPTER 5	92

MODELING OF AC AND DC FLASHOVER ON ICE-COVERED INSULATORS	92
5.1. Introduction.....	93
5.2. Model description	95
5.3. The equivalent circuit components	96
5.3.1. Arc channel characteristics	97
5.3.2. Ice section characteristics	98
5.3.2.1. Electrical surface conductivity.....	100
5.3.2.2. Variation of water film thickness along the ice-covered insulator	104
5.3.3. Propagation criterion and arc velocity	106
5.4. Two –arc model of flashover	107
5.5. General description of the proposed dynamic model	109
5.6. Conclusion	111
CHAPTER 6	112
MODEL VALIDATION AND NUMERICAL SIMULATIONS	112
6.1. Introduction.....	113
6.2. Validation of the equivalent surface conductivity mathematical model.....	114
6.3. Validation of the proposed two-arc model.....	119
6.3.1. Validation of the DC two-arc model.....	119
6.3.2. Validation of the AC two-arc model.....	121
6.4. Numerical simulations of potential and electric-field distributions along an ice-covered post insulator.....	123
6.4.1. Potential distribution along the insulator under DC voltage.....	124
6.4.2. Potential and electric-field distributions along the insulator under AC voltage.....	127
6.5. Conclusion	131
CHAPTER 7	132
CONCLUSIONS AND RECOMMENDATIONS	132
7.1. Concluding Remarks.....	133
7.2. Recommendations for future work	138
REFERENCES	140

LIST OF FIGURES

Figure 2.1. Relationship between electrical surface conductivity and applied water conductivity under AC voltage [26].	18
Figure 2.2. Relationship between electrical surface conductivity and applied water conductivity, (a) DC+, (b) DC- [31].	18
Figure 2.3. Configuration of tested insulators [82].	27
Figure 2.4. Obenaus's model for flashover on ice-covered insulators.	30
Figure 2.5. Model of arc discharge on ice surface.	32
Figure 2.6. Principal model of arc propagation on an ice-covered insulator surface [33].	36
Figure 3.1. HV AC transformer with its associated regulator.	43
Figure 3.2. HV DC transformer with its associated regulator.	43
Figure 3.3. Big cold room (6m (width) × 6m (length) × 9m (height)).	44
Figure 3.4. Geometrical characteristics of the 735-kV station post insulator used in the tests.	45
Figure 3.5. Camera set-up.	47
Figure 3.6. Ice on monitoring cylinder.	48
Figure 3.7. Physical aspect of an insulator during ice accretion.	48
Figure 3.8. Sequences of the icing regime test procedure [24].	49
Figure 3.9. Sequences of the melting regime test procedure [24].	50
Figure 3.10. Air gap configuration along an ice-covered insulator under DC voltage: a) upper air gap, b) lower air gap, c) lower and upper air gaps.	52
Figure 3.11. Air gap configuration along an ice-covered insulator under AC voltage: a) 2 air gaps, b) 3 air gaps, c) 4 air gaps.	53
Figure 3.12. Schematic diagram of the experimental setup.	55
Figure 4.1. Ice-covered insulator flashover sequence at 87 kV of DC negative voltage.	59
Figure 4.2. Flashover test results under DC+.	59
Figure 4.3. Flashover test results under DC-.	60
Figure 4.4. Flashover test results under AC.	60
Figure 4.5. Ice accretion under high wind velocity.	61
Figure 4.6. Flashover results for configuration 1-dc (173cm dry arc distance) with a conductivity of 80 μ S/cm under DC+.	64
Figure 4.7. Flashover results for configuration 2-dc (173cm dry arc distance) with a conductivity of 80 μ S/cm under DC+.	64
Figure 4.8. Flashover results for configuration 3-dc (173cm dry arc distance) with a conductivity of 80 μ S/cm under DC+.	65
Figure 4.9. Flashover results for configuration 1-dc (173cm dry arc distance) with a conductivity of 80 μ S/cm under DC-.	65
Figure 4.10. Flashover results for configuration 2-dc (173cm dry arc distance) with a conductivity of 80 μ S/cm under DC-.	66

Figure 4.11. Flashover results for configuration 3-dc (173cm dry arc distance) with a conductivity of 80 $\mu\text{S}/\text{cm}$ under DC-.....	66
Figure 4.12. Flashover results for configuration 1-dc (173cm dry arc distance) with a conductivity of 150 $\mu\text{S}/\text{cm}$ under DC+.....	67
Figure 4.13. Flashover results for configuration 2-dc (173cm dry arc distance) with a conductivity of 150 $\mu\text{S}/\text{cm}$ under DC+.....	67
Figure 4.14. Flashover results for configuration 3-dc (173cm dry arc distance) with a conductivity of 150 $\mu\text{S}/\text{cm}$ under DC+.....	68
Figure 4.15. Flashover results for configuration 1-dc (173cm dry arc distance) with a conductivity of 150 $\mu\text{S}/\text{cm}$ under DC-.....	68
Figure 4.16. Flashover results for configuration 2-dc (173cm dry arc distance) with a conductivity of 150 $\mu\text{S}/\text{cm}$ under DC-.....	69
Figure 4.17. Flashover results for configuration 3-dc (173cm dry arc distance) with a conductivity of 150 $\mu\text{S}/\text{cm}$ under DC-.....	69
Figure 4.18. Flashover results for configuration 1-ac (275cm dry arc distance) with a conductivity of 80 $\mu\text{S}/\text{cm}$ under AC.....	70
Figure 4.19. Flashover results for configuration 2-ac (275cm dry arc distance) with a conductivity of 80 $\mu\text{S}/\text{cm}$ under AC.....	71
Figure 4.20. Flashover results for configuration 3-ac (275cm dry arc distance) with a conductivity of 80 $\mu\text{S}/\text{cm}$ under AC.....	71
Figure 4.21. Flashover results for configuration 3-dc (173cm dry arc distance) with a conductivity of 80 $\mu\text{S}/\text{cm}$ under AC voltage.....	72
Figure 4.22. Flashover results for configuration 3-dc (173cm dry arc distance) with a conductivity of 150 $\mu\text{S}/\text{cm}$ under AC voltage.....	72
Figure 4.23. Flashover results for configuration 1-ac (dry arc distance of 275cm) with a conductivity of 150 $\mu\text{S}/\text{cm}$ under AC.....	73
Figure 4.24. Proposed mechanism of arc propagation.....	74
Figure 4.25. Flashover occurrences on an ice-covered post insulator.....	75
Figure 4.26. Flashover process of post insulator under DC+.....	76
Figure 4.27. Flashover process of post insulator under DC-.....	76
Figure 4.28. Flashover process of post insulator under AC.....	77
Figure 4.29. Ice-covered insulator flashover sequence; (a): first stage, (b): second stage, (c): last stage.....	78
Figure 4.30. Variation of water film conductivity under DC+.....	80
Figure 4.31. Variation of water film conductivity under DC-.....	80
Figure 4.32. Variation of water film conductivity under AC.....	80
Figure 4.33. Volume flow rate of water film.....	82
Figure 4. 34. DC Positive flashover stress versus ISP for different air gap configurations.....	86
Figure 4. 35. DC Negative flashover stress versus ISP for different air gap configurations.....	86

Figure 4. 36. Comparison of AC flashover stress versus ISP for dry arc distances of 173 and 275 cm.....	87
Figure 4. 37. Comparison of flashover stress obtained from different research.....	89
Figure 5.1. Different stages of arc development on an ice-covered insulator.....	94
Figure 5.2. The basic equivalent circuit model of arc propagation on an ice-covered insulator surface.....	96
Figure 5.3. Capacitance of the rod and finite plane geometry [153].....	98
Figure 5.4. Laminar flow on an iced-covered vertical insulator.....	100
Figure 5.5. Water film thickness.....	103
Figure 5.6. Water film on ice-covered insulator, (a): uniform water film, (b):non-uniform water film.....	104
Figure 5.7. (a): two arcs model, (b): equivalent model for two arcs.....	108
Figure 5.8. A simplified equivalent electric circuit.....	108
Figure 5.9. General flowchart of AC and DC modeling.....	110
Figure 6.1. Comparison of the measured and computed leakage current of the positive arc with dry arc distance of 173 cm.....	115
Figure 6.2. Comparison of the measured and computed leakage current of the negative arc with dry arc distance of 173 cm.....	115
Figure 6.3. Measured leakage current of AC arc with dry arc distance of 173 cm.....	115
Figure 6.4. Simulated leakage current of AC arc with dry arc distance of 173 cm.....	116
Figure 6.5. V_{MF} for different freezing water conductivities under DC+ with dry arc distance of 173 cm.....	117
Figure 6.6. V_{MF} for different freezing water conductivities under DC- with dry arc distance of 173 cm.....	117
Figure 6.7. V_{MF} for different freezing water conductivities under AC with dry arc distance of 173 cm.....	118
Figure 6.8. Calculated and experimental flashover voltages for different freezing water conductivities.....	118
Figure 6.9. Comparison of the measured and computed leakage current under DC+ by two-arc model.....	119
Figure 6.10. Comparison of the measured and computed leakage current under DC- by two-arc model.....	120
Figure 6.11. V_{MF} for different freezing water conductivities under DC+ with dry arc distance of 173 cm.....	120
Figure 6.12. V_{MF} for different freezing water conductivities under DC- with dry arc distance of 173 cm.....	121
Figure 6.13. V_{MF} for different freezing water conductivities under AC with dry arc distance of 173 cm.....	121
Figure 6.14. V_{MF} for different freezing water conductivities under AC with dry arc distance of 275 cm.....	122

Figure 6.15. The calculated and experimental results for different dry arc distance under AC . 122
 Figure 6.16. The calculated and experimental results for different dry arc distance under AC . 123
 Figure 6.17. Equipotential lines distributions for a wet ice- covered insulator: a) upper air gap, b) lower air gap, c) lower and upper air gaps..... 125
 Figure 6.18. Potential distributions under DC voltage. 125
 Figure 6.19. Electric field distributions under DC voltage. 126
 Figure 6.20. Equipotential lines distributions for a wet ice- covered insulator: a) 2 air gaps, b) 3 air gaps, c) 4 air gaps. 127
 Figure 6.21. Potential distributions under AC voltage. 128
 Figure 6.22. Electrical field distributions under AC voltage. 128

LIST OF TABLES

Table 2.1 Characteristics of ice formed on structures [20]. 14
 Table 2. 2. Characteristics of insulators tested. 21
 Table 2. 3. Arc Parameters of an ice-covered insulator under AC and DC conditions. 34
 Table 3. 1. Geometric characteristics of the suspension IEEE standard insulator..... 45
 Table 3. 2. Experimental conditions of the tests..... 47
 Table 4. 1. Propagation velocities of AC and DC arcs. 79
 Table 4. 2. Coefficients of A and α in Equation (4.1)..... 87
 Table 4. 3. Coefficients of A and α in Equation (4.1)..... 88
 Table 6. 1. Simulation parameters [155]. 124
 Table 6.2. Voltage drop along air gaps. 129
 Table 6.3. Voltage drop along air gaps after the formation of a partial arc along second air gap. 130

CHAPTER 1

INTRODUCTION

Rapport-Gratuit.com

CHAPTER 1

INTRODUCTION

1.1. Overview

Delivering a reliable power supply to consumers has always been the main objective of any power utility from both technical and economic viewpoints. As power networks are expanding and the voltage level of transmission lines is being increased, the performance of outdoor insulators plays an increasingly important role in assuring the secure operation of power systems. The insulator performs dual functions, i.e. mechanical and electrical. Indeed, an insulator as a component of power networks at three levels, i.e. production, distribution and transmission, has to support an energized conductor physically and keeps it electrically isolated from other conductors or grounded structures for an indefinite period of time.

All insulators have external surfaces which will be subjected to various atmospheric conditions. Atmospheric icing of power transmission systems is now well-known to be a serious problem in many cold regions of the world. The power outages caused by flashover on insulators due to the combination of atmospheric ice and pollution have been reported in many cold climate countries in North America [1], [2], [3], [4], [5] as well as in many cold climate countries of Europe [6], [7], [8], [9] and Asia [10], [11], [12]. Under such conditions, in addition to the mechanical damage due to the excessive static and dynamic loads created by the combination of atmospheric ice and wind, the electrical performance of insulators may be adversely affected. Under certain conditions, a concomitant drastic decrease in the electrical insulation strength can lead to insulator flashover and consequent power outages [13], [14].

Due to the similarity between the mechanisms of the flashover phenomena on polluted and iced insulators, the hypothesis considered for arc propagation along polluted insulators was used to explain electrical discharge mechanisms on ice-covered insulator surfaces.

Recall that for polluted insulators, the dry contaminant layer on insulator surfaces becomes conductive when exposed to light rain, fog or dew. As wetting progresses, the growth of leakage current dries the conducting layer and forms dry bands around the areas of high current density. Due to these dry bands, the current flow cannot cross the insulator surface, and consequently most of the applied voltage appears across these narrow dry bands. If the electric field along the dry bands exceeds its dielectric strength, an arc is initiated and may lead to flashover [15], [16], [17].

In order to improve our understanding of discharge initiation on an iced insulator surface and its development into a flashover arc, a research program was set up under the auspices of the NSERC / Hydro-Quebec / UQAC Industrial Chair on Atmospheric Icing of Power Network Equipment (CIGELE) and Canada Research Chair on Engineering of Power Network Atmospheric Icing (INGIVRE) at the Université du Québec à Chicoutimi. The insulating performance of ice-covered equipment is an extremely complex phenomenon resulting from the interaction between the following factors: a decrease in effective leakage distance caused by ice bridging, an increase in surface conductivity caused by the presence of a water film, the presence of a pollution layer on the surface of the insulator, and the formation of air gaps [18], [19]. However, it is well established that several ice parameters, including type, density, amount and distribution, as well as the conductivity of applied water, may also have a significant influence on flashover voltage [20], [21].

The mechanisms of flashover on ice-covered insulators are not yet fully understood. From field observations as well as from laboratory investigations, it has been found that the flashover of insulators covered with a very thick layer of ice is not an instantaneous phenomenon, although it results from a process involving ice and discharges. Hence, the flashover process can generally be summarized as follows [19], [22], [23], [24]. Following ice accretion, several sections of the insulators, especially the areas near the electrodes, may become free of ice mainly due to sunshine or the heating effect of partial discharges as well as non-uniform distribution of applied voltage along the insulator. These ice-free zones are referred to as air gaps. The presence of a water film on the surface of the ice is an essential factor for an arc to propagate on an ice-covered insulator. This water film can be produced by many factors, such as wet ice accretion, condensation, the heating effect of leakage current and partial arcs or, in many cases, by a rise in air temperature or the effect of sunshine. The high conductivity of water film, due to the rejection of impurities from the solid part of ice toward its surface during solidification, and by pollution of the water and ice surface from corona discharge by-products, leads to voltage drops across the air gaps [19], [25]. If the voltage strength across the air gaps is high enough, corona discharges are initiated, leading to the development of partial arcs at these zones. This may cause an increase in leakage current and consequent ice melting rate. If the leakage current continues to increase, an unstable white arc will form along the insulator. When the white arc reaches its critical length [26], flashover occurs along the whole insulator string.

In order to study the mechanism of arc propagation over an ice surface [27], [28] and estimate the critical flashover voltage [18], [22], [29], [30], different static and dynamic models were originally established under AC and DC voltages [26], [31], [32], [33]. Contrary to static models which calculate the critical flashover voltage of ice-covered insulators, dynamic models

can contribute to a better understanding of the discharge mechanisms involved in the time dependent evolution of the main parameters of the flashover.

One of the problems facing governments and utilities today is how to supply large amounts of electrical energy efficiently to growing populations with a minimal impact on the environment. Transmission lines sometimes have to cross long distances under severe climate conditions. Ultra High Voltage (UHV) and Extra High Voltage (EHV) offer the promise to meet this challenge. An extension of this technology is the challenge of keeping the performance of equipment up to par, especially under adverse conditions like icing. Despite several efforts on this topic, many aspects of the flashover phenomena of ice-covered insulators, particularly for extra high voltage AC and DC insulators are still not well understood. Indeed, in such a case, more than one partial arc is observed during flashover. The necessity of a two-arc dynamic model representing the behavior of electric arcs on long ice-covered insulators is therefore inevitable. Also, due to the limiting conditions of available laboratory facilities, experimental results for the flashover voltage of full scale insulators under icing conditions are limited. Therefore, this situation makes it difficult to validate the existing models to long ice-covered insulators. Hence, further studies are required to advance knowledge on this phenomenon and develop current mathematical models, applicable to long ice-covered insulators under AC and DC voltages.

1.2. Research objectives

Generally, the overall objective of this thesis is to improve our understanding of the AC and DC flashover phenomena occurring on ice-covered insulators. To achieve this aim, the existing dynamic mathematical models developed at CIGELE should be improved for predicting

the flashover voltage of ice-covered insulators used on EHV and UHV DC and AC transmission lines and their substations. Hence, the specific objectives of this research can be classified in two parts; experiments and simulations, as follows:

1.2.1. Experiments

- **Experimental observation of the arc propagation on ice-covered EHV insulators**

The velocity of arc propagation on ice-covered post insulator surface, considering the effect of water film conductivity under AC and DC voltage, is an important parameter that will help closing major gaps in our understanding. Another important aspect to regard is identification of the number of arcs relative to insulator length. These investigations provided fundamental information for understanding the different behaviors of ice-covered insulators under different voltage types and polarities.

- **Determination of the minimum flashover voltage of a short insulator covered with ice under DC and AC service voltages**

A series of experiments was carried out for both AC and DC voltages under high speed wind velocity to investigate the effect of voltage type and polarity on the minimum flashover voltage.

- **Investigation of the flashover performance of full-scale EHV insulators covered with ice under AC and DC service voltages**

The aim of this part is to describe the performance of insulators used for AC and DC EHV networks. Moreover, the effect of air gap numbers and positions on minimum flashover

voltage of insulators was investigated. This might suggest an optimized configuration of air gaps which can be used for installation of booster sheds on insulators.

- **Measurement of the water film flow rate and conductivity**

Some experimental attempts were performed to measure the variation of water film flow and its conductivity to determine water film thickness as well as the equivalent surface conductivity. These investigations may provide a more accurate estimation of residual ice resistance distributed along insulators.

1.2.2. Simulations

- **Computing the potential and electrical field distributions around an ice-covered insulator**

In order to interpret the effect of the number of air gaps and their position on the minimum DC and AC flashover voltages, voltage distribution along the ice-covered insulator under different air gap positions were calculated using the Finite Element Method (FEM) based software.

- **Establishing a relationship between the equivalent surface conductivity and the freezing water conductivity during a melting period**

In order to improve the existing models, a novel method was presented to determine the equivalent surface conductivity based on fluid mechanics concept under both AC and DC voltages.

- **Establishing a two-arc dynamic model**

Based on the available models and those presented for polluted insulators, a two-arc mathematical model allowing the prediction of the minimum flashover voltage of ice-covered insulators for EHV AC and DC networks was developed. The flowchart of the developed model should allow the prediction of important flashover characteristics such as leakage current and minimum flashover voltage. Finally, the proposed model was validated against the experimental data.

1.3. Methodology

To achieve the above objectives, this study is based on both computational and experimental investigations at CIGELE laboratory. The proposed methodology is briefly described as follows.

A series of tests was carried out to determine the flashover voltage and to investigate the relationship between the variations of freezing water conductivities and ice-covered insulator flashover voltages using a high voltage source and a data acquisition system. For this purpose, wet-grown ice with predetermined thickness was accumulated on the surface of an insulator using several expected freezing water conductivities and dry arc distances. In order to investigate the effect of air gap numbers and positions, once the ice thickness on the post insulator reached a desirable value, the icing process was stopped and then the air gaps, normally 7-8% of insulator's length were artificially created by removing ice at the given positions. Shortly after air gap creation, flashover voltage was applied to the ice-covered insulator based on IEEE Std

1783 [34]. Maximum withstand voltage, V_{WS} is considered to be the maximum voltage at which flashover does not occur in at least three tests out of four. The minimum flashover voltage, V_{MF} corresponded to a voltage level higher than V_{WS} .

In order to interpret the effect of air gap positions and numbers on the experimental results, the potential distribution along an ice-covered station post insulator was calculated during a melting period using the Finite Element Method (FEM). An actual ice-covered station post insulator assuming uniformly accumulated with ice was simulated. The potential and electric field distributions were computed on a vertical plane cutting the insulator into four symmetrical parts.

In order to estimate instantaneous flashover behavior under relevant conditions, it is necessary to develop an appropriate dynamic model. Therefore, in this regard, a relationship between electrical surface conductivity and freezing water conductivity during melting period under both DC and AC voltages was established. Hence two parameters that play an important role in the accuracy of surface conductivity, thickness and conductivity of the water film on ice surfaces were measured.

Incidentally, a traditional method has been used to date. This method consists in recovering water resulting from the melting ice by a plastic pipe which conveys it to a tray where several glasses of water are stored. The conductivity of this water is measured by using the conductivity meter (Model SC 72), and then recorded. This conductivity measurement system makes it possible to measure in a precise way the conductivity of the water film during the melting regime. Water film thickness, as an effective factor on surface conductivity, can be determined through an approach similar to that presented by Fox [35] in fluid mechanics

concept. It is assumed that the water flows downward along the insulator under the influence of gravity.

Using an appropriate mathematical model is probably one of the most efficient ways of estimating the minimum flashover voltage of ice-covered insulators. Since the instantaneous behavior of arc parameters needs to be observed, a dynamic model must be developed based on equations and information related to the dynamic behavior of the arc [32], [33] as well as on the consideration of static multi-arc concepts [36] under DC and AC voltages. Therefore, to reach this goal, an AC and DC two-arc dynamic model was developed to analyze the flashover of ice-covered insulators used under EHV network. Finally, the proposed model was validated by experimental tests carried out on real insulators covered with artificial ice at CIGELE.

1.4. Statement of the originality of the thesis

The lack of mathematical models for forecasting the electrical flashover performance of long insulators under icing conditions has motivated the present study, which aims at developing reliable dynamic models to investigate the AC and DC flashover phenomena. Such models would do away with the need for performing full scale high-cost tests on ice-covered insulators which require major infrastructures and a highly specialized team of engineers and technicians. Also, the fast development of HVAC and HVDC projects has been well recognized worldwide due to several economic and technical advantages. The development of this technology and related performance of equipment could be seriously threatened by severe icing conditions. Therefore, the proposed model will be unique and may allow a more appropriate design of EHV insulators under icing conditions.

1.5. Structure of the thesis

This dissertation discusses major topics dealing with modeling of flashover of ice-covered insulators, as follows:

Chapter 1 presents overall information related to the problematic, research objectives and originality and offers a brief description of the methodology of this PhD thesis.

Chapter 2 recalls the flashover mechanisms of ice-covered insulators along with the effect of major parameters influencing the flashover voltage. Moreover, a survey of the mathematical models for predicting the flashover voltage of polluted and ice-covered insulators is introduced.

Chapter 3 describes the test facilities and the methodology for performing the experiments in the laboratory.

Chapter 4 presents and discusses the experimental results.

Chapter 5 focuses on the modeling of the flashover of ice-covered insulators.

Chapter 6 provides a comparison between the simulated results and those obtained from experiments. Furthermore, numerical simulations by FEM will be presented to explain the role of air gaps in the performance of ice-covered insulators.

Chapter 7 provides the general conclusions of this work and also highlights several recommendations for future researches.

CHAPTER 2

LITERATURE REVIEW

CHAPTER 2

LITERATURE REVIEW

2.1. Introduction

Due to the continuous increase of energy demand, long distance power transmission lines and high voltage substations have been widely used in power networks. Hence, the performance of outdoor insulators as one of the main and essential devices in the power network is playing a vital role for the safe operation of overhead power transmission lines and related substations. From the electrical viewpoint, the main function of insulators is to withstand electrical stress with a low failure probability under the environmental and meteorological conditions to which they are subjected. Over recent decades, atmospheric ice accretion has been recognized to be a serious threat to power transmission lines. Therefore, it has been the subject of many investigations with the aim of improving understanding of the icing phenomenon and the atmospheric factors influencing the electrical performance of insulators under icing conditions. Therefore, a review of the literature pertinent to this thesis is presented in this chapter. The first part of this chapter provides a brief review of the theoretical studies and experimental investigations on the mechanism of ice accretion on an insulator surface, flashover of ice-covered surfaces and the effects of atmospheric parameters on insulator performance. Then, the present chapter continues with the review of basic flashover modeling of insulators under pollution conditions. Lastly, the current dynamic and static models developed to predict flashover parameters of ice-covered insulator surfaces are presented.

2.2. Mechanism of ice accretion on insulator surface

Natural atmospheric ice deposits on insulators mainly result from a variety of conditions including hoarfrost caused by condensation of water vapor on cold surfaces, in-cloud icing involving the freezing of suspended super-cooled droplets in clouds or fog, and precipitation icing resulting from freezing rain and drizzle, as well as wet and dry snow [14], [20].

The mechanism of ice accretion on various insulator types depends on the environmental conditions, such as air temperature, wind velocity, water droplet size, and liquid water content. Based on the investigations carried out by Imai [37], Oguchi [38] and Kuroiwa [39], [40], three types of ice, namely hard rime, soft rime and glaze, under different atmospheric conditions were formed on the insulator surface and other energized equipment of the power network. Hard rime is opaque and has a density between 0.6 and 0.9 g/cm³. Soft rime is white and opaque, with a density less than 0.6 g/cm³. Glaze is transparent and has a relatively high density of about 0.9 g/cm³. The main characteristics of the above mentioned ice types are summarized in Table 2.1.

Table 2.1 Characteristics of ice formed on structures [20].

Type of ice	Density (g/cm ³)	Appearance	Shape
Glaze	0.8-0.9	Transparent and clear	Cylindrical icicles
Hard rime	0.6-0.9	Opaque	Eccentric pennants into wind
Soft rime	<0.6	White and opaque	Feathery and granular

The studies of the icing phenomenon have also been extended to the investigations of electrical performance of insulators. With the aim of investigating the flashover of ice-covered insulators, a variety of ice types was formed in the climate chamber of the high voltage laboratory of CIGELE, UQAC. Two regimes of icing, dry and wet, were used by Farzaneh *et al.* to investigate the performance of ice-covered insulators [22], [30], [41], [42]. The ice grown process is referred to a dry regime when the ice deposit temperature remains below 0°C. Both hard rime and soft rime ice were grown under a dry regime [18], [39], [43]. Under the dry regime, all the water droplets impinging on an insulator surface were completely frozen. In contrast, glaze is grown under a wet regime at a temperature of 0°C where icicles can be formed around the insulator sheds [18], [39], [43]. This type of ice deposition simulated ice accretion during freezing rain precipitation.

2.3. Conductivity of ice surface

It is well acknowledged that flashover characteristics of an insulator are affected by the ice surface properties. Over the last few decades, ice surface properties have been the subject of many scientific studies from chemical and mechanical point of views. Faraday observed that the surface layers of ice crystals, at temperatures near melting point, have physical properties which seem to differ considerably from those of the bulk [44]. Much of the research in recent decades has been carried out on the topic of ice surface conductivity. Experimental results showed that ice surface has electrical conductivity which varies in the range of 10^{-11} to 10^{-8} S, even with a small amount of impurities in ice [45], [46], [47], [48], [49], [50]. Another approach to studying ice surfaces is through observing the thickness of the liquid-like layer on the surface at temperatures close to the melting point of ice. Over the past few decades, several techniques

such as semi-quantitative thermodynamic modeling [51], proton backscattering [52], optical ellipsometry [53], X-ray diffraction [54], molecular dynamics calculations [55], atomic force microscopy [56], photoelectron spectroscopy [57] and infrared spectroscopy [58] have been used to measure the thickness of the liquid-like layer. The thickness measurements of this thin surface melting layer reveal a remarkable variation up to 200 nm depending on the experimental condition, the nature of the ice samples and environment temperature.

The presence of a water film on the ice surface accreted on an insulator string is one of the main conditions for flashover to occur. The water film on the ice surface of an energized insulator submitted to icing condition can be produced not only by a rise in air temperature, wet ice accretion, condensation or the effect of sunshine but also by many other factors, including the heating effect of leakage current and partial arcs [14], [19]. The high conductivity of the water film is caused by the rejection of ionic impurities from the bulk ice toward its surface during solidification/freezing process. This increase in conductivity can also be related to pollution of the ice surface by corona discharge by-products. As a consequence, the voltage drop across the air gaps increases [19], [25]. If the electric field across the air gaps is high enough, an arc propagating along the ice surface of the insulator may lead to flashover. Experimental results obtained by P. G. Buchan *et al.* showed that wet ice can be considered to have both volume and surface conductivity [59]. H. T. Bui noticed that the value of the electrical resistance of ice during the icing period is higher than that of the de-icing period [60]. Sugawara *et al.* showed that the average conductivity of the water film on the bottom of ice plates is approximately 2.5 times higher than the applied conductivity [61]. Over the last years, the CIGELE research group has investigated leakage current distribution and the corresponding surface conductivity using a triangular ice sample. It was observed that at 0°C, water film thickness and leakage current are

not uniformly distributed. However, when the air temperature is higher than 2.5°C, the distribution of leakage current is uniform [62]. Also, it was found that the current flows through both the inner and the outer interface of the ice [63]. The range of the conductivity of dripping water was reported to be 5 to 11 times greater than that of applied water conductivity [64]. Moreover, it was observed that surface conductivity of the ice increases rapidly with an increase in applied voltage [65].

2.3.1. Electrical surface conductivity of ice

The flashover process on an ice surface is a function of the distributed resistance of an ice layer built up in parallel with the leakage resistance of an insulator. For a uniform water film on a rectangular slab ice layer having a length L and width W , the total ice layer resistance R can be expressed as the parallel combination of two terms, as follows [24]:

$$R = \frac{L}{W} \left[\frac{1}{\sigma_{\text{ice}} h_{\text{ice}} + \sigma_{\text{water}} h_{\text{film}}} \right] \quad (2.1)$$

where σ_{ice} is the conductivity of the ice, h_{ice} is the thickness of the ice layer, σ_{water} is the conductivity of the surface film of water, and h_{film} is the thickness of the surface film of water on the ice.

The term $\sigma_{\text{water}} h_{\text{film}}$ is normally expressed as a product, defined as the equivalent surface conductivity, γ_e . As the water film conductivity, σ_{water} is typically 100–300 times higher than that of dry ice, for typical ice layers, this term will dominate the equivalent bulk conductivity [66]. Farzaneh *et al.* [26], [31] carried out a series of tests to determine the electrical

surface conductivity γ_e based on measured values of the resistance $R(x)$ of a thin triangular ice sample. The value of electrical surface conductivity was found to vary with applied water conductivity σ_{20} over the range of 1-200 $\mu\text{S}/\text{cm}$ for AC and 1-300 $\mu\text{S}/\text{cm}$ for DC voltage as shown in Figures 2.1 and 2.2.

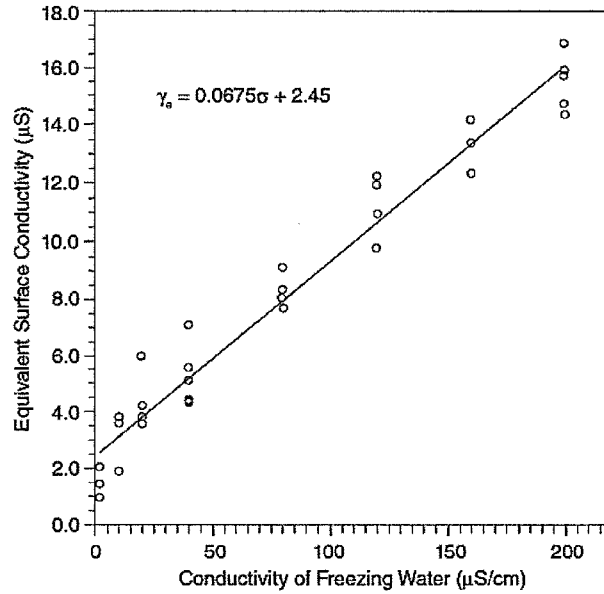


Figure 2.1. Relationship between electrical surface conductivity and applied water conductivity under AC voltage [26].

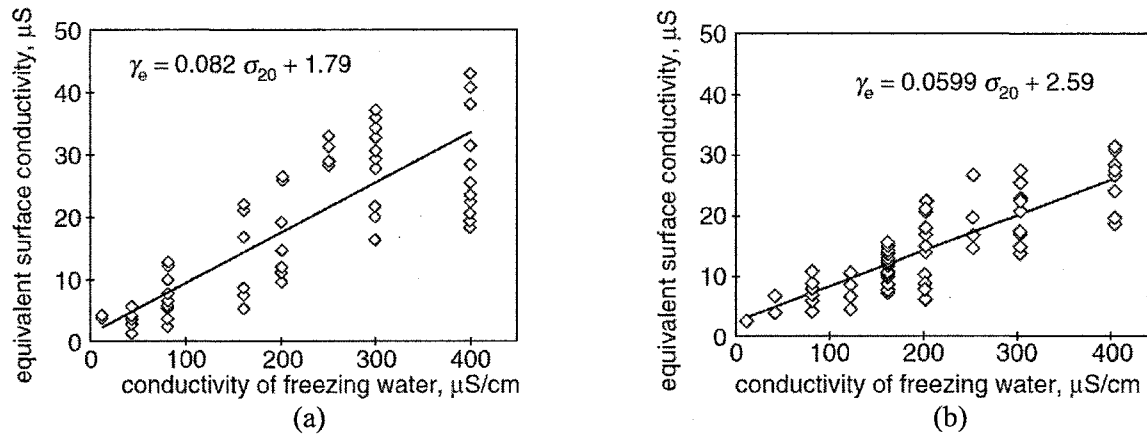


Figure 2.2. Relationship between electrical surface conductivity and applied water conductivity, (a) DC+, (b) DC- [31].

2.4. Flashover mechanisms of ice-covered insulators

Researchers do agree that ice surface flashover resulting from an interaction involving service voltage, wet and polluted ice surface, presence of air gaps at the ice surface, environmental conditions, and the geometry of the insulators is a complex phenomenon [6], [18], [19], [22], [23], [29], [67], [68]. In general, it is agreed that the presence of a water film on the surface of the ice is necessary for flashover to occur [19], [22]. The appearance of this water film may be due to an increase in the ambient temperature or it may be a result of melting ice due to partial arcs and corona [1], [62]. The presence of a highly conductive water film increases the voltage across the air gaps. These air gaps are formed during the growth period of icicles due to the activity of corona discharge at the icicle tips [5], [19], [20], [69], [70], [71]. If the electric field across the air gaps is high enough, corona discharges will appear across them. In this condition, several small partial arcs appearing along the air gaps emit additional heat, which further contributes to ice melting, which further increases the water film on the surface, along with a substantial increase in leakage current and a simultaneous melting of ice. If the applied voltage is sufficiently high, a local arc grows along the ice surface, forming a white arc. When the white arc reaches a certain length [72], [73], depending on surface conductivity and the length of the remaining ice layer, the whole insulator may suddenly undergo complete flashover.

Though the process of ice surface flashover has been investigated for many years in different laboratories and at outdoor locations across the world, the understanding of the physical process of arc formation is not yet fully understood. It has been observed that performance of insulators covered with ice depends upon various factors such as the icing process, environmental conditions, applied voltage types as well as insulator shape and configuration. In

the following sections, further discussions on the different parameters affecting the performance of insulators under icing conditions are briefly reported.

2.4.1. Effect of ice type and thickness

The type of ice accretions depends on several major parameters, such as the size and velocity of droplets and the ambient temperature. Each type of ice has its own relative density as presented in Table 2.1. Laboratory investigations show that the ice type has a considerable effect on withstand voltage.

Phan *et al.* [74] observed the performance of a short insulator string covered with three types of ice: soft rime, hard rime or glaze. The lowest level of minimum flashover voltage was observed under hard rime type.

Sugawara *et al.* [75] investigated the effect of ice density on the AC withstand voltage for two standard suspension insulator units covered with ice. The withstand voltage decreased slightly with an increase in the ice density from 0.6 to 0.8 g/cm³ related to hard rime. For an ice density of 0.9 g/cm³ related to glaze, the withstand voltage was markedly smaller than that observed for an ice density of 0.6 or 0.8 g/cm³.

Fujimura *et al.* [10] determined the withstand voltage of an ice- and snow-covered suspension insulator strings. The AC withstand voltage of an ice-covered insulator was approximately 40% lower than the withstand voltage of an insulator covered with snow.

Farzaneh *et al.* found that the glaze ice was the most dangerous type of ice because it is associated with a high probability of flashover of ice-covered insulators [14], [18], [22], [29]. In the case of glaze ice, the water film on the ice surface during the accretion and melting regime creates the most critical flashover conditions.

The thickness of the ice layer has a significant effect on the maximum withstand voltage (V_{ws}). Due to the non-uniformity of ice, the exact thickness of ice cover on an insulator surface is difficult to measure. Therefore, the ice weight was measured to characterize the amount of ice on insulators [10], [76]. It was noted that the V_{ws} lowered and tended towards a constant value as the weight of the ice increased.

Farzaneh *et al.* suggested a rotating monitoring cylinder as a reference parameter to monitor the ice thickness ranging from 5–30 mm [14]. They observed that the critical ice thickness levels at which V_{ws} remains constant are 2 cm, 2.5 cm and 3 cm for anti-fog insulators, IEEE standard and EPDM insulators respectively [19], [22], [29], [30]. The characteristics of insulators are presented in Table 2.2.

Table 2. 2. Characteristics of insulators tested.

	IEEE standard	Anti-fog	EPDM
Shed diameter (mm)	254	320	90 and 105
Shed spacing (mm)	146	170	55
Leakage distance (mm)	305	545	2171

Another important factor affecting the uniformity of ice is wind velocity during ice accretion. Experimental laboratory results showed that the higher the wind velocities are, the lower the value of flashover [10], [18], [29]. It was also found that the icicles formed at a

relatively high wind velocity (7 m/s) were nearly always tilted away by the wind, while they remained almost vertical for the lower wind velocity (3.3 m/s) [77].

2.4.2. Effect of applied water conductivity

Natural rain, which is the origin of icing on the insulator surface, can be conductive through sea salt, nitrates, sulphates and various industrial pollutants. Therefore, the conductivity of applied water, which is one of the most important parameters, influences the insulating strength of ice-covered insulators. In general, the higher the conductivity, the lower the flashover voltage is. Since the water conductivity varies with the ambient temperature, it is necessary to correct and express its value at a reference temperature of 20°C [78].

Fikke *et al.* [8] investigated the flashover voltage of insulators in the mountainous areas under icing conditions. The considered ice type contained a high ion concentration due to salt or the combustion of fossil fuels.

Kannus *et al.* [79] studied the influence of freezing water resistivity on the leakage current of AC flashover voltages. The flashover voltage of two suspension insulator units was found to be related to the square root of the freezing water resistivity.

Chisholm *et al.* [80] presented a cold-fog test method to reproduce a flashover on an insulator while considering surface contamination, ice and fog by rising temperature to 0 °C. The electrical performance of outdoor insulators, designed for a 115 kV, 230 kV and 500 kV substations, degrades severely under these conditions.

Also, the performance of insulators, covered with ice formed under different water conductivities were examined by Fujimura *et al.* [10], Matsuda *et al.* [11] and Vouckovic *et al.* [7]. They reported that the flashover voltage of insulators covered with ice decreases with increase in the conductivity of the applied water.

Several investigations have been carried out to evaluate the performance of ice-covered insulators considering pollution levels in China. Jiang *et al.* [81], [82], Su *et al.* [83] and Liu *et al.* [84] confirmed the influence of pollution on ice-covered insulator flashover.

Over the past years, comprehensive investigations have been carried out at CIGELE to study the effect of applied water conductivity on the V_{ws} of different types of ice-covered insulators under AC and DC voltages [18], [22], [29], [72], [85], [86], [87]. It is now an established fact that any increase in the freezing water conductivity lowers the flashover voltage.

2.4.3. Effect of dry arc distance

Under heavy icing conditions, sheds may be bridged by icicles; the effective leakage distance may therefore be reduced to the dry arc distance. The flashover voltage can therefore be expressed as a function of the dry arc distance for short string insulators. According to several laboratory investigations, the relationship between flashover voltage and dry arc distance is mostly linear for short string insulators, [29], [41], [74], [88], whereas it becomes non-linear for long insulators [36], [89].

The nonlinearity of this relationship, in the case of long insulators, can be traced to the non-uniform distribution of ice along the insulator, changes in physical properties of melting ice, such as water film conductivity and electrical discharge phenomena [89].

2.4.4. Effect of air gaps

In general, it was observed that the sections of the insulator that are free of ice (air gaps) formed during the ice accretion period are physically close to the high voltage (HV) and ground electrodes, independent of the insulator's type and configuration [5], [22], [69].

Across the air gaps, the higher electric field strongly affects the growth of icicles by inducing partial discharges at their tips [90], [91]. The appearance of partial arcs prevents the icicles from becoming longer and may even melt them.

The presence of a partial arc along an air gap leads to a redistribution of voltage along the ice-covered insulators. Some investigations have dealt with the influence of air gaps on the potential and electric field distribution along an EHV post insulator [67], [68], [92], [93]. Concerning voltage distribution and phenomena preceding flashover, numerical results obtained by the Finite Element Method (FEM) showed that an ice accretion with two air gaps seems to be more dangerous than one with three gaps [93].

In addition, the study of the effect of number and position of air gaps on the flashover voltage of a single short string of five IEEE standard insulators, covered with ice, showed that in the 4 air-gap configurations tested, the critical flashover voltage is lowest in the case of two air gaps at the top and bottom of insulator string [94], [95], [96].

Concerning the effect of the air gaps on the voltage distribution along ice-covered insulators, several solutions consisting in the addition of booster sheds [24] and grading rings [97] to improve the insulating performance of insulators under icing conditions have been offered. The applications of the booster sheds (BS) and grading rings provide several air gaps along the insulator covered with the ice. Manitoba Hydro [98] reported the application of booster sheds in preventing the flashover of 450 kVdc bushings under fog, rain and wet snow conditions.

2.4.5. Effect of insulator type and configuration

Among major parameters influencing insulator performance under icing conditions, the type and configuration of insulators play an important role in their selection for applications in cold climate regions.

Wu *et al.* [99] tested the insulating performance of composite and glass insulators. They found a high insulating performance for composite insulators, such as silicone rubber or EPDM, compared to that of a glass cap-pin insulator string.

The study of five different types of long-rod insulators covered with ice by Cherney [3] indicated that the insulating performance of a composite insulator was superior to IEEE standard insulators. Furthermore, the experimental results offered a better performance of ice-covered insulators for a composite insulator with alternate long/short sheds rather than one with uniform sheds. The insulator consists a shed spacing of 90 mm and alternating-diameter sheds of 170 and 132 mm.

The performance of various types and configurations of short portions of post insulators such as the insulator with three alternating sheds (type A and B), standard post insulator and semiconducting glaze insulator, were investigated under wet-grown ice during icing regime [30]. It was observed that the semiconducting glaze insulator presented the best performance of V_{ws} , with an increase of 16% under the icing regime, when compared to the standard one.

In addition, three types of suspension insulators (IEEE standard, anti-fog and EPDM) with characteristics presented in Table 2.2 and one post-type insulator covered with uniform wet ice, of a thickness of 2 cm and with the same dry arc distance, were examined [18]. The shed diameter, shed spacing and leakage distance of the post-type insulator are 250, 51 and 2525 mm respectively. The results showed that all the insulators tested under icing conditions had a higher V_{ws} compared to IEEE standard insulators. In particular, the V_{ws} of EPDM insulators offered the best insulating performance with a V_{ws} 36% higher than that of IEEE insulators.

Jiang *et al.* [82] selected seven types of short samples of composite insulators (type A to type G) as shown in Figure 2.3 to analyze the influence of the configuration parameters of the sheds on the DC flashover gradient under various conditions of ice thickness, pollution and air pressure. Among these configurations, Type G was proposed as having the best set of external insulation characteristics under the comprehensive effect of high altitude, pollution and icing conditions.

The diameter of the insulator is a major factor influencing air gap formation and the electrical performance of insulators under icing conditions. Farzaneh *et al.* [100] investigated the effect of the insulator diameter by controlling the width of the ice layer on insulator performance. The 50% withstand voltage (V_{50}) decreased as the diameter of the insulator increased.

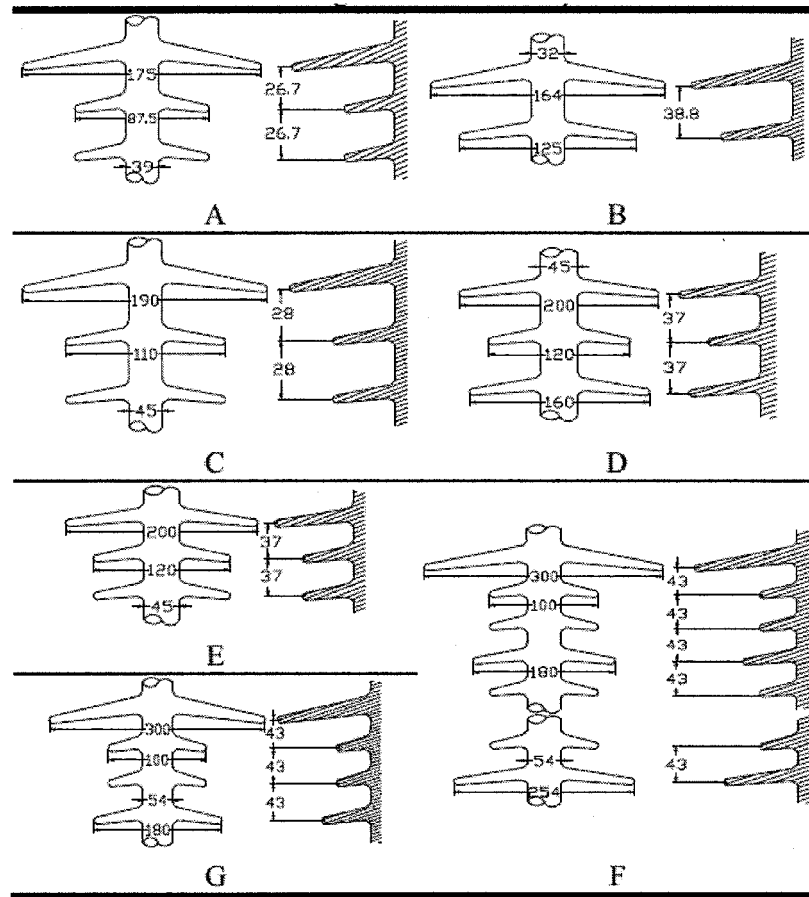


Figure 2. 3. Configuration of tested insulators [82].

2.4.6. Effect of voltage polarity

While extensive studies have been performed on AC flashover of ice-covered insulators in the last decades, only a few investigations have been made in regard to the flashover of ice-covered insulators under DC voltages.

Watanabe [101] carried out several DC flashover tests on an insulator covered with ice or snow. The minimum flashover voltage was found to be higher under DC- than that measured under DC+ under both ice and snow conditions.

Contrarily, Fujimura *et al.* [10] reported that the flashover voltage of an ice-covered insulator was higher under DC+ and consequently conducted the experiments exclusively under DC- voltage conditions.

However, Renner *et al.* [102] found that the flashover voltage of ice-covered insulators under DC- voltage was only slightly lower than the flashover voltage measured under DC+ voltage. Consequently, the effect of voltage polarity could be neglected.

Also, a number of experiments were carried out under DC voltage at CIGELE [19], [31], [103], [104]. It was found that the minimum flashover voltage of a short suspension insulator string under DC- was approximately 17% lower than under DC+ voltage.

2.4.7. Effect of air pressure

The air pressure has a considerable influence on the minimum flashover voltage of ice-covered insulators. At high altitudes, the electric performance of insulators is enhanced by increasing air pressure [82], [103], [105], [106], [107]. Li *et al.* [87] introduced a relationship between the critical flashover voltage V_c at any pressure and that, at standard sea level V_0 is as follows:

$$V_c = \left(\frac{P}{P_0}\right)^m V_0 \quad (2.2)$$

where P_0 and P are respectively the standard pressure (101.3 kPa) and the pressure at high altitudes, V_0 and V are the flashover voltages corresponding to the pressures P_0 and P respectively; and exponent m indicates the degree of influence that air pressure has on the critical

flashover voltage. The value of m depends on a number of elements such as insulator shape, pollution severity, and voltage type [87]. Several investigations showed the flashover voltage decreases up to 40%, when the air pressure drops from its sea level value of 101.3 kPa to 30 kPa [104].

2.5. Flashover modeling of insulators surfaces

Insulator flashover is not an instantaneous phenomenon, but a complex process that occurs through different phases; the appearance of water film on the ice surface, the formation of air gaps, the initiation of corona discharges, the development of local arcs, and the increase in leakage current. Finally, if conditions are suitable, flashover occurs. The study of such complex phenomena require sophisticated investigation facilities. However, because of the limited facilities in laboratories, experimental results for the flashover voltage of full scale HVDC insulators under atmospheric conditions are scarce. Thus, mathematical modeling may be one of the most attractive ways to estimate the flashover performance of insulators over a wide range of atmospheric conditions. Also, it can be a powerful tool for the design and selection of HV insulators, specifically subjected to severe environmental conditions.

2.5.1 Basic models of polluted surface flashover

The pioneering work of Obenaus [108] can be considered as the first attempt to model flashover propagation on the surface of insulators covered with a conductive layer. The flashover on a polluted surface is considered as an arc in series with a residual resistance consisting of a pollution layer that is not bridged by the arc as shown in Figure 2.4.

Considering the circuit equation, Obenaus deduced the critical current and the general expression for the minimum direct voltage U_{cx} necessary to sustain an arc of length x in series with a resistance R_p as follows:

$$i_{cx} = \frac{n}{n+1} I_{sc} \quad (2.3)$$

$$U_{cx} = \frac{n+1}{n^{n+1}} N^{1/n+1} x^{1/n+1} R_p^{n/n+1} \quad (2.4)$$

where n and N are static arc characteristic constants, I_{sc} is the current that would flow if the arc were replaced by a short circuit. It was assumed that the same current which passes through the arc also flows through the resistive layer.

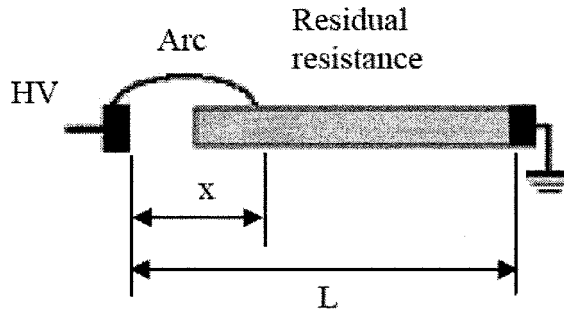


Figure 2. 4. Obenaus's model for flashover on ice-covered insulators.

Neumarker [109] developed those equations proposed by Obenaus further and considered a uniform resistance per unit length of wet polluted layer instead of a constant resistance of pollution layer in series with arc. He calculated critical values of voltage, length and current.

Alston and Zoledziowski [110] introduced some modifications to the model of Neumarker and confirmed his results. They stated that the required voltage to maintain the discharge on polluted insulators may increase with an increase in discharge length, and if the

voltage exceeds the applied voltage, the discharge extinguishes without flashover occurrence. They stated that the flashover cannot happen if the applied voltage and the initial arc length are less than the critical values.

Hampton [15] stated that a necessary condition for arc development along the polluted layer is when the electric field in the arc becomes less than that of the pollution layer.

Under AC voltage, however, the arc current decays to zero every half - cycle. However, the remaining hot gas in the arc can easily be reignited by the applied voltage in the next half - cycle. Based on this knowledge, several essential criteria were proposed to adapt the Obenaus's model for AC flashover. Claverie [111], [112] described the peak reignition voltage as a function of the peak current in the previous half – cycle and maximum arc length. Rizk [113] established a mathematical model for reignition of an AC arc in series with a uniform pollution layer, based on the energy balance criterion.

2.5.2. Modeling of flashover on ice-covered surfaces

In spite of the large number of contributions on the flashover phenomena of ice-covered insulators, mostly concentrated on determining the flashover voltage, a few research projects have been done to study and model the arc discharge on ice-covered surfaces. Recently, systematic and comprehensive studies carried out at CIGELE dealing with the modeling of flashover on ice-covered insulators; a variety of elements characterizing their flashover phenomena was considered. In the next section, an overview of the different existing

mathematical models of arc discharge on an ice-covered insulator surface, mostly static models of DC arc, is provided.

2.5.2.1. Static models

Flashover of an ice-covered insulator is due to the initiation and development of local arcs across air gaps. This creates a situation similar to the flashover of a polluted insulator represented by an arc in series with a residual resistance (consisting of an ice layer which is not bridged by the arc). One of the first quantitative analyses of arcs on contaminated surfaces was carried out by Obenaus [108]. On the basis of the model established for a polluted insulator, as represented in Figure 2.4, an electric circuit model was proposed by Farzaneh and Zhang [26], [31] for an ice surface as shown in Figure 2.5.

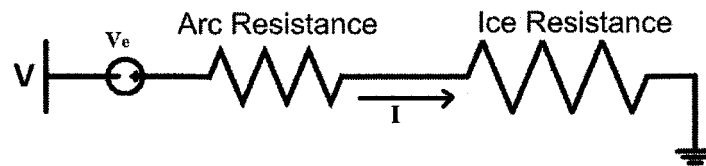


Figure 2.5. Model of arc discharge on ice surface.

Based on the model of the simple circuit shown in Figure 2.5, the governing equation of this circuit leads to:

$$V = xAI^{-n} + R(x)I + V_e \quad (2.5)$$

where V is applied voltage, V_e is the electrode voltage drop of arc which can be neglected for AC arcs; x (cm) is the arc length; I is leakage current; $R(x)$ is the residual resistance of ice layer; while A and n are the arc constants.

The resistance of the ice layer consisting of a thin conductive film of water is calculated taking into account the insulator geometry and the constriction of the current at the arc root. For a narrow ice band, where the width of the ice layer is less than its length, this resistance can be represented based on Wilkins' resistance model [114] as follows:

$$R_{ice} = \frac{1}{2\pi\gamma_e} \left[\frac{\pi(L-x)}{w} + \ln \left(\frac{w}{2\pi r} \right) \right] \quad (2.6)$$

where w is ice layer width, x is arc length, L is insulator length, r is arc channel radius and γ_e is the equivalent surface conductivity.

The critical leakage current I_c and critical arc length x_c can be calculated by employing a method similar to that used for polluted insulator [114], [115], by solving the following equations:

$$\frac{\partial V}{\partial x} = 0 \quad (2.7)$$

$$\frac{\partial V}{\partial I} = 0 \quad (2.8)$$

Since, under AC voltages, flashover occurs around the peak value of the applied voltage, the same analysis for DC applied voltage is used to calculate the AC critical flashover voltage. Under AC voltage, the current is interrupted twice during each cycle and, consequently, the local arc decays and re-ignites twice per cycle. Therefore, not only Equation (2.5) must be satisfied but

also the arc re-ignition condition must also be fulfilled. The re-ignition condition can be expressed as follows [26], [112]:

$$V_m \geq \frac{kx}{I_m^b} \quad (2.9)$$

where k and b are the arc re-ignition constants and V_m is the peak value of applied voltage; x is the local arc length; I_m is the peak value of leakage current.

Table 2.3 summarizes the parameters introduced in the above-mentioned equations using a series of experiments on triangular physical ice sample [31], [116], [117], [118], [119], [120].

Table 2.3. Arc Parameters of an ice-covered insulator under AC and DC conditions.

Voltage type Parameters	AC	DC+	DC-
A	204.7	208.9	84.6
n	0.56	0.45	0.77
k	1118	-	-
b	0.5277	-	-
$V_e(V)$	-	799	526
γ_e	$0.0675\sigma + 2.45$	$0.082\sigma + 1.79$	$0.0599\sigma + 2.59$
r	$\sqrt{\frac{I}{0.875\pi}}$	$\sqrt{\frac{I}{0.648\pi}}$	$\sqrt{\frac{I}{0.624\pi}}$

The proposed static model described in this section has been applied to wet grown cylindrical ice samples [121] of various dry arc distances and a short string of five IEEE standard insulators [26]. There was a good concordance between the experimental results and those predicted by the model.

The above-mentioned mathematical models were successfully applied to short insulator strings under icing conditions. However, when this model is applied to an insulator longer than 1

m, there is a quite large deviation between the results calculated from the model and those obtained by experiments. In fact, from the laboratory observations of flashover occurrence for long insulators, more than one arc can be initiated along the insulator. Hence, based on previous single-arc model a multi-arc model was developed by Farzaneh and Zhang [36]. Thus, the residual ice resistance for N arcs can be expressed by the following equation.

$$R_{ice} = \frac{1}{2\pi\gamma_e} \left[\frac{4(L-x)}{D+2d} + (N_1 + 2N_2) \ln \left(\frac{D+2d}{4r} \right) \right] \quad (2.10)$$

where D is insulator diameter, d is ice thickness, N_1 and N_2 are the number of arcs with one and two roots respectively. Also, L, x, and r are insulator length, arc length and arc channel radius. The multi-arc model was applied to different types and configurations of insulators covered with ice [36], [122]. There is good agreement between the calculated and experimental results.

2.5.2.2. Dynamic models

The static model has proved to be useful in predicting the critical flashover voltage of ice-covered insulators, although several questions still remain unanswered. Static models are not structured in such a way as to provide time-dependent evolution of parameters such as current or resistance of the components. The major purpose of this type of model is the determination of the critical flashover voltage, rather than the dynamic evolution of various parameters during different phases of the flashover phenomenon. Due to the time scale of arc parameters, dynamic models are more suitable for understanding the arc development and propagation on an ice surface than static models.

In order to describe the arc propagation on ice-covered insulators, a simplified dynamic arc model developed by Tavakoli *et al.* [33] based on Mayr's dynamic arc equation [123].

Figure 2.6 shows an RLC electrical circuit proposed for arc propagation. In this model, the arc channel is assumed to be cylindrical in shape, with radius r and length x . The impedance associated with the arc channel is represented by the resistance $R_{arc}(x, t)$ in series with inductance $L_{arc}(x, t)$, and capacitance $C(x, t)$ between the arc tip and the opposite electrode. $R_{ice}(x, t)$ depicts the non-bridged ice-layer resistance. $V_c(t)$ is the voltage drop across the capacitance $C(x, t)$. The arc and ice elements vary with time according to the channel characteristics and discharge geometry. When the arc propagates, the voltage $V_{ap}(t)$ and current $I_{arc}(t)$ waves initiated are described by [33], [124]:

$$V_{ap}(t) - V_c(t) = R_{arc}(x, t)I_{arc}(t) + L_{arc}(x, t) \frac{dI_{arc}(t)}{dt} \quad (2.11)$$

$$I_{arc}(t) = C(x, t) \frac{dV_c(t)}{dt} - \frac{1}{R_{ice}(x, t)} V_c(t) \quad (2.12)$$

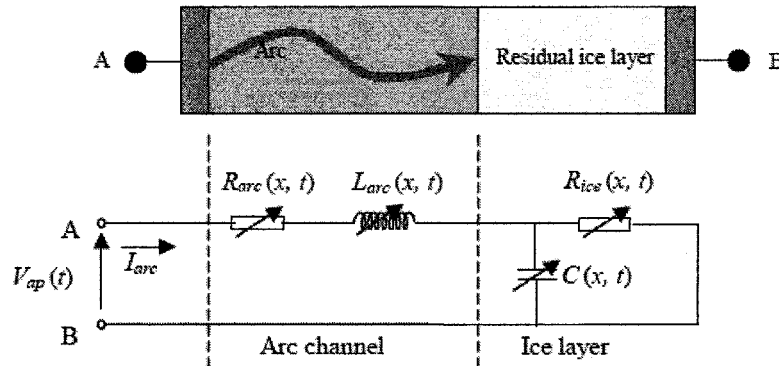


Figure 2.6. Principal model of arc propagation on an ice-covered insulator surface [33].

The input data of the model were the insulator geometry, ice parameters, ambient conditions and certain initial values. The model makes it possible to predict the minimum flashover voltage, leakage current and corresponding charges, arc channel radius, trajectory and electric stress, propagation velocity and energy injected into the air gaps.

Based on the equivalent circuit model shown in Figure 2.6 for AC flashover, the relevant equations for DC are similar to AC conditions. However, some parameters related to arc resistance needed to be modified [32].

In order to take into account the arc temperature as a function of the applied voltage level for DC+ and DC-, formulas were also derived based on a series of simulations and experiments related to short insulators [32].

The flashover characteristics, as a function of surface conductivity, insulator length, and insulator diameter, determined by the dynamic model were quite satisfactory when compared to the experimental results of an insulating cylinder [32], [33], [125], [126], a short string of five IEEE standard insulators [32], [124], [125] and a post insulator [33], [125], [127] covered with artificial ice.

Volat *et al.* [128] developed a model based on dynamic electric field analysis to predict the AC flashover voltage of the ice-covered HV insulators during a melting period, for an arc distance up to two meters. The residual ice resistance can be determined for complex geometries of ice accretion and consequently provides a more powerful method than the analytical formula

of Wilkins [114]. Furthermore, the criterion of arc propagation was determined based on potential and electric field calculations.

Yang *et al.* [129], [130] developed a flashover model of the ice-covered insulator based on those published by CIGELE group. The model was built on the base of analyzing the electric field around the ice-covered insulator before and after the arc initiation and combining with the U-I characteristic of arc. It can be found that the results simulated by the developed model provide good agreement with those obtained by the experimental results not only under uniform but also under complex ice accretion.

2.6. Conclusion

The literature review showed that the flashover of an ice-covered insulator has received much attention from many researchers. In this chapter, different types of ice and their characteristics were reviewed. It was observed that wet-grown ice or glaze, which has a relatively high density, is the most dangerous type of ice from an electrical point of view. Then, several major parameters such as applied water conductivity, ice type, dry arc distance and air pressure influencing the performance of high voltage insulators were introduced. Generally, shorter insulator length, larger insulator diameter, lower air pressure and higher applied water conductivity may lead to a lower flashover voltage.

Also, a series of fundamental mathematical models for flashover of polluted insulators was presented. Additionally, existing static and dynamic flashover models of ice surfaces relied on the basic models of polluted insulator, in particular, Obenaus's model considering an arc in

series with a residual resistance, were studied. The static model provides more quantitative results for flashover voltage prediction whereas the dynamic models provide more precise results about instantaneous evolution of arc parameters. However, the need for dynamic mathematical models for predicting the flashover performance of long ice-covered insulators where two arcs may appear during flashover occurrence is justified.

CHAPTER 3

**EXPERIMENTAL FACILITIES AND
TEST PROCEDURES**

CHAPTER 3

EXPERIMENTAL FACILITIES AND TEST PROCEDURES

3.1. Introduction

As mentioned in Chapter 2, during the recent years, many attempts have been made experimentally and mathematically by research groups to analyze icing and flashover phenomena on the surface of insulators. In spite of these efforts, however, many aspects of the flashover phenomena for ice-covered insulators, particularly EHV insulators, are still not well understood. In addition, because of lack of proper and accurate facilities, experimental researches on the subject are infrequent. Hence, in order to achieve the objectives of this thesis, a series of experiments was systematically carried out in the HV laboratory of CIGELE on the flashover performance of short and long insulators under both AC and DC voltages. For this purpose, the electrical performance of insulators under atmospheric icing conditions was evaluated based on test methods described in IEEE Std 1783[34]. Leakage current and applied voltage, which are important parameters in the electrical measurement categories, were measured using a current transformer (Pearson coil) and/or shunt resistance via the DAQ system. Furthermore, the arc propagation velocity - considering the effect of freezing water conductivity - is observed using high-speed imaging technique.

In addition, in order to determine the electrical surface conductivity on the ice surface of an energized insulator submitted to icing conditions, a series of tests was carried out under a melting regime to measure the flow rate, thickness and conductivity of the water film.

This chapter proceeds with a brief explanation of the facilities of the High Voltage laboratory at CIGELE, followed by a presentation of the test procedures used to determine the required parameters and achieve the relevant experimental results.

3.2. Test facilities

In order to perform the experiment, a variety of experimental equipment is required. These include high-voltage source, voltage and current measuring devices, climate chamber, high-speed camera and test samples, which should be properly arranged and synchronized.

3.2.1. High-voltage equipment

In order to investigate the electrical performance of HV insulators, two types of AC and DC high voltage power sources are necessary. For the tests described herein, the voltages were supplied by an AC source of 350 kV/700 kVA, and a DC source of 300 kV/600 kVA. Their associated voltage regulators are shown in Figures 3.1 and 3.2 respectively. This system is especially designed for flashover tests on insulators under icing conditions and with potential for further research under ice and polluted conditions. The voltage was increased either manually or automatically at different optional rates, and was regulated at a fairly constant rate of about 3.9 kV/s. Since flashover tests on ice-covered insulators are carried out in a closed cold chamber, and the transformer is kept outside this chamber in the HV section of the laboratory, the security system set in place for this type of experiment is of vital importance. Two circuit-breakers and an accurate relay, which interrupts the voltage instantaneously on demand, are a part of this security system. The system may be adjusted to cut off the voltage and de-energize automatically if any

member of personnel enters the test areas. Tested insulator can be supplied by high voltage through bushing connected to the walls of the cold room.

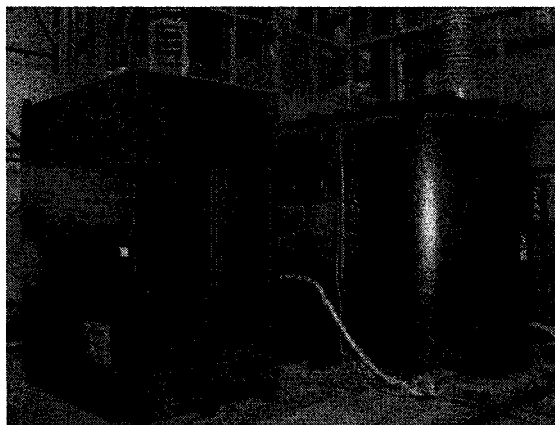


Figure 3.1. HV AC transformer with its associated regulator.



Figure 3. 2. HV DC transformer with its associated regulator.

3.2.2. Climate Chamber

In order to achieve repeatable and comparable tests among researchers, all experiments were carried out at CIGELE laboratory in a uniquely designed climate room (6 m (w) × 6 m (l) × 9 m (h)) for long insulator and (6 m (w) × 6 m (l) × 4 m (h)) for short insulator. These climate rooms are deemed sufficient to meet clearances required by the standard IEEE Std 1783 [34]. The temperature inside two cold rooms can be adjusted to values as low as $-60 \pm 0.2^\circ\text{C}$ and -30



$\pm 0.2^{\circ}\text{C}$ where the long and short insulators were tested respectively. The climate rooms are equipped with such appropriate facilities as a wind generator and a water-droplet spray system. Super-cooled droplets are generated and applied to the insulator by oscillating nozzles which are of the air-atomizing type. The experimental set up related to the big cold room is presented in Figure 3.3.

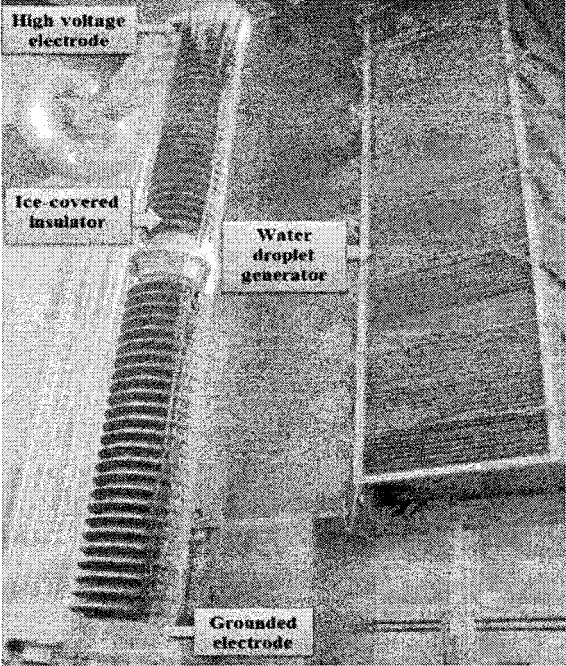


Figure 3.3. Big cold room (6m (width) \times 6m (length) \times 9m (height)).

The water used to produce the droplets, and eventually the ice, is produced by filtration and demineralization of tap water. This filtered water is stored in tanks before starting ice accumulation. This enables adjusting the water conductivity to reflect the desired environmental pollution level.

3.2.3. Physical Objects

In order to perform the experiments and to obtain the desired data, a standard post insulator unit and a line insulator string were chosen. Therefore, to investigate the flashover performance of long insulators, a standard post-type porcelain insulator was selected. This type of insulator is commonly used in Hydro-Quebec 735 kV substations (Figure 3. 4). In order to assess the flashover phenomena on short line insulator, a string of five IEEE standard insulators under given conditions were selected (Table 3. 1). The results related to the line insulator made it possible to study the arc propagation process, as well as to determine flashover voltage for the short-scale insulator.

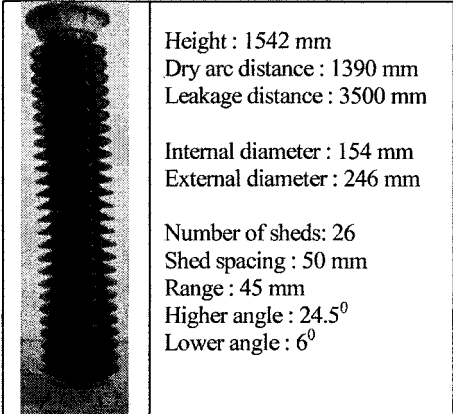


Figure 3. 4. Geometrical characteristics of the 735-kV station post insulator used in the tests.

Table 3. 1. Geometric characteristics of the suspension IEEE standard insulator

Diameter of shed (mm)	Shed spacing (mm)	Leakage distance (mm/unit)	Dry arc distance for 5 units (mm)
254	146	305	809

3.2.4. Current and voltage measurement devices

Dynamic modeling of the arc provides the temporal evolution of a number of arc parameters. The voltage signal and the leakage current were attenuated by using a voltage divider and a shunt or current transformer. In order to be able to compare these curves with the ones produced experimentally, a Labview™ graphical software program was used to acquire high quality data. The test signals were connected to a measuring set through a conditioning box providing protection and isolation. A NI-DAQ device, model PCI-6035E, was used for this purpose. Using the Labview user-interface features, a visual program was specifically designed and developed for these experiments to acquire and save data for further analysis.

3.2.5. High-speed camera

A high-speed video camera (FASTCAM SA1) having a recording capacity up to 675,000 frames per second was used to record arc propagation during flashover occurrence. It was controlled either by a PC through the Gigabit Ethernet port, or by an RS-422 remote control keypad with a LCD monitor for complete camera set-up and operation. It also enabled the user to select the playback rate, step through video one frame at a time even after saving the data, and selectively save video sequences in a variety of compressed and uncompressed formats. Figure 3.5 shows the camera set-up for recording the arc propagation through the cold room window.



Figure 3.5. Camera set-up.

3.3. Test Procedures

The experimental conditions were adjusted, under the conditions described in Table 3.2, to form glaze ice with icicles as this type of ice is associated to the highest probability of flashover on energized insulators. Parameters such as air temperature, wind velocity, as well as both the vertical and horizontal components of precipitation intensities were properly controlled and kept constant for each test.

Table 3. 2. Experimental conditions of the tests

Ice type	Glaze
Ambient air temperature	-12°C ($\pm 0.2^\circ\text{C}$)
Droplet size	80 μm
Ice thickness on rotating monitoring cylinder	2 cm for line insulators, 1.5 cm for post insulators
Rate of water flow	250 ml/s/nozzle
Wind velocity	7 m/s for line insulators, 3.3 m/s for post insulator
Air pressure	10 psi (70 kPa)

The thickness of ice is an important factor influencing the flashover voltage of ice-covered insulators. The accumulated ice thickness on the insulator was measured at 5 different points on a 3.8 cm diameter monitoring cylinder, rotating at one revolution per minute (rpm) [14]. Then, the average value was used to determine the ice thickness as shown in Figure 3.6. The physical aspects of the ice-covered insulator strings under DC+ voltage at different time sequences during ice accumulation are shown in Figure 3.7.

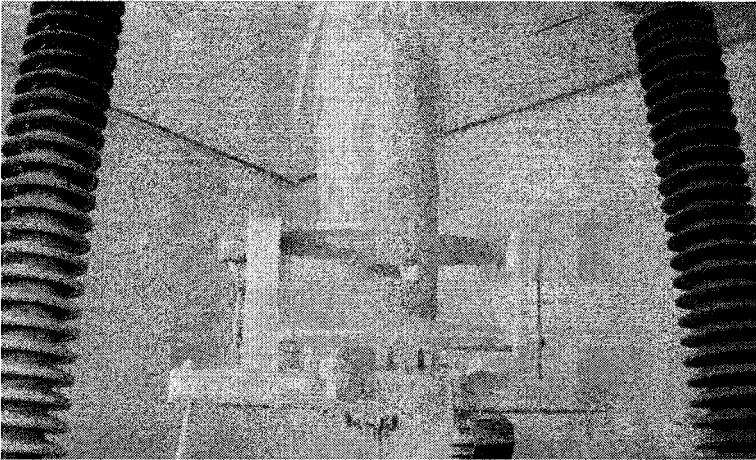


Figure 3.6. Ice on monitoring cylinder.

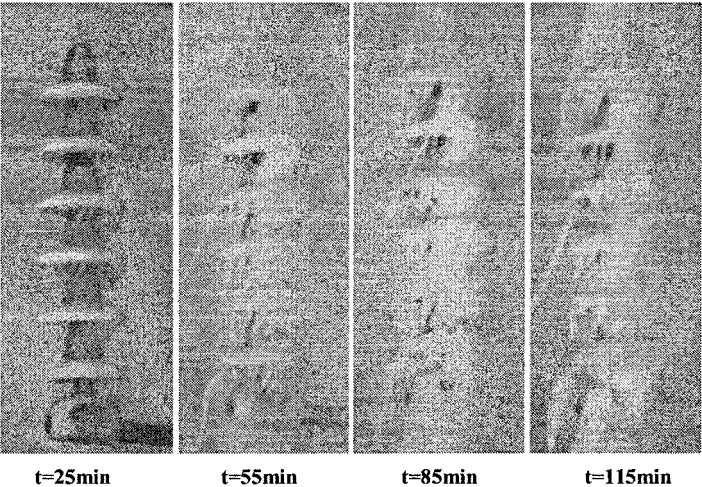


Figure 3.7. Physical aspect of an insulator during ice accretion.

3.3.1. Ice test preparation prior to flashover

A preparation period is needed between the end of the ice accretions at sub-zero temperature and the moment when test voltage is applied for flashover voltage evaluation. The procedure may be adjusted according to two approaches; “icing regime” or “melting regime” [14], [24]. Testing under “icing regime” corresponds to the case where the flashover performance test is carried out shortly after the ice accretion is completed and a water film is still present on the ice surface. In such a case, the preparation period is short, typically about 2 to 3 min, which gives enough time for taking pictures, adjusting the test setup, installing/removing the collector, receiving dripping water from test insulators, and measuring ice thickness (Figure 3.8).

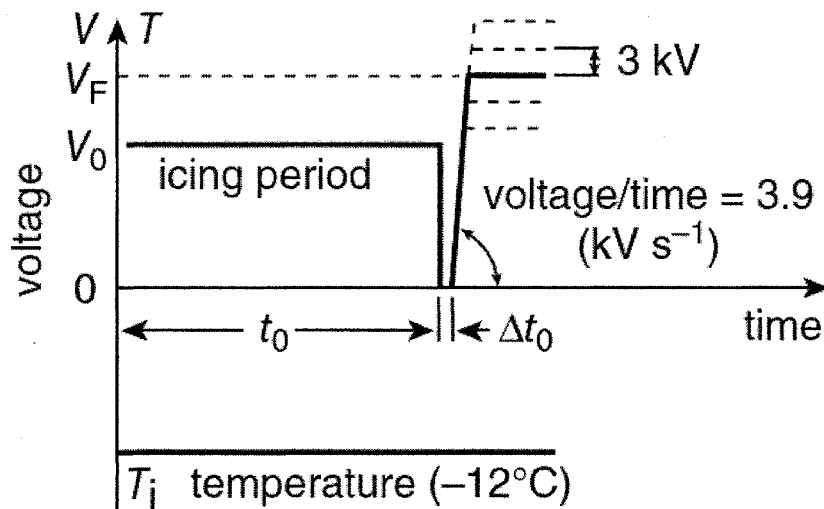


Figure 3.8. Sequences of the icing regime test procedure [24].

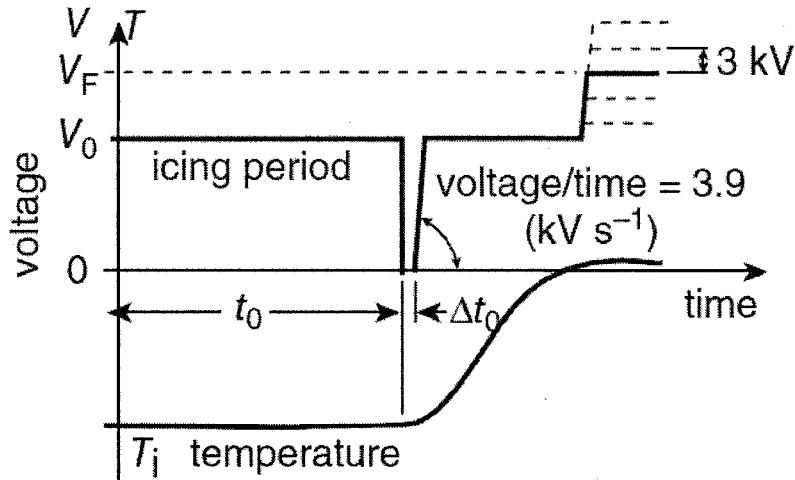


Figure 3.9. Sequences of the melting regime test procedure [24].

The melting sequence shown in Figure 3.9 was preceded by an “ice hardening” sequence. In a recommended 15-minute hardening sequence, voltage was turned off, wind speed was continuous and air temperature remained the same as during the icing period. These conditions ensured complete hardening of the ice and equalization of insulator and ice temperatures. During the melting sequence, immediately after the hardening sequence, while service voltage was applied, the air temperature was increased progressively from subzero to melting level at a rate of 2–3 °C/hour above -2 °C. The most important decision in this step was the identification of the “critical moment,” which corresponds to the time at which the probability of flashover is the highest. This is the moment when flashover voltage should be applied. Several major signs of this moment are the presence of a water film on the ice surface, the gloss of the ice surface, the start of water droplet ejection from the icicles, and/or an increase in leakage current to values over 15 mA [14]. In order to measure the conductivity and volume flow rate of water film over ice surface, the melting regime method was used.

Based on experimental results in [72], maximum withstand voltage values under icing regime are around 3% lower than those obtained from melting regime. Therefore, both the melting and icing regime methods can be used to carry out flashover tests of ice-covered insulators. Hence, in order to save time, the “icing regime” test procedure was used for all flashover experiments.

In the case of flashover tests on post insulators, in order to eliminate problems related to randomness in the position and size of air gaps, the ice was accumulated without voltage application to determine the effect of air gap position and numbers on insulator surface on the maximum withstand voltage as well as to establish the two-arc dynamic model. Once the ice thickness on the cylinder reached 15 mm, the icing process was stopped and a series of artificial gaps with a given length corresponding to 6-8% of insulator length was then artificially created near the high voltage electrodes and/or the middle of the insulator by cutting a part of the ice, following procedures from previous work [86].

Under DC voltage, each test can be categorized into two voltage polarities. For each polarity, for an arc distance of 173 cm, one of three air gap configurations close to the electrodes was chosen as follows:

Configuration 1-dc: one 14-cm air gap at the top of insulator (Figure 3.10-a);

Configuration 2-dc: one 14-cm air gap at the bottom of insulator (Figure 3.10-b);

Configuration 3-dc: one 14-cm air gap at the bottom and one 14-cm air gap at the top of insulator (Figure 3.10-c).

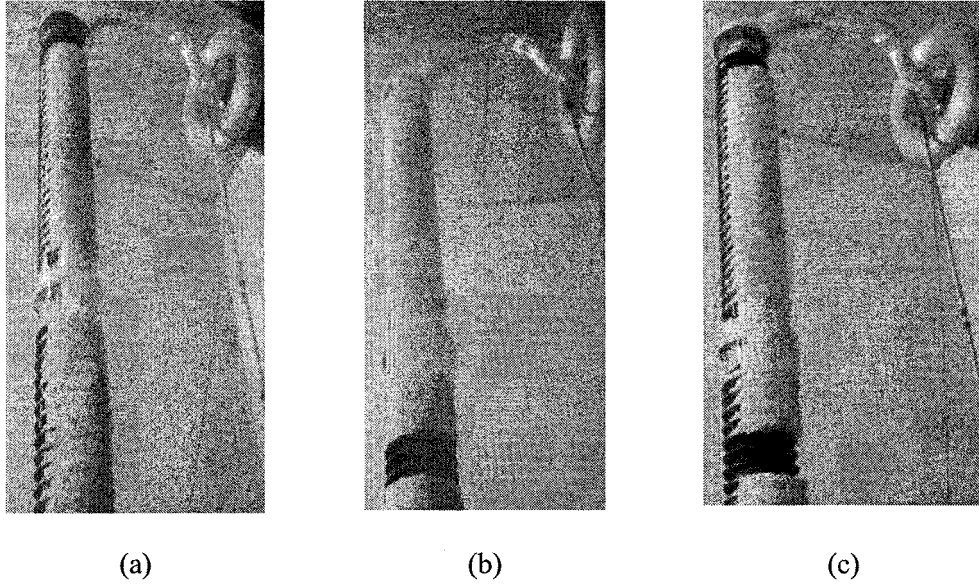


**Figure 3.10. Air gap configuration along an ice-covered insulator under DC voltage:
a) upper air gap, b) lower air gap, c) lower and upper air gaps.**

Under AC voltage for an arc distance of 275 cm, the following three air gap configurations were used:

Configuration 1-ac: two 14 cm air gaps at the top and bottom of insulator (Figure 3.11-a);

Configuration 2-ac: three 14 cm air gaps at the top, bottom and middle of two post insulator units (Figure 3.11-b);

Configuration 3-ac: three 14 cm air gaps at the top, bottom and middle of two post insulator units, and also one 14-cm air gap at middle of the upper insulator unit (Figure 3.11-c).

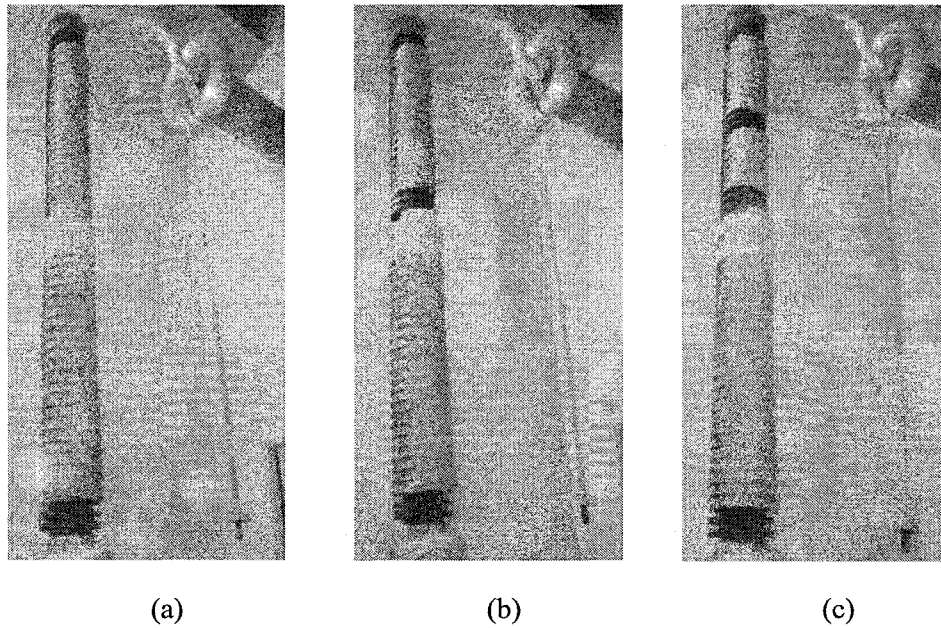


**Figure 3.11. Air gap configuration along an ice-covered insulator under AC voltage:
a) 2 air gaps, b) 3 air gaps, c) 4 air gaps.**

3.3.2. Evaluation sequence

This sequence consists in determining the maximum withstand voltage (V_{ws}) of the insulators under a given ice thickness during the melting period, based on IEEE Std 1783 [34]. Using this method, after the first successful flashover result, the voltage was decreased by less than 5% of the nominal voltage, and then, after any withstand or flashover result, the voltage was increased or decreased once more by the same value, or else it was maintained. Based on this method, the maximum withstand voltage is the maximum level of applied voltage at which flashover does not occur for a minimum of 3 tests out of 4, under similar experimental conditions. It is also recommended that for each withstand test, the insulator is kept at the test voltage for a period of at least 15 minutes to ensure that no flashover occurs during this period. The minimum flashover voltage (V_{MF}) corresponded to a voltage level 5% higher than V_{ws} at which two flashovers out of a maximum of three tests were produced.

3.3.3. Water film conductivity and volume flow rate measurement procedure

In order to estimate instantaneous flashover behavior under relevant conditions, it is necessary to develop an appropriate dynamic model. There are several parameters that could play an important role on accuracy of this model, and they should thus be measured precisely. Surface conductivity is an example of such a parameter, since it has an effective role in the calculation of electrical resistance of the ice surface. Therefore, a relationship between surface conductivity and freezing water conductivity during melting period under both DC and AC voltages were established. Incidentally, two other parameters, thickness and conductivity of water film, were measured in order to calculate the precise value of surface conductivity. Hence, a series of tests was performed on a post insulator to determine the conductivity and the volume flow rate of the water film during flashover occurrence. These experiments were carried out on a 172.6 cm arc length insulator with three different water conductivities of 30, 80 and 150 $\mu\text{S}/\text{cm}$ under different voltage polarities and types.

During the melting period, ice accreted on an insulator melts and forms a water film on its surface, which increases greatly the conductivity and causes a corresponding decrease of withstand voltage of the insulator string. Since the water film conductivity has its highest value at the beginning of the melting stage and then decreases gradually, the time variation of the dripping water film conductivity is required. Incidentally, a traditional method has been presented to date. Once water started dripping from the icicles, flashover voltage was applied. During this period, the melted water was collected in a funnel and was conveyed to a tray where its conductivity was measured while, simultaneously, water film volume variation was measured. This conductivity measurement system makes it possible to measure in a precise way the conductivity of water film during the melting regime. The experimental setup is presented schematically in Figure 3.12.

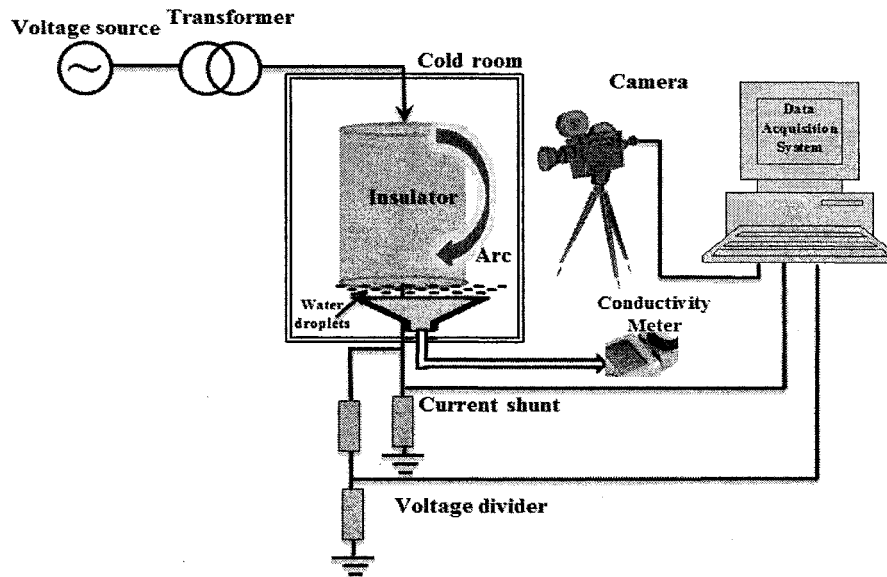


Figure 3.12. Schematic diagram of the experimental setup.

3.4. Conclusion

The necessary facilities and test procedures to carry out the experiments were presented in this chapter. A standard post insulator, typically used in Hydro-Quebec 735 kV substations, and a line insulator string were used as long and short insulators respectively. A wet-grown ice layer was accumulated on the insulator surface in a uniquely designed climate room at an ambient temperature of -12°C by seven pneumatic nozzles at a wind velocity of 3.3 m/s. The voltages were supplied by an AC source of 350 kV, 700 kVA and a DC source of 300 kV, 600 kVA. Arc propagation was observed by a high-speed video camera with recording capacity up to 675,000 frames per second. Then, the flashover tests were carried out under icing period based on IEEE Std 1783. Test methods to determine water film conductivity and volume flow rate were described.

CHAPTER 4

**EXPERIMENTAL RESULTS AND
DISCUSSIONS**

CHAPTER 4

EXPERIMENTAL RESULTS AND DISCUSSIONS

4.1. Introduction

Using the facilities and test procedures described in Chapter 3, a series of experiments was carried out to meet the stated objectives. First, the effects of voltage type and polarity on the maximum withstand voltage of a string of five IEEE standard insulators (as short insulators) were investigated under icing conditions. Then, the flashover performance of EHV standard porcelain post insulators was tested under icing conditions and the influence of air gap positions and number on maximum withstand voltage were also examined. Moreover, the effect of voltage type and polarity on the arc propagation velocity - considering the effect of freezing water conductivity - was observed using high-speed imaging techniques. Also, several tests were carried out to measure the water film flow rate and conductivity in order to determine water film thickness. Finally, the flashover stress of an ice-covered post insulator is presented as a function of the icing stress product (ISP) for each air gap configuration. Flashover results obtained from present work are compared with those reported from other laboratories.

4.2. Withstand voltage measurement of a string of five standard insulator units under icing conditions

In order to improve our understanding of the flashover process of short ice-covered insulators, a series of tests was carried out under DC+, DC- and AC voltages. These tests were

performed with the aim of examining the influence of the type and polarity of the applied voltage on the flashover voltage and leakage current. The five IEEE standard insulators with shed diameter, unit spacing and leakage distance of 254, 146 and 305 mm respectively were positioned vertically in the center of a climate room under high wind velocity (7m/s).

The AC and DC minimum flashover and maximum withstand voltages of the insulator were determined under the conditions given in Table 3.1. A positive arc appeared when DC-voltage was applied to the bottom electrode, and a negative arc manifested when DC+ voltage was applied. Due to the discharge activities during ice accumulation, the air gap was formed close to the HV electrode. At the end of the accumulation period (70 min.), the windward side of insulator was completely covered with ice. Following the icing regime, described in Chapter 3, the voltage was applied shortly after ice accumulation and it was increased at a constant rate up to the estimated flashover voltage. As the voltage increased, visible discharges (violet arc) appeared along the air gap for a certain time, and then the visible discharges changed to a stable white arc across this air gap. If the applied voltage was high enough the white arc could elongate up to flashover, otherwise after certain time, the white arc could extinguish due to the melting and shedding of the ice. Concerning the arc propagation mechanism, it was observed from Figure 4.1 (taken by high speed camera) that the local arc consistently started from the grounded top electrode and propagated towards the HV bottom electrode, regardless of the voltage polarity. It was also found that only one air gap was formed close to the HV electrode for insulator strings shorter than 1 m.

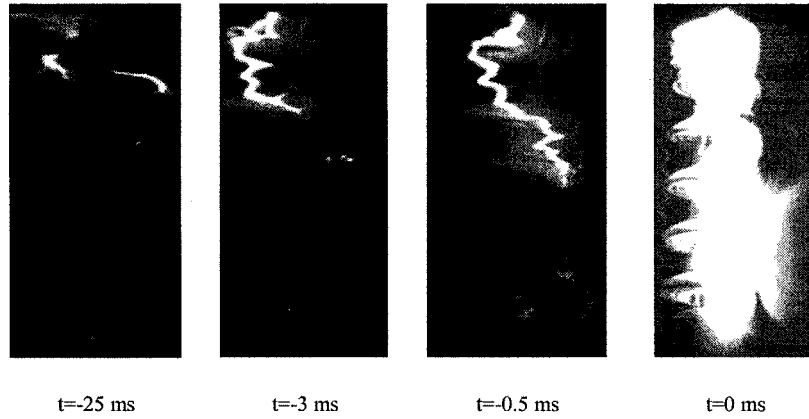


Figure 4. 1. Ice-covered insulator flashover sequence at 87 kV of DC negative voltage.

The flashover test results were obtained from three different series of experiments, under DC+, DC- and AC voltages for the freezing water conductivity of $80 \mu\text{S}/\text{cm}$ and ice thickness of 2 cm. The experimental results related to flashover and withstand voltages under DC+, DC- and AC conditions are presented in Figures 4.2, 4.3 and 4.4 respectively.

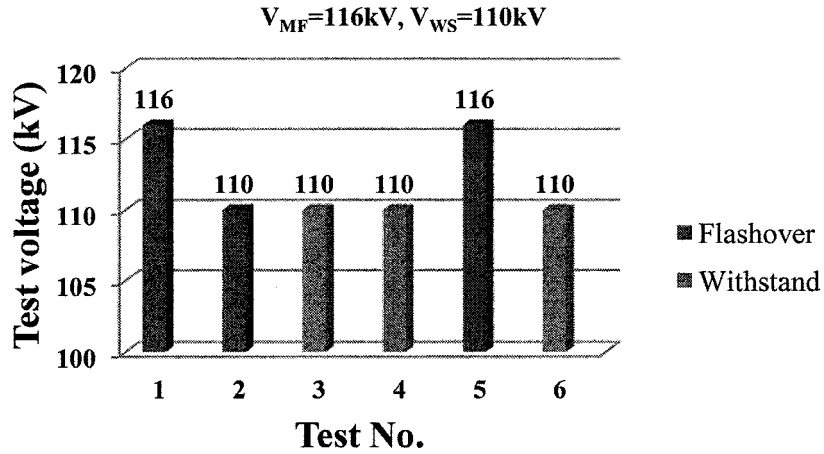


Figure 4.2. Flashover test results under DC+.

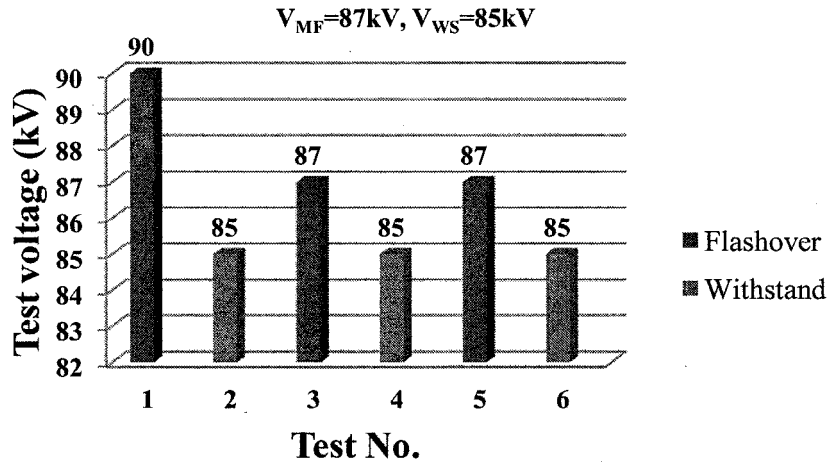


Figure 4.3. Flashover test results under DC-.

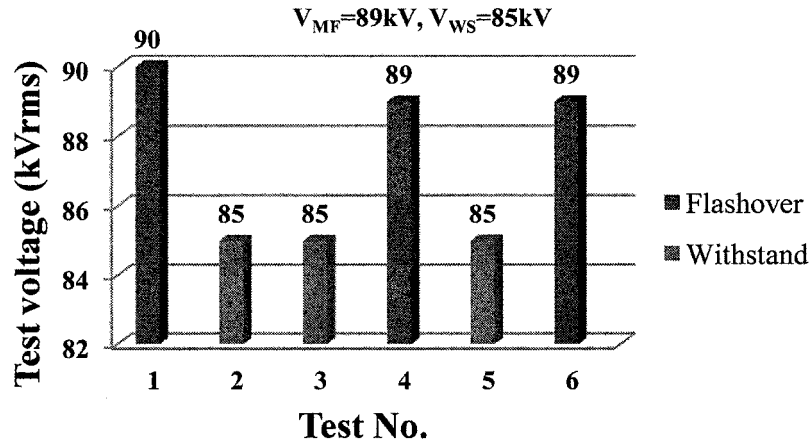


Figure 4.4. Flashover test results under AC.

These results show that the effect of polarity on the insulator string is around 25%, which is in accordance with the results presented in [32]. Consequently, from the results obtained, it can be concluded that the minimum flashover voltage is lower under DC- and AC than under DC+. It was also found that the icicles formed at a relatively high wind velocity (7 m/s) were nearly tilted away by the wind, as shown in Figure 4.5, while they were nearly vertical for the lower wind velocity (3.3 m/s). Therefore, the higher the wind speeds, the longer the leakage distance is. Compared to previous studies, mostly at low wind velocities, the withstand voltage is higher at a high wind velocity [29].

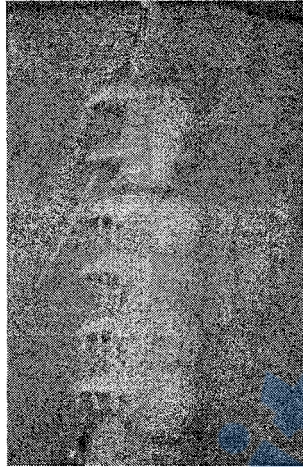


Figure 4.5. Ice accretion under high wind velocity.

4.3. Withstand voltage measurement of post insulator units under icing conditions

As the voltage applied to a moderately ice-covered insulator was increased, local arcs first initiated across the air gaps and propagate along the surface. The arc lengthens not only because of longitudinal propagation alongside the ice but also due to bowing of the hot channel resulting from buoyancy force. Arc propagation observation showed that the arc path on ice surface is random. Therefore, arc propagation may be completed through the shortest path having the highest conductivity. In the case of short insulators, the discharge path usually initiated from a point close to the HV electrode. For the long insulators, used in the EHV and UHV networks, voltage distribution was highly non-uniform, particularly after the formation of icicles. Under these conditions, more than one air gap may be formed depending on insulator length, and therefore on the number of insulator units. For post type insulators, the space between the sheds is relatively small compared to that between the shed and the metallic part. Consequently, the shed spacing can easily be bridged by icicles, with air gaps usually formed between the shed and the metallic part.

As presented in Chapter 3, to eliminate the problems related to randomness in the position and size of air gaps, the air gaps were created manually. Therefore, once the ice thickness on the monitoring cylinder reached 15 mm, the icing process was stopped and then a series of artificial gaps with a given length corresponding to 6-8% of insulator length was artificially created at places where the formation of an air gap are most probable. The tests under DC voltage are classified into three air gap configurations, namely one air gap at the lower part, one air gap at the upper part and two air gaps (at the upper and lower parts of the insulator), as shown in Figure 3.10. In the same way, under AC voltage two units of post insulator were considered with three different air gap positions, as shown in Figure 3.11, namely:

- two air gaps at top and bottom of insulator;
- three air gaps at top, bottom and middle of the insulator;
- four air gaps positions : top, bottom and middle of two post insulator units and one at the middle of the upper insulator unit.

In order to save time, the icing regime method was also selected to investigate the flashover performance of EHV insulators covered with ice under different air gap position and voltage types. According to the evaluation method, each series was constituted of at least five tests, which, under optimum conditions, include 2 flashovers and 3 withstands. Also, the flashover test results were obtained from a series of experiments with different applied water conductivities, i.e. 80 and 150 $\mu\text{S}/\text{cm}$ and different dry-arc distance, i.e. 173 and 275 cm.

4.3.1. Experimental results and discussion under DC Voltage

Based on the above-mentioned air gap configurations, the flashover test results were obtained from several series of experiments, under DC+ and DC- voltages. The experimental results related to the minimum flashover and the maximum withstand voltages under DC+ and DC- voltage with different air gap positions and applied water conductivity are presented in Figures 4.6 to 4.17.

It may be observed that the number and position of air gaps have a significant effect on the minimum flashover voltage of ice-covered insulators. The lowest level of minimum flashover voltage was obtained with the configuration 3-dc and the highest, with the configuration 2-dc. From these results, it may be concluded that configuration 2-dc presents the best combination of air gaps. By comparing the minimum flashover voltage of configuration 2-dc to that of configuration 3-dc, which was taken as reference, an improvement of 8% in the minimum flashover voltage was observed. Moreover, the experimental results reveal that flashover voltage under DC+ is higher than DC-. In addition, the minimum flashover voltage decreased as the freezing water conductivity increased.

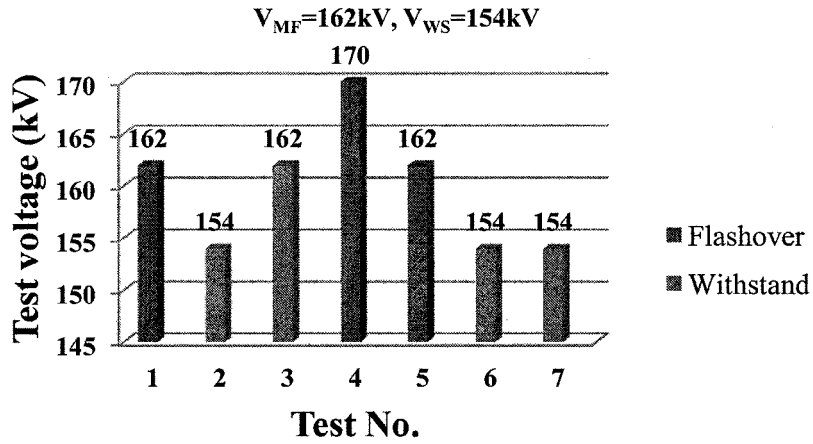


Figure 4.6. Flashover results for configuration 1-dc (173cm dry arc distance) with a conductivity of $80 \mu\text{S}/\text{cm}$ under DC+.

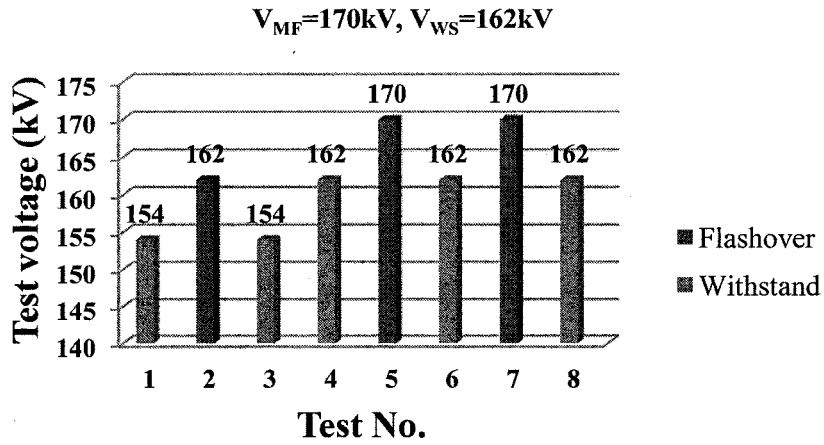


Figure 4.7. Flashover results for configuration 2-dc (173cm dry arc distance) with a conductivity of $80 \mu\text{S}/\text{cm}$ under DC+.

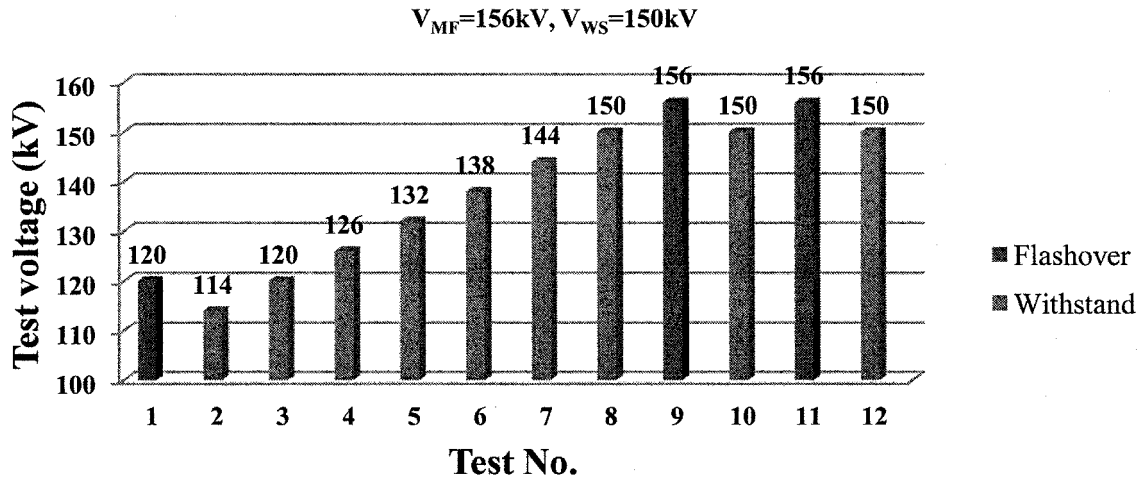


Figure 4.8. Flashover results for configuration 3-dc (173cm dry arc distance) with a conductivity of 80 $\mu S/cm$ under DC+.

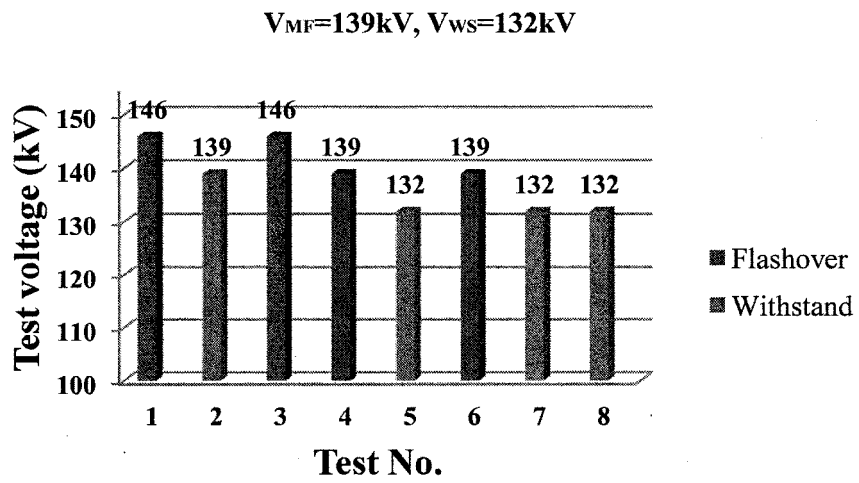


Figure 4.9. Flashover results for configuration 1-dc (173cm dry arc distance) with a conductivity of 80 $\mu S/cm$ under DC-.

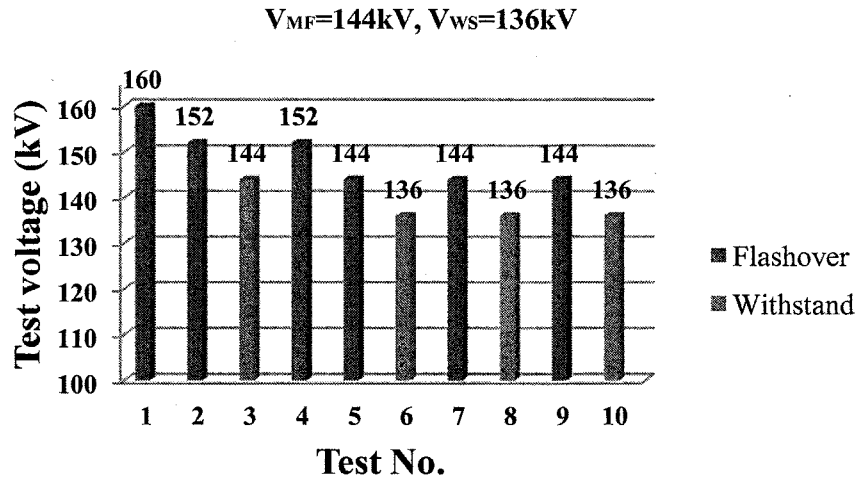


Figure 4.10. Flashover results for configuration 2-dc (173cm dry arc distance) with a conductivity of $80 \mu S/cm$ under DC-.

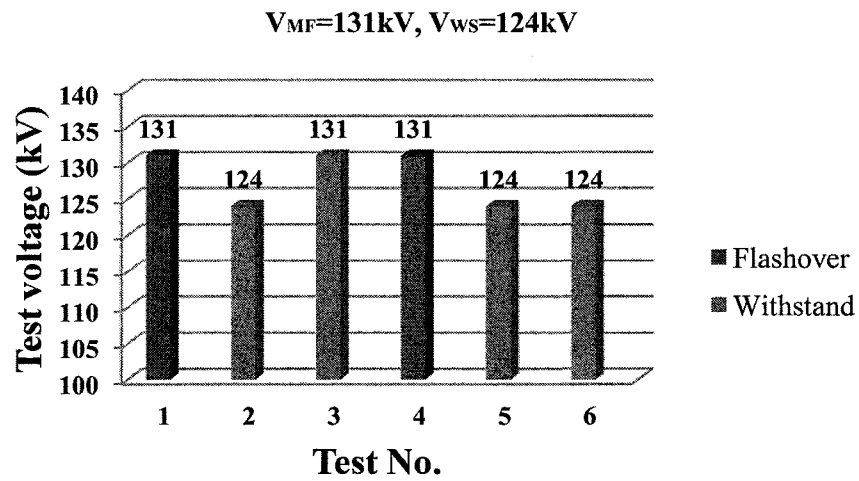


Figure 4.11. Flashover results for configuration 3-dc (173cm dry arc distance) with a conductivity of $80 \mu S/cm$ under DC-.

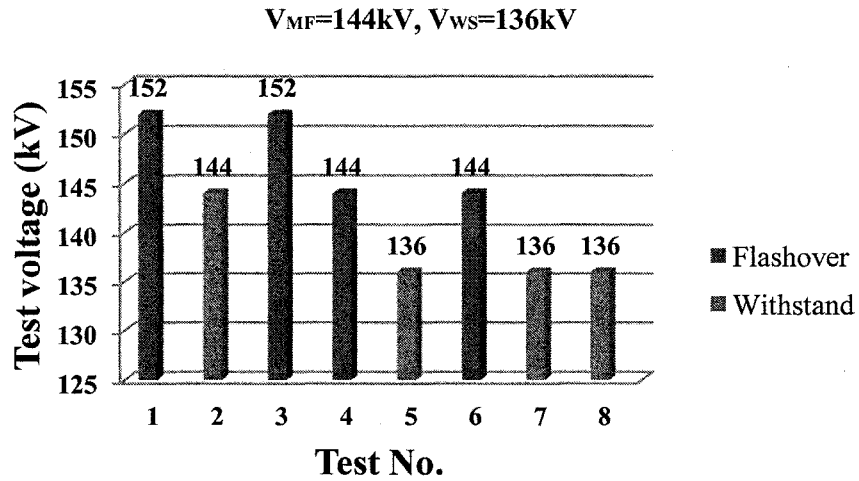


Figure 4.12. Flashover results for configuration 1-dc (173cm dry arc distance) with a conductivity of 150 $\mu S/cm$ under DC+.

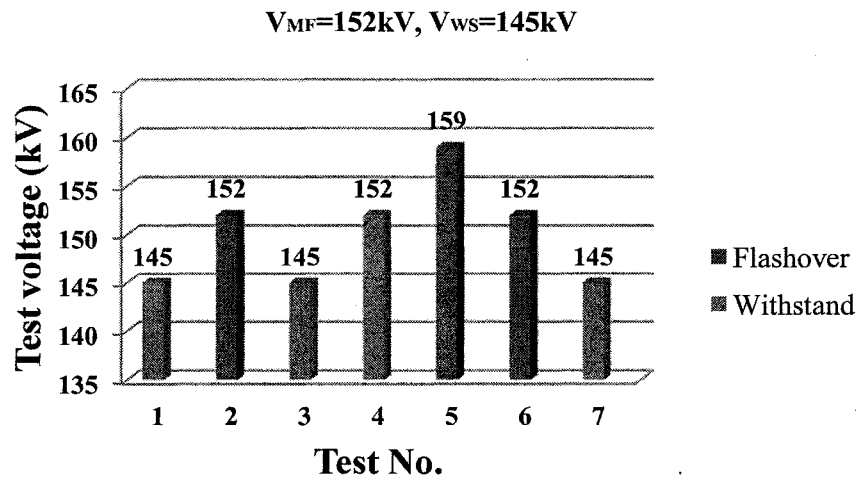


Figure 4.13. Flashover results for configuration 2-dc (173cm dry arc distance) with a conductivity of 150 $\mu S/cm$ under DC+.

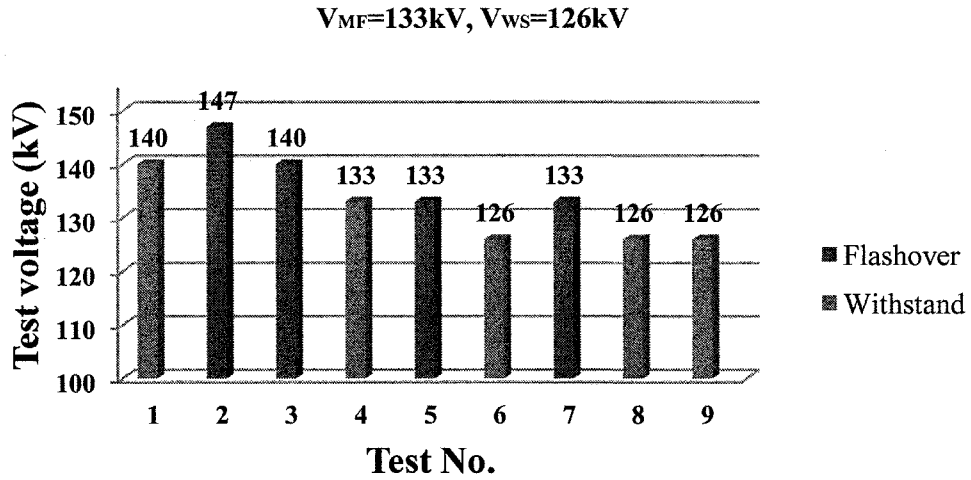


Figure 4.14. Flashover results for configuration 3-dc (173cm dry arc distance) with a conductivity of $150 \mu S/cm$ under DC+.

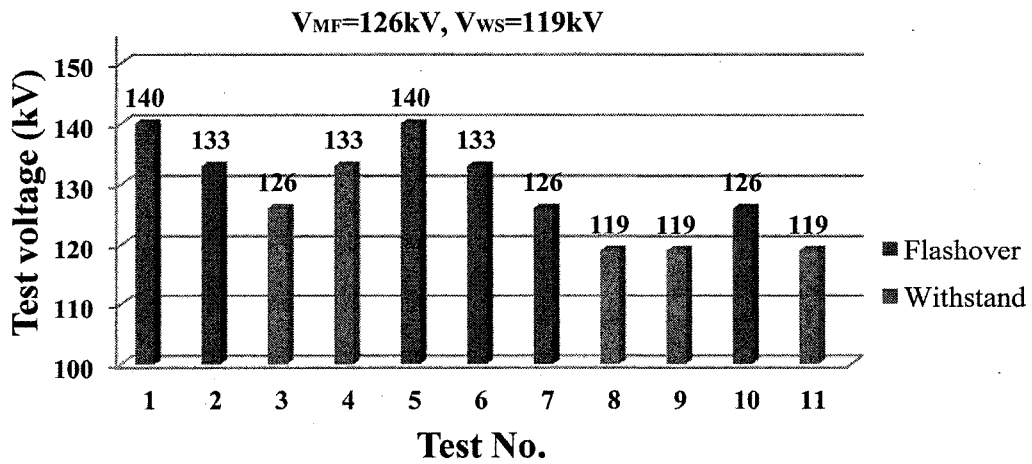


Figure 4.15. Flashover results for configuration 1-dc (173cm dry arc distance) with a conductivity of $150 \mu S/cm$ under DC-.

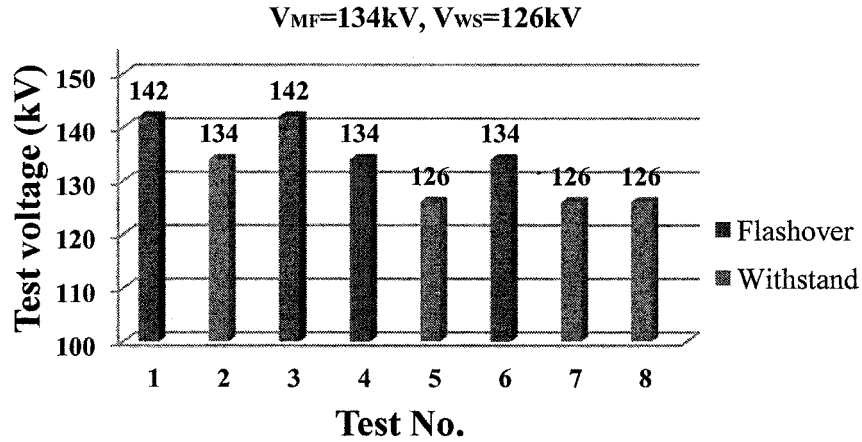


Figure 4.16. Flashover results for configuration 2-dc (173cm dry arc distance) with a conductivity of $150 \mu\text{S}/\text{cm}$ under DC-.

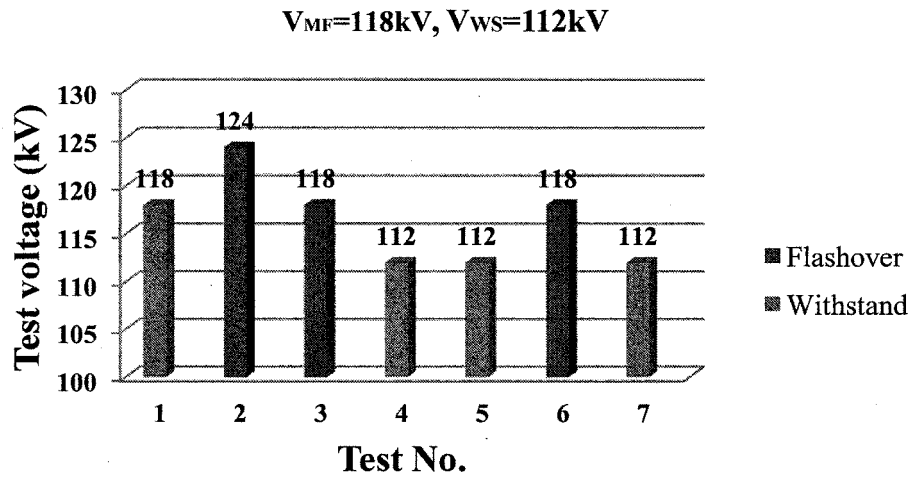


Figure 4.17. Flashover results for configuration 3-dc (173cm dry arc distance) with a conductivity of $150 \mu\text{S}/\text{cm}$ under DC-.

4.3.2. Experimental results and discussion under AC Voltage

A series of tests was carried out under AC voltage to evaluate the performance of long insulators covered with ice. Using the test procedures described in Chapter 3, the minimum flashover voltage was determined and the results for three different air gap configurations are presented in Figures 4.18, 4.19 and 4.20. In contrast to configuration 1-ac, consisting of two air gaps at the top and bottom of the insulator, there are three air gaps in the case of configurations

2-ac. In this case, the local arc has a longer initial length and could reach its critical length sooner when compared to configuration 1-ac. This could explain why the value of the V_{MF} is lower for configurations 2-ac than for configuration 1-ac. On the other hand, configuration 3-ac with four air gaps has the highest minimum flashover voltage. This is probably due to the fact that the voltage needed for breaking down a total of four air gaps and establishing initial arcs is higher than the required voltage for the configurations 1-ac and 2-ac. From these results, it may be concluded that configuration 3-ac presents the best combination of air gaps. By comparing the V_{MF} of configuration 3-ac to that of configuration 2-ac, which is taken as reference, an improvement of 15% in V_{MF} is observed.

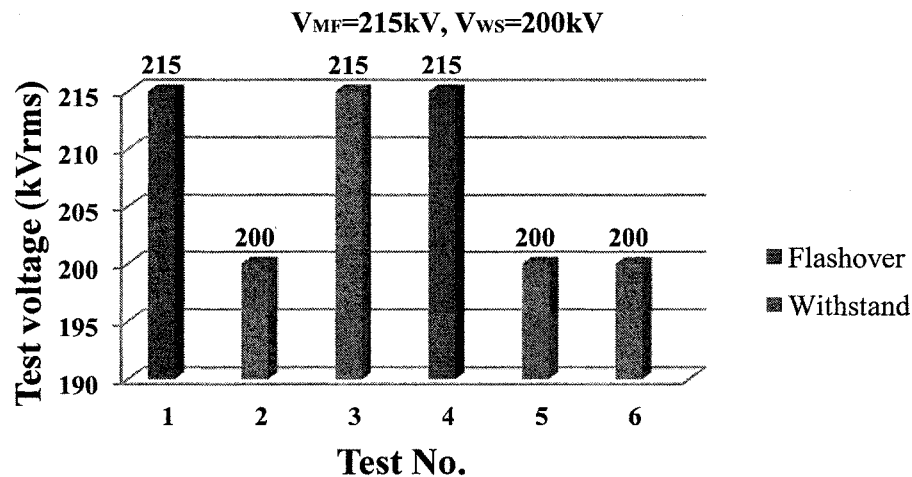


Figure 4.18. Flashover results for configuration 1-ac (275cm dry arc distance) with a conductivity of $80 \mu\text{S}/\text{cm}$ under AC.

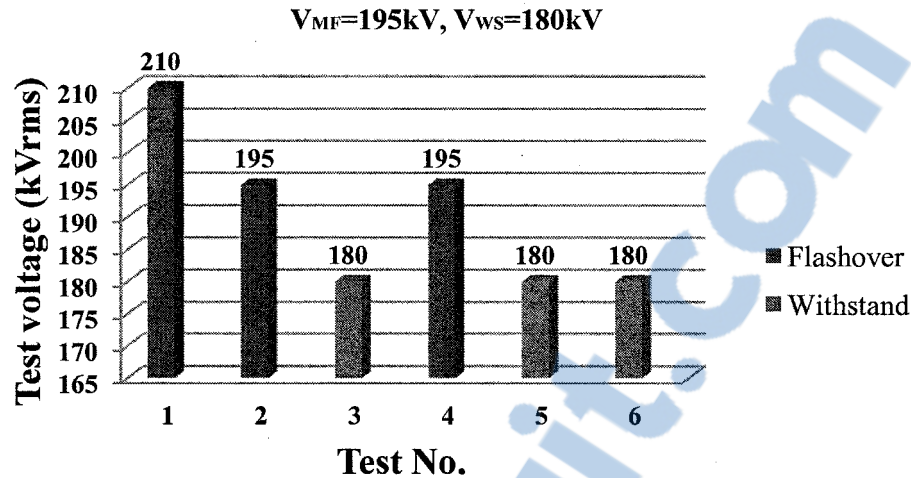


Figure 4.19. Flashover results for configuration 2-ac (275cm dry arc distance) with a conductivity of $80 \mu\text{S}/\text{cm}$ under AC.

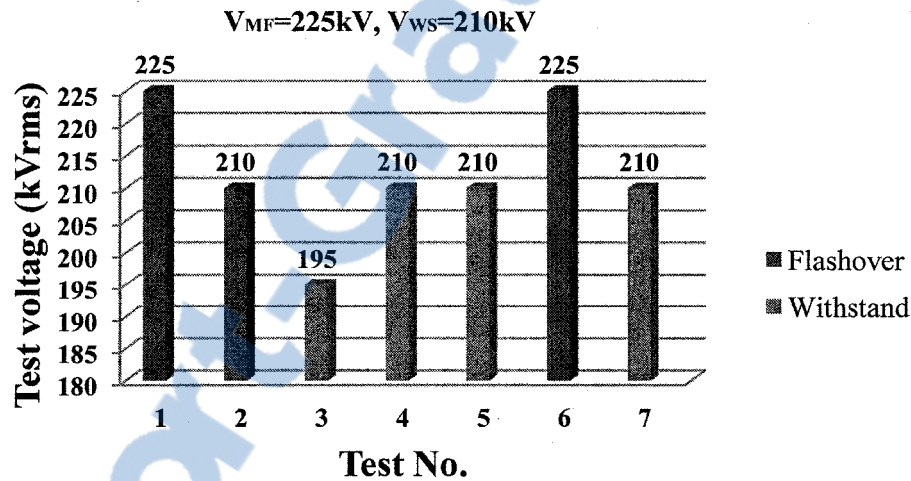


Figure 4.20. Flashover results for configuration 3-ac (275cm dry arc distance) with a conductivity of $80 \mu\text{S}/\text{cm}$ under AC.

One of the main factors that should be considered while selecting the insulator length is the voltage level of power network. Thus, a series of tests under AC voltage, corresponding to configuration 3-dc, has also been carried out to determine the effect of arc distance on the minimum flashover voltage with two freezing conductivities, i.e. 80 and $150 \mu\text{S}/\text{cm}$. Also, the results clearly show the effect of voltage type. The experimental results presented in Figures 4.21

and 4.22 claim that the minimum flashover voltage decreases with increasing the freezing conductivity. Moreover, it can be concluded that the behavior of an ice-covered insulator under AC voltage is similar in the case of DC-. Also, the level of minimum flashover voltage under AC voltage is slightly higher than that of DC- and lower than DC+ voltages. The study of arc propagation under AC voltage may reveal its similarity with a negative arc.

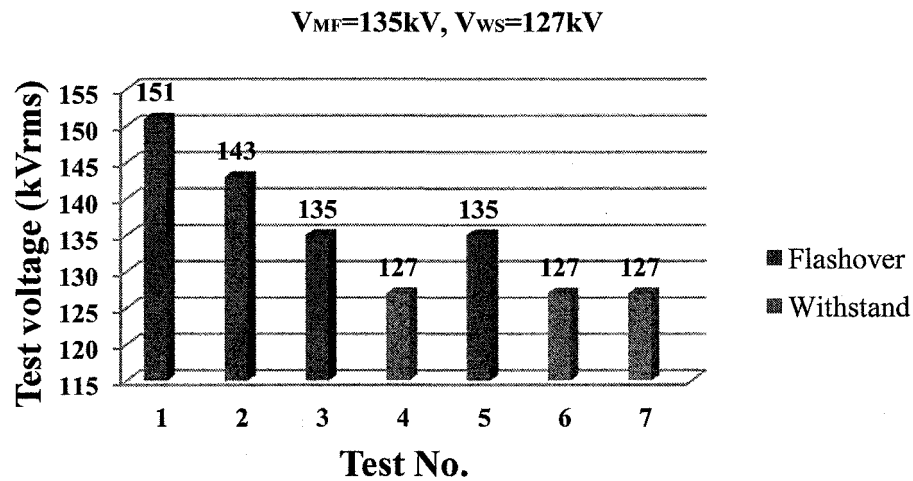


Figure 4.21. Flashover results for configuration 3-dc (173cm dry arc distance) with a conductivity of $80 \mu S/cm$ under AC voltage.

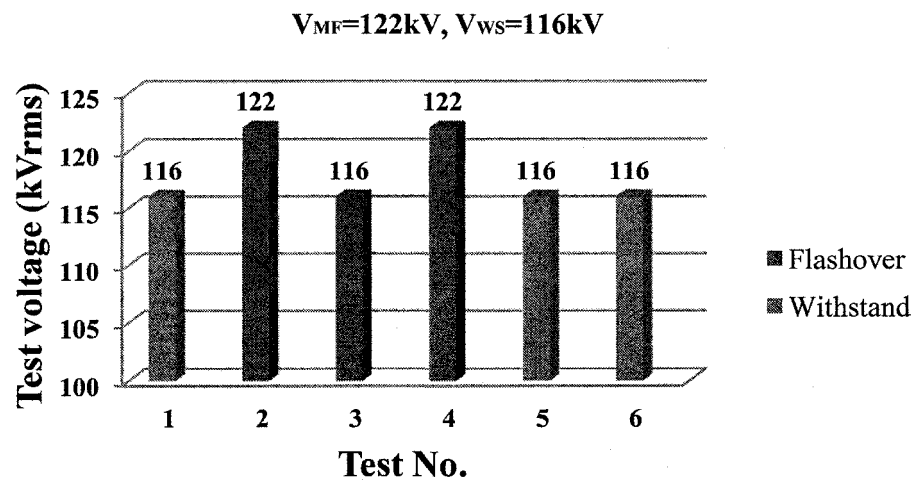


Figure 4.22. Flashover results for configuration 3-dc (173cm dry arc distance) with a conductivity of $150 \mu S/cm$ under AC voltage.

The level of pollution is an important parameter which may affect the insulators performance especially under icing conditions. Therefore in order to determine the effect of the freezing water conductivity on the V_{MF} , a series of tests was carried out at $150 \mu\text{S}/\text{cm}$, a value of conductivity considered to be high. The experimental results presented in Figure 4.23, compared to Figure 4.22 for the same conductivity, validate the theoretical premise that the minimum flashover voltage increases with increasing insulator length.

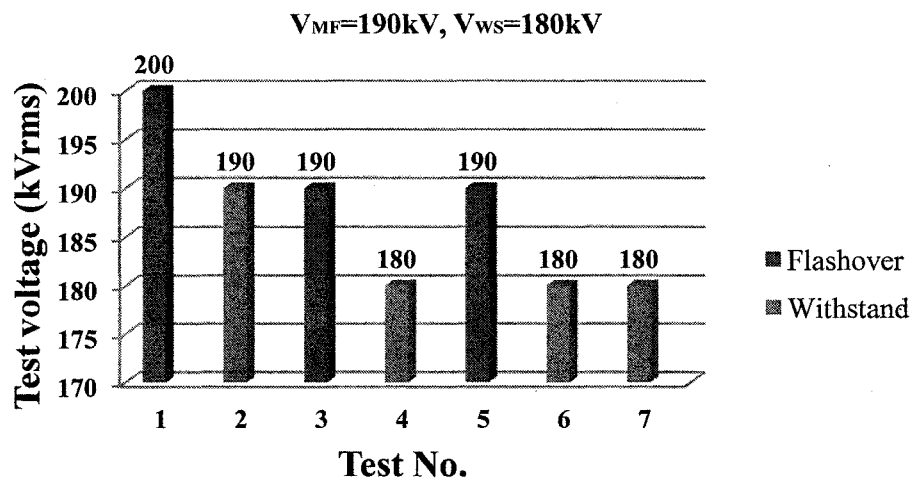


Figure 4.23. Flashover results for configuration 1-ac (dry arc distance of 275cm) with a conductivity of $150 \mu\text{S}/\text{cm}$ under AC.

4.4. Arc propagation on the ice surface

The initiation of corona discharges leading to the development of partial arcs in the air gaps causes a substantial increase in leakage current. Based on a theory already proposed by Wilkins [131] on electrolytic surfaces, a mechanism of arc propagation by ionization on ice surface is suggested. The theory suggests that elongation is produced by three ionization paths, in parallel, through the bulk ice, the water film layer and the air along the water film surface as shown in Figure 4.24. The leakage currents I_{ice} , I_{water} and I_{air} are related to the bulk ice, the water

film layer and the air paths respectively. Indeed, previous investigations have shown that the conductivity of the bulk ice itself, during a melting period, is very low compared to that of the ice surface [63]. Therefore, it has to be noticed that the current flowing through the bulk ice is negligible. In addition, the conductivity of the air before ionization is low. Finally, experimental observations show that arc propagation velocity over an ice surface is much higher than in air. Hence, leakage current as well as arc propagation is forced to flow mainly on the surface of the water film, as shown in Figure 4.25 for several arc propagations.

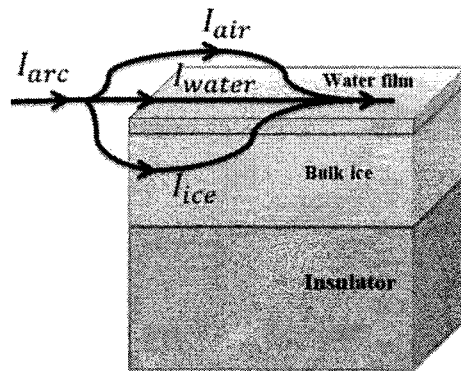


Figure 4.24. Proposed mechanism of arc propagation.

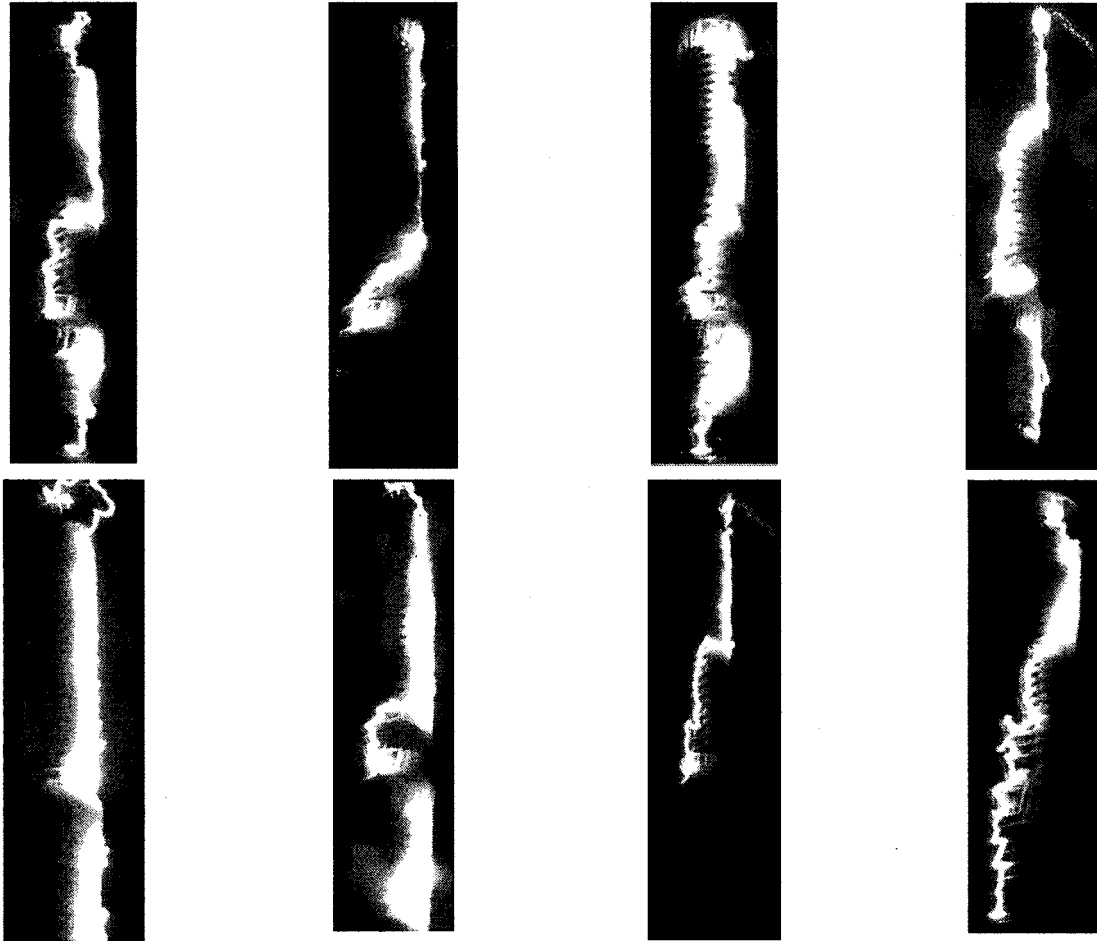


Figure 4.25. Flashover occurrences on an ice-covered post insulator.

Arc propagation is a complex phenomenon which can be affected by several factors including voltage type, rate of voltage application, humidity and insulator length. The arc lengthens because of buoyancy forces that move the arc forward or by a convection effect. Arc propagation observations showed that arc trajectory on ice surface is a random process. Therefore, the arc propagation may be completed through the shortest path having the highest conductivity. In the case of short scale insulator, the discharge path always initiated from a point closer to the HV electrode whereas for the long scale insulator in the meantime, another arc initiates from the grounded electrode and joins the first arc approximately in the middle of the

insulator. Figures 4.26, 4.27 and 4.28 show the flashover process under DC positive, negative and AC applied voltages based on digital high-speed image recording techniques, respectively. It can be seen that under the same icing conditions, the duration of arc development from 40% of insulator length to flashover occurrence with the application of DC+ is longer than under DC- and AC. In this case, the duration of arc development under DC+ and DC- were, respectively, 49, 35 and 41 ms.

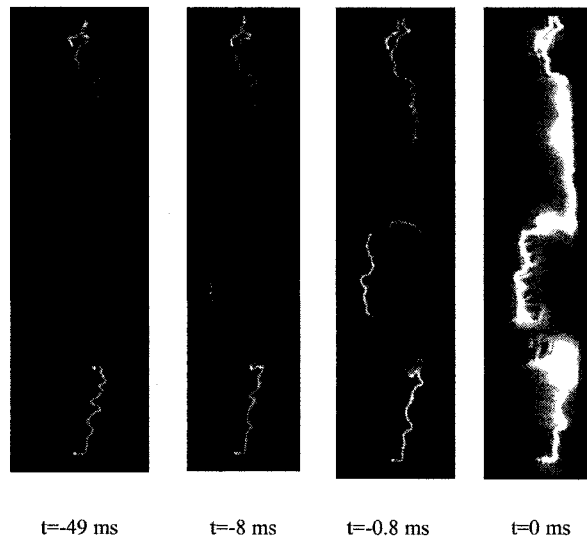


Figure 4.26. Flashover process of post insulator under DC+.

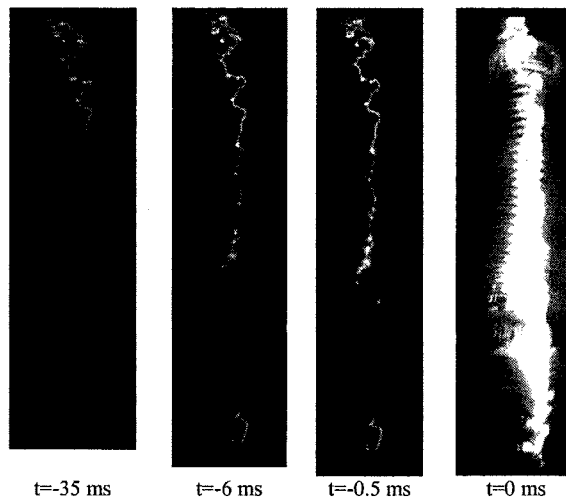


Figure 4.27. Flashover process of post insulator under DC-.

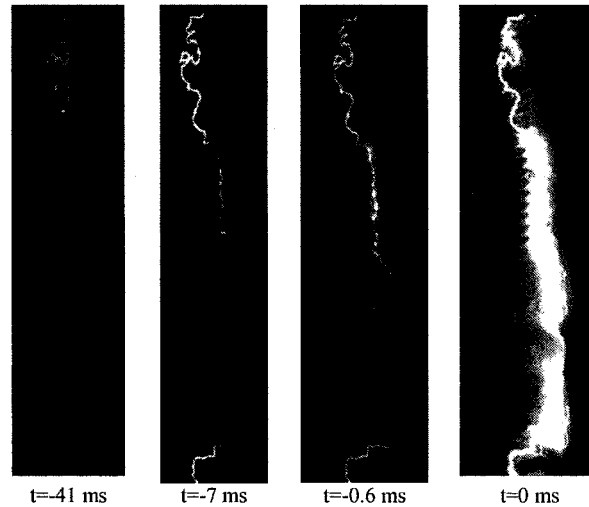


Figure 4.28. Flashover process of post insulator under AC.

4.4.1. Arc propagation velocity on the ice surface

Previous researches, mainly on short scale insulators, have shown that the arc propagation process may lead to flashover in two stages [103], [120]. However, it can be observed from the arc propagation process on long scale insulators, recorded by high speed camera, that the arc propagation process is completed in three stages, as shown in Figure 4.29. The first stage starts at the moment a violet arc is established with an initial length of about 7% of insulator length, (corresponding to the air gap length), and ends when the arc length reaches about 40% of insulator length. In this stage, the arc extends relatively slowly.

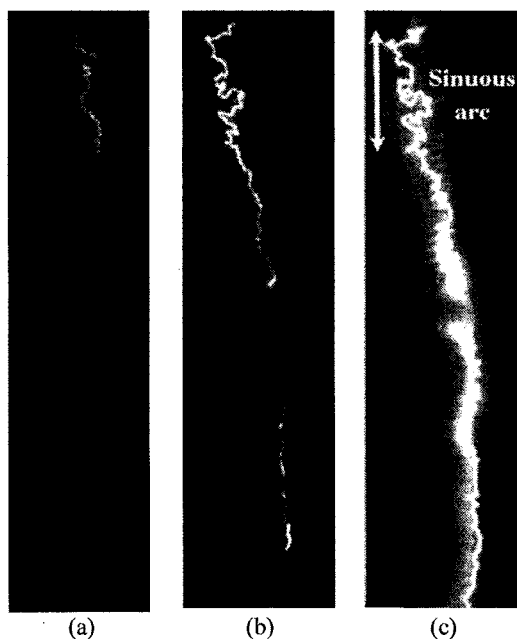


Figure 4.29. Ice-covered insulator flashover sequence; (a): first stage, (b): second stage, (c): last stage.

The second stage corresponds to an arc length extending from 40% to 80% of insulator length. In this stage, the arc propagation velocity increases suddenly. The arc at the final stage (final jump) is related to flashover occurrence at the moment it reaches its maximum length, which occurs considerably faster than at the previous stages. Under AC conditions, the local arc extinguishes and re-ignites at each cycle of the applied voltage. However, the plasma does not disappear instantly because the time constants for plasma decay are usually not negligible at the scale of the other durations involved in the phenomenon [132]. Arc propagation observations show that the arc path on an ice surface is relatively straight whereas it is sinuous across the sections free of ice. Figure 4.29c shows the sinuous path of propagation of an arc through air along an insulator surface which has a sinuous path. Based on digital high-speed image recording techniques, arc propagation velocities at different water conductivities, under DC and AC voltages, are listed in Table 4.1. Arc propagation velocity is significantly influenced by water conductivity. The higher the water conductivity, the faster the arc propagation is. In addition, it can be seen that the velocity of a DC+ arc during the last stage is lower than that observed for

DC- and AC arcs, for a given water conductivity. This could also explain why flashover happens at lower voltage for DC- and AC than DC+.

Table 4. 1. Propagation velocities of AC and DC arcs.

Voltage type	$\sigma_w(\mu\text{s/cm})$	Arc velocity (m/s)		
		Stage 1	Stage 2	Stage 3
AC	80	0.58-2.96	218-272	984-1154
	150	0.54-3.12	415-446	1450-1857
DC+	80	0.45-2.74	215-242	867-1108
	150	0.47-2.84	413-461	1363-1533
DC-	80	0.52-2.87	204-232	1043-1384
	150	0.54-3.24	407-524	1674-2106

4.5. Volume flow rate and water film conductivity

Laboratory observations show that water film conductivity, at the first melting stage, has its highest value and then decreases gradually. In order to measure the water film conductivity, the methodology described in Chapter 3 was used. This method consists in recovering water resulting from the melting by a funnel which conveys it to a tray where several cups are stored, from where water conductivity is measured using a conductivity meter. Simultaneously, the variation of water film volume collected in cups as a function of time was measured. Therefore, a series of tests was performed on a post insulator to determine the thickness and the volume conductivity of the water film during flashover occurrence. These experiments were carried out on a 172.6 cm arc length insulator with water conductivities of 30, 80 and 150 $\mu\text{S/cm}$ under different voltage polarities and types. The variation of water film conductivity measured by this method under DC+, DC- and AC voltages are respectively shown in Figures 4.30, 4.31 and 4.32. The measurements show that the water film conductivity depicts its highest value at the first melting stage, and then decreases gradually.

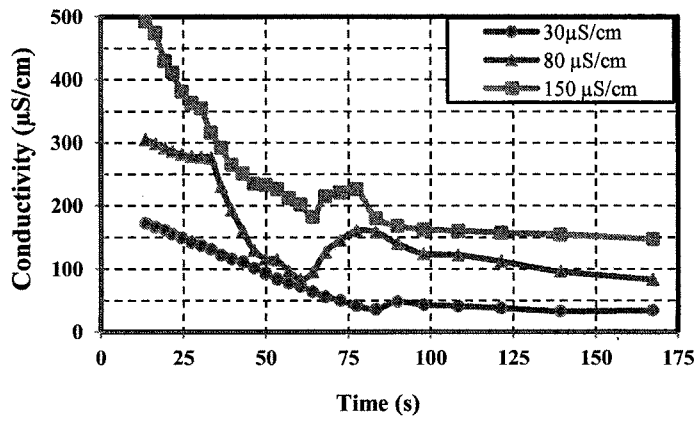


Figure 4.30. Variation of water film conductivity under DC+.

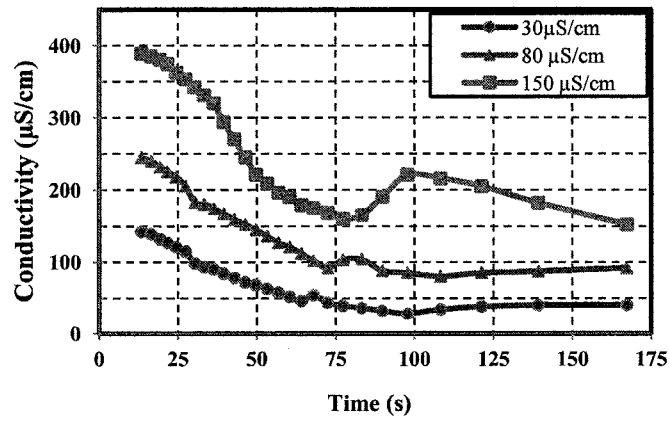


Figure 4.31. Variation of water film conductivity under DC-.

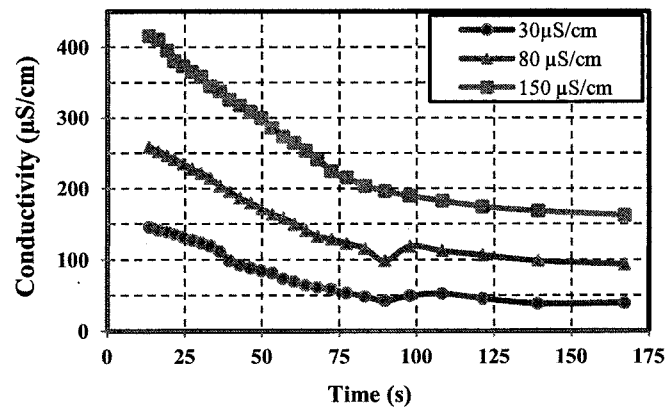


Figure 4.32. Variation of water film conductivity under AC.

The high conductivity of the water film is caused by the rejection of impurities - non-volatile and insoluble in ice - from the solid portion of the ice towards the surface during the solidification and freezing processes [19], [25]. As salt is removed from the ice surface by the water film flow during partial arc and flashover occurrence, the conductivity decreases gradually to a very low level. It is to be noticed that for each flashover test performed under the same experimental conditions, the dripping water conductivity presents a similar evolution. It can be observed that the electric activity before the establishment of the white arc are not hot enough to produce enough melted water for conductivity measurement. It was observed that the small amount of water collected at that moment came from the upper part of iced insulator (close to HV electrode). During the flashover tests, the arc heats the ice and melts it rapidly. This process is similar to natural melting: the part of the ice containing more salt melts first and flashover occurs when the surface conductivity reaches its maximum value. This later decreases gradually to a very low level compared with the conductivity of freezing water. The experimental results show that the range of dripping water conductivity is 3 to 12 times greater than the freezing water conductivity, depending on the measuring point along the insulator. This is in agreement with what was previously measured by Farzaneh and Melo [25]. Once flashover occurs, the volume flow rate, which is at its maximum value, decreases gradually in a short delay to nearly zero as shown in Figure 4.33. The reduction of the flow rate may be explained by the disappearance of the flashover heat source. Furthermore, the surrounding temperature of ice-covered insulator is too low to melt the remaining ice.

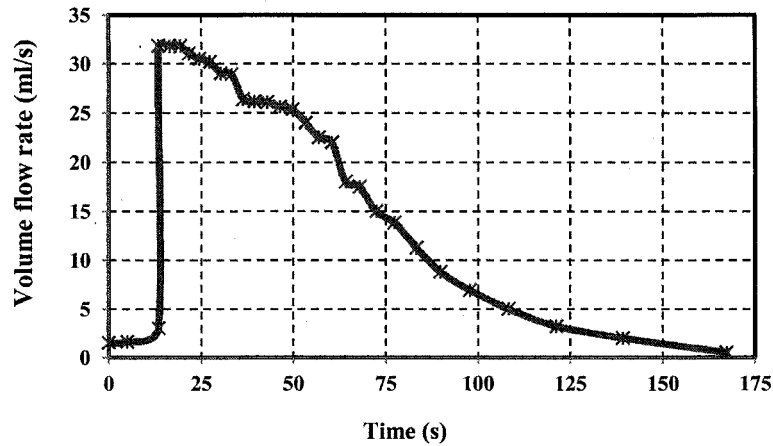


Figure 4.33. Volume flow rate of water film.

4.6. Discussions

4.6.1. Effect of voltage polarity on minimum flashover voltage

The experimental results showed that for a given experimental condition the minimum flashover voltage was highest when the voltage was positive. The ratio of positive-to-negative flashover voltage varied from 1.10 to 1.25. The asymmetry of results between positive and negative voltages is interesting since it implies a difference in insulation requirements for the two poles of a DC line. The polarity effect in the maximum withstand voltage of an ice-covered insulator is likely to be caused by the different characteristics of the partial arcs in each polarity. Hence, the investigation of the partial arcs structures under positive and negative voltages can help in interpreting the difference between positive and negative arcs.

From the arc propagation, it was observed that the positive partial arc lies close to the surface [133] and is strongly cooled by the cold surface, resulting in a thin and hot arc column [134], [135]. In contrast to a positive arc, these bright spots in a negative arc are floating away from the surface. At a later time, the central part of a negative arc floats much higher than a positive arc [133]. An interaction exists between the conductive ice surface and the column of

the positive partial arc, which prevents the positive arc from floating. This interaction involves the motion of Na atoms from the surface into the arc column. Since on the ice surface contaminated with sodium chloride, light emitted from the arc column is solely from the Na atoms [136], [137], [138], and the luminosity of positive arcs are brighter than negative arcs. Therefore, more Na atoms may evaporate from the surface with positive arc than the negative arc, and transported into the channel by diffusion. The gradient of the Na density may attract the arc column close to the surface, because Na atoms supply electrons and raise air conductivity [134]. Hence, arc velocity under DC- is higher than under DC+, resulting in the higher maximum withstand voltage under DC+.

Arc propagation pictures reported in [139], [140] show that under positive DC voltage, the arc foot appeared branched and consisted of multiple small spots. Therefore, the discharge current entered the ice surface at more than one contact point. The added resistance - due to the current constriction - causes the additional voltage drop, increasing the flashover voltage under positive polarity [141].

Moreover, it is well recognized that in some circumstances arcs will spontaneously extinguish due to cathodic phenomena [142]. Such phenomena on the water surface could make the positive arc less stable than the negative arc and hence increase the positive flashover voltage.

Experimental results confirmed that the minimum flashover voltage under AC is lower than under DC+. The reason for this lower AC flashover voltage is because half the AC wave acts as an opposing pre-stress to the following half wave. Therefore the charge created on the surface of the solid insulator causes an enhancement in the electric field at both electrodes,

leading to a lower flashover voltage [143]. In the case of an AC arc, more investigations related to its arc roots structures are still required.

4.6.2. Effect of water film conductivity on arc velocity

An arc needs a high ionization degree at its tip and enough energy to heat it to plasma temperature and to compensate for heat losses [144]. During arc propagation, the energy is supplied to the arc channel by leakage current through the ice surface. Thus, the energy injected into the channel is determined by the ohmic resistance of the water film. The flow of leakage current over the surface is accompanied by Joule effect and the formation of a water film. This increases the conductivity and the leakage current that can increase the energy supply to the arc channel, thus accelerating its development in the later stages. Therefore, the higher the freezing water conductivity, the higher the arc velocity is. Additionally, the arc length growth was observed using the ultra high-speed camera and was found to fall within 60-80% of the total length of the insulator a few moments before flashover occurrence, independently of the initial air gap length. Furthermore, the measured arc propagation velocity during the whole process showed that the arc will reach its maximum velocity in the range of 1000 to 2000 m/s depending on the voltage type and freezing water conductivity.

4.6.3. Effect of freezing water conductivity and dry arc distance on maximum withstand voltage

The experimental results imply a noticeable decrease in the minimum flashover voltage with an increase in the freezing water conductivity (when below 100 $\mu\text{S}/\text{cm}$). For higher values

(above 100 $\mu\text{S}/\text{cm}$), the effect of the variation of this parameter is less significant. The flashover measurements showed that the lower the breakdown voltage along the air gaps is, the lower the flashover occurrence is. Moreover, for freezing conductivity higher than 100 $\mu\text{S}/\text{cm}$, ice surface is assumed to reach its required conductance to drop whole voltage across air gaps, while for low conductivity, the voltage distributes along the insulator's length. This may explain why the flashover voltage may not change significantly for high freezing water conductivity. The dry arc distance is one of the main factors affecting the number of partial arcs initiated from insulator surface. The experimental results indicate that the minimum flashover voltage increases slightly nonlinearly with an increase in insulator's dry arc distance. This is due to the fact that when the insulator length increases, free ice zones (air gaps) also increase. These added air gaps may change the real equivalent arc distances of an ice-covered insulator due to the addition of leakage distance because of the air gaps. Therefore, a slightly nonlinear relationship between the V_{MF} and arc distance could be seen.

4.7. Flashover results presentation using Icing Stress Product (ISP)

An important parameter, so far used as a flashover index, is the Icing Stress Product (ISP). The ISP ($\text{g}/\text{cm} \times \mu\text{S}/\text{cm}$) is the product of the ice layer weight (g/cm of dry-arc distance) and the conductivity of the melted ice layer ($\mu\text{S}/\text{cm}$) [24]. The weight of accreted ice per centimeter of dry arc distance (g/cm) was assumed to be four times the ice thickness (mm) on the reference cylinder [21]. Considering an ice thickness of 15 mm, an ice layer weight of 60 g/cm can be considered for the present work. Moreover, based on the ice layer conductivity measured at the CIGELE laboratory (UQAC), this value is fairly close to the applied water conductivity.

Based on the above-mentioned assumptions, the flashover stresses in kV per meter of dry arc distance versus the ISP in $\text{g/cm} \cdot \mu\text{S/cm}$ for different air gap configurations are shown in Figures 4.34 and 4.35 under DC+ and DC- respectively. As can be seen, the flashover stress decreases with increasing ISP.

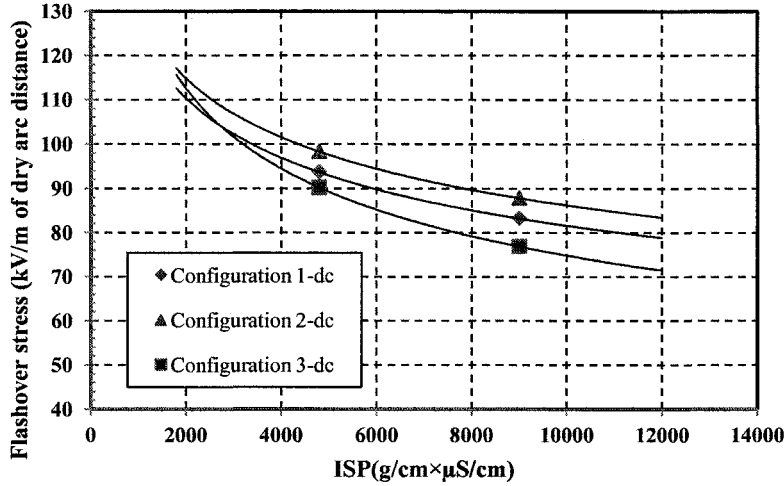


Figure 4. 34. DC Positive flashover stress versus ISP for different air gap configurations.

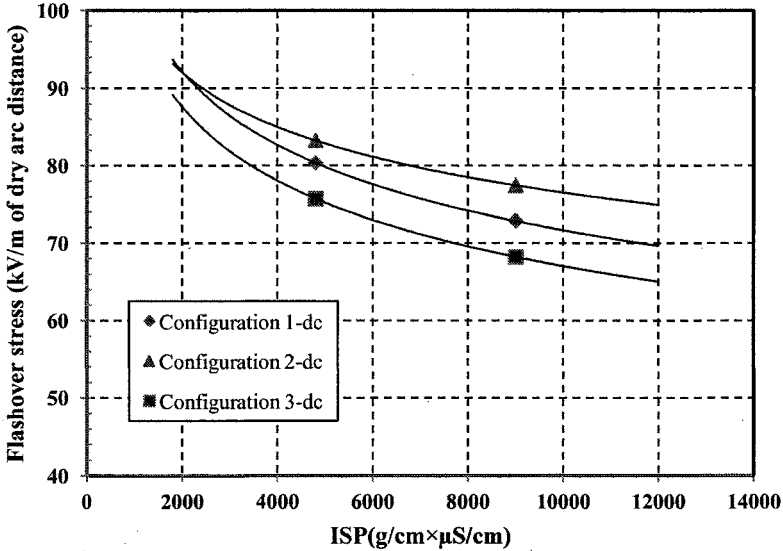


Figure 4. 35. DC Negative flashover stress versus ISP for different air gap configurations.

Figure 4.36 shows the AC flashover stress results as a function of the ISP for Configurations 3-dc and 1-ac respectively for dry arc distances of 173 and 275 cm. Similar flashover stresses could be seen for different dry arc distances.

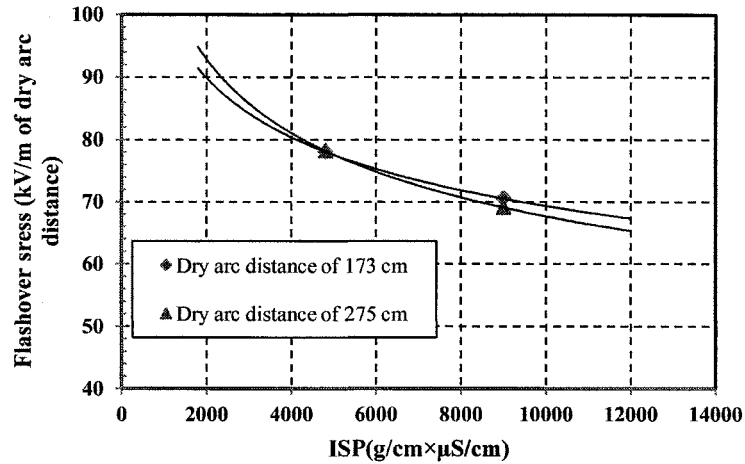


Figure 4. 36. Comparison of AC flashover stress versus ISP for dry arc distances of 173 and 275 cm.

The flashover stress results versus the ISP for different air gap configurations can be represented by following general equation.

$$E = A(ISP)^\alpha \quad (4.1)$$

Table 4.2 summarizes coefficients of A and α under AC and DC voltage with different air gap positions.

Table 4. 2. Coefficients of A and α in Equation (4.1)

Voltage	DC+			DC-			AC	
	1-dc	2-dc	3-dc	1-dc	2-dc	3-dc	3-dc	1-ac
A	458	444	775	302	220	310	414	306
α	-0.19	-0.18	-0.25	-0.15	-0.11	-0.16	-0.2	-0.16

4.7.1. Comparison of flashover results from different laboratories under icing conditions

As mentioned in Chapter 2, over the last years, problems due to ice accretion have necessitated some laboratory investigations. Due to the limitations in laboratory equipment, experimental results, in particular, flashover results are still insufficient to evaluate properly the performance of ice-covered EHV insulators. Moreover, because of different ice and pollution severity of each region, typical test conditions, evaluation methods as well as insulators have been used. Hence, flashover results from different laboratories are sometime hardly comparable. However, an attempt was made to compare the flashover results achieved from this research with those obtained from other laboratories.

The relations between flashover stress in kV per meter of dry arc distance, and ISP in ($\mu\text{S.g.cm}^{-2}$) were presented in Equation (4.1) using results from different laboratories. Table 4.3 summarizes the coefficients of A and α under AC and DC voltage for different test conditions.

Table 4.3. Coefficients of A and α in Equation (4.1)

	DC+	DC-	DC+ Farzaneh[24]	DC- Farzaneh[24]	DC Jiang[81]	DC- Shu[145]	AC	AC Farzaneh[24]	AC Jiang [146]	AC Shu[145]
A	534	272	400	340	1173.5	1831	355	396	2320.5	2376
α	-0.205	-0.145	-0.19	-0.19	-0.26	-0.3	-0.18	-0.19	-0.32	-0.314

From the relations obtained from several laboratory results (Equation (4.1) as per Table 4.3), the flashover stresses versus ISP are shown in Figure 4.37. The discrepancies between laboratory results can be related to the different test conditions.

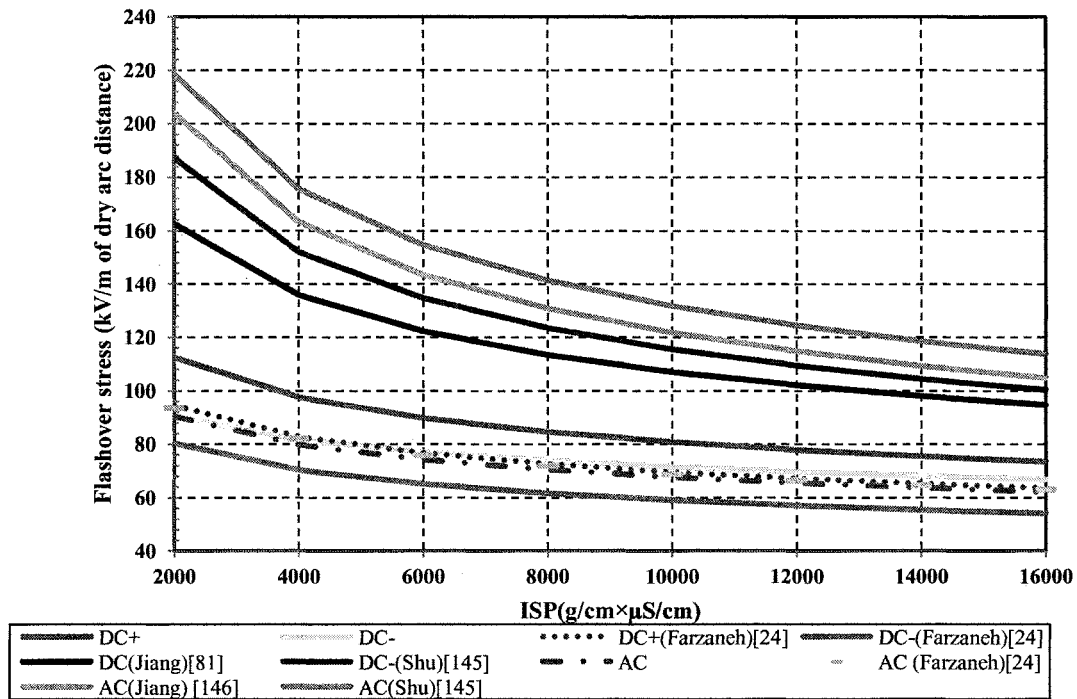


Figure 4. 37. Comparison of flashover stress obtained from different research.

Expressions of DC+, DC- and AC are related to relations achieved by the mean flashover stresses versus ISP of different air gap configurations. Farzaneh and Chisholm presented relations related to AC and DC maximum withstand stresses obtained from a short string of IEEE standard insulators under artificial wet-grown ice [24]. The average relationship between the DC flashover stress versus ISP for four types of insulators (porcelain, glass and two SIR specimens with different geometry) was presented by Jiang *et al.* using the icing-water conductivity method [81]. Jiang *et al.* [146] determined the relationship between the AC minimum flashover stress of an ice-covered insulator string including nine IEC standard suspension units and ISP as per the U-shaped curve method. A series of AC and DC flashover tests on porcelain, glass and composite insulators was carried out using melting regime method

by Shu *et al.* [145]. The relations between the flashover stress and ISP were extracted from AC and DC test results obtained from an insulator string of seven porcelain units.

4.8. Conclusion

A number of experiments were carried out in order to determine the minimum flashover voltage and record the leakage current on ice-covered post and line insulators under AC and DC voltages. The effect of two main parameters, freezing water conductivity and insulator length, on the minimum flashover voltage was investigated. Higher freezing water conductivity results were observed in lower minimum flashover voltages. The minimum flashover voltage increases with an increase in the insulator length. Also, the influences of the number and position of air gaps on the maximum withstand voltage of insulators under icing conditions were investigated. The results obtained might be helpful in designing HVDC insulators with high electrical performances under icing conditions. This may be achieved by controlling the number of air gaps with appropriate settings of corona rings or booster sheds.

Furthermore, a novel method was proposed to establish a linear relationship between the equivalent surface conductivity and the freezing water conductivity of an ice-covered post insulator during flashover. This method was based on a number of measurements, carried out to determine the flow rate and the volume conductivity of the water film through the ice surface.

Moreover, the effects of freezing water conductivity, which governs surface conductivity, on the arc velocity under AC and DC voltages were investigated. These results revealed

differences in the propagation processes of AC and DC arcs, which might explain the effect of voltage type and polarity on the minimum flashover voltage of an ice-covered insulator.

The icing stress product (ISP) was considered as a characteristic parameter to indicate the flashover performance of an ice-covered post insulator. In general, the flashover stress of an ice-covered insulator decreases with increasing the ISP.

Rapport-Gratuit.com

CHAPTER 5

MODELING OF AC AND DC FLASHOVER ON ICE-COVERED INSULATORS

CHAPTER 5

MODELING OF AC AND DC FLASHOVER ON ICE-COVERED INSULATORS

5.1. Introduction

Because of the limited facilities in laboratories, experimental investigations for determining the flashover performance of full scale ice-covered insulators under icing conditions are scarce and sometimes costly and time consuming. Therefore, the mathematical model appears as one of the most interesting ways to estimate the flashover behavior of ice-covered insulators. A detailed understanding of all aspects of the flashover process on ice-covered insulators is required in order to establish a dynamic model to predict the behavior of electric arc parameters during flashover occurrence. Such a task would essentially involve an examination of the main tenets of the physical, electrical, mechanical, thermal and thermodynamic aspects of flashover processes on ice surface.

The flashover on ice-covered insulators is still one of the most challenging problems of power systems in cold climate regions. To the best of our knowledge, the substantial study concerning basic phenomena occurring during the flashover of ice-covered insulators was pioneered by Farzaneh *et al.* [18], [22]. The flashover phenomenon over an ice surface generally takes place in three main stages. First, the appearance of water film on the ice surface and the initiation of corona discharges across the air gaps as shown in Figure 5.1a. Then, if the applied voltage is higher than V_{ws} , the local arcs can change within seconds to a white arc and extend along the ice surface as shown in Figure 5.1b. Finally, when the arc reaches a critical length

(about 60-80% of the insulator length), this may result in a complete flashover, shown in Figure 5.1c.



Figure 5.1. Different stages of arc development on an ice-covered insulator.

In this chapter, the parameters necessary to establish DC and AC dynamic models were introduced and, from these parameters, the currently available one-arc model was expanded to a two-arc dynamic model for both AC and DC voltages. Moreover, a novel approach to determine the equivalent surface conductivity is proposed based on fluid mechanics and the Navier-Stokes equations, as well as a series of experiments presented in Chapter 4 to measure the water film flow rate and conductivity. Finally, the relevant algorithm to predict the behavior of arc parameters during AC and DC flashover occurrences are established. The proposed improved models offer a great advantage over the currently available static or dynamic mathematical models as they constitute a powerful and accurate tool for predicting the flashover voltage of ice-

covered post insulators. Hence, such models might be used for selecting and dimensioning of HV and EHV insulators under different icing conditions.

5.2. Model description

Recall that the flashover of an ice-covered insulator is due to the initiation and development of local arcs across air gaps. This creates a situation similar to that of the flashover of a polluted insulator represented by an arc in series with a residual resistance consisting of an ice layer (which is not bridged by the arc). One of the first quantitative analyses of arcs on contaminated surfaces was carried out by Obenaus [108]. The same basic idea has been used to model arc propagation on iced insulators at CIGELE laboratory [32], [33]. The phenomenon is modeled by a simple electrical equivalent circuit consisting of an arc in series with an electrical resistance. The air gaps on the ice-covered insulators in series with the accumulated ice which have a relatively high surface conductivity, present situations similar to those of the dry bands in series with the wet parts of polluted insulator surfaces. In this model, the arc channel is assumed to be cylindrical with radius r and length x represented by a RLC electrical network, as shown in Figure 5.2. In order to describe the production of electrical charges, a capacitance is inserted in the model. When the arc propagates, the voltage and current waves initiated are described by [32], [33]:

$$V_{ap}(t) - V_c(t) - V_e = R_{arc}(x, t)I_{arc}(t) + L_{arc}(x, t) \frac{dI_{arc}(t)}{dt} \quad (5.1)$$

$$I_{arc}(t) = C(x, t) \frac{dV_c(t)}{dt} - \frac{1}{R_{ice}(x, t)} V_c(t) \quad (5.2)$$

where $R_{arc}(x, t)$, $L(x, t)$ and $C(x, t)$ represent respectively, arc channel resistance, inductance and capacitance between the arc tip and the opposite electrode capacitance. $R_{ice}(x, t)$ depicts the non-bridged ice-layer resistance, $V_{ap}(t)$ is the applied voltage, V_c is voltage drop across capacitance $C(x, t)$ and V_e , represents the voltage drop at the electrodes under DC voltage. Under AC voltage, this value (V_e) is negligible. The value of this latter for negative and positive arcs on the ice surface has been determined experimentally at 526 and 799 V respectively [31], [147].

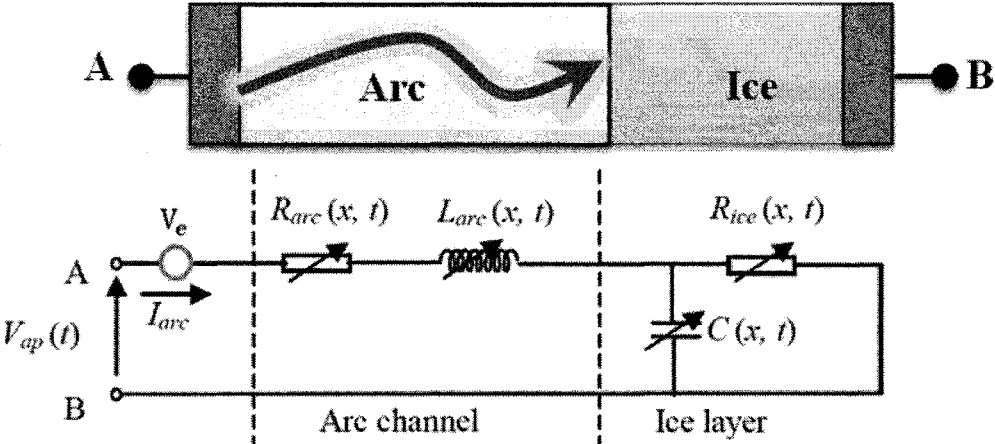


Figure 5.2. The basic equivalent circuit model of arc propagation on an ice-covered insulator surface.

5.3. The equivalent circuit components

The pertinent relationships for determining the circuit elements are essential to successful simulation and modeling. These relationships should reflect all known physical properties of the intervening/involved parameters. The electrical circuit used to calculate the arc parameters include some parts such as arc resistance, arc inductance, capacitance and ice resistance which can be introduced as follows:

5.3.1. Arc channel characteristics

The impedance of the arc, constituted of a resistance in series with an inductance and a capacitance in parallel with the ice resistance, should consider the electromagnetic aspects of the channel through which the current flows.

In order to determine arc channel inductance, a simplification already proposed for discharge in long air gaps modeling is used [148]. The inductance per unit length of the channel (H/m) L_{arc} is also given by:

$$L_{\text{arc}} = \frac{\mu_0}{2\pi} \left[0.25 + \ln \left(D_f / r \right) \right] \quad (5.3)$$

where D_f represents the distance far from the discharge axis at which the magnetic field is considered to be zero, μ_0 is the vacuum permeability and r is the arc channel radius (cm) calculated from Equation (5.4) [120]:

$$r = \sqrt{I / k\pi} \quad (5.4)$$

where I is the arc current (A). The parameter k has been previously determined by Farzaneh *et al.* [120] as 0.648 for DC+ and 0.624 for DC-.

The arc channel resistance is obtained from energy balance equations. In order to derive an expression which would connect the electrical conductivity of the channel with the electrical characteristics of the circuit, it may be assumed that the discharge occurs in such a short time that radiation and heat loss by conduction are negligible. Indeed, the arc channel, the so-called positive column, is a volume of normally non-linear ionized gas [132], [149]. The arc channel resistance, based on the energy balance equation, can be calculated using Mayr's equation [123].

$$\frac{1}{r_{\text{arc}}} \frac{dr_{\text{arc}}}{dt} = \frac{1}{\tau} \left(1 - \frac{r_{\text{arc}} I_{\text{arc}}^2}{P_0}\right) \quad (5.5)$$

where τ is the arc time constant which may be taken at 100 μs (for air) [150], [151], [152], P_0 is the heat conduction rate which, in this case, is 204.7(VA/cm) [86] and r_{arc} is the arc resistance (Ω/m).

The capacitance $C(x, t)$ between arc tip and the opposite electrode (F), which depends on the geometry of the system, is calculated using a spherical approximation, as shown in Figure 5.3 [153]:

$$C(t) = 2\pi\epsilon\alpha \left[1 + \left(\frac{r}{L-x}\right)\right] \quad (5.6)$$

with:

$$\alpha = 1 - 1/\sqrt{1 + \left[\left(\frac{\phi}{2L}\right)\left(\frac{1}{1-x/L}\right)\right]^2} \quad (5.7)$$

where ϕ represents the diameter of opposite electrode.

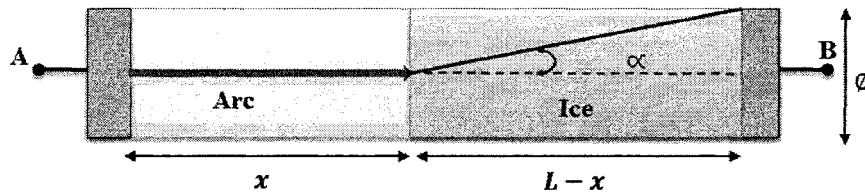


Figure 5.3. Capacitance of the rod and finite plane geometry [153].

5.3.2. Ice section characteristics

The reflection of ice section behavior in the electrical circuit is represented as the ice resistance. The resistance of the ice layer consisting of a thin conductive film of water is

calculated taking into account the insulator geometry and the constriction of current at the arc root. For a narrow ice band, where the width of the ice layer is less than its length, this resistance yields [114]:

$$R_{ice} = \frac{1}{2\pi\gamma_e} \left[\frac{\pi(L-x)}{w} + \ln\left(\frac{w}{2\pi r}\right) \right] \quad (5.8)$$

where w is ice layer width and γ_e is the equivalent surface conductivity.

Since ice is almost considered as a non-conductive material [121], the resistance of this part is mainly due to a thin water layer at the ice surface. If an axially symmetrical insulator is covered with a thin uniform conductive film of a constant thickness, the equivalent surface conductivity γ_e is equal to the product of equivalent water film conductivity σ_s and its equivalent thickness h , defined by [24]:

$$\gamma_e = h \cdot \sigma_s \quad (5.9)$$

Pervious investigations on the determination of surface conductivity resulted in a linear relationship between surface conductivity (γ_e) and the freezing water conductivity (σ_w) [31].

$$\gamma_e(\mu s) = \alpha \sigma_w \left(\frac{\mu s}{cm} \right) + \beta \quad (5.10)$$

where α and β are functions of voltage type and polarity.

The electrical surface conductivity, determined by equating the measured surface resistance and its analytical relationship, displays a relatively large standard deviation, from 10 to 50% [31]. Therefore, a relatively high error is expected in the flashover voltage prediction of long ice-covered insulators by the existing models.

Accordingly, a novel approach is proposed to establish a linear relationship between the equivalent surface conductivity and the freezing water conductivity of an ice-covered post insulator based on the measurement of the water film conductivity and flow rate during flashover occurrence, described in Chapter 4.

5.3.2.1. Electrical surface conductivity

The surface conductivity, γ_e at any point of an axially symmetrical insulator is covered with a thin uniform conductive film of a constant thickness h and constant conductivity σ_s , is defined by Equation (5.9). Hence, in order to derive Equation (5.9) under icing conditions, it is essential to determine water film thickness as well as water film conductivity during the melting process and flashover.

In order to determine the water film thickness, an approach similar to that used by Fox, based on fluid mechanics and Navier-Stokes equations, was applied [35]. It was considered that the water flow originates from the top of the vertical insulator and flows downward due to the gravity in a steady, developed and incompressible laminar flow as shown in Figure 5.4.

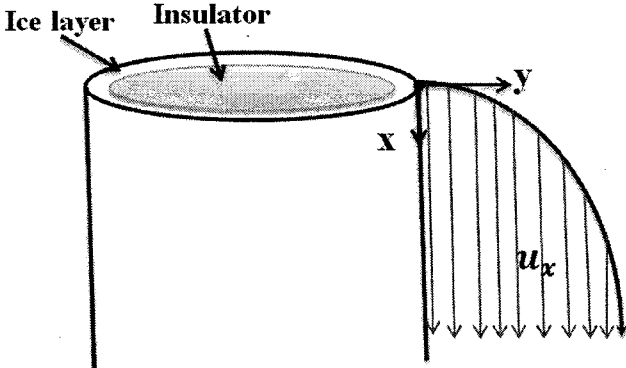


Figure 5.4. Laminar flow on an iced-covered vertical insulator.

According to continuity and Navier-Stokes equations, the governing equations written for incompressible flow with constant viscosity are as follows [35]:

$$\frac{\partial u}{\partial x} + \frac{\partial v}{\partial y} + \frac{\partial w}{\partial z} = 0 \quad (5.11)$$

$$\rho \left(\frac{\partial u}{\partial t} + u \frac{\partial u}{\partial x} + v \frac{\partial u}{\partial y} + w \frac{\partial u}{\partial z} \right) = \rho g_x - \frac{\partial p}{\partial x} + \mu \left(\frac{\partial^2 u}{\partial x^2} + \frac{\partial^2 u}{\partial y^2} + \frac{\partial^2 u}{\partial z^2} \right) \quad (5.12)$$

$$\rho \left(\frac{\partial v}{\partial t} + u \frac{\partial v}{\partial x} + v \frac{\partial v}{\partial y} + w \frac{\partial v}{\partial z} \right) = \rho g_y - \frac{\partial p}{\partial y} + \mu \left(\frac{\partial^2 v}{\partial x^2} + \frac{\partial^2 v}{\partial y^2} + \frac{\partial^2 v}{\partial z^2} \right) \quad (5.13)$$

$$\rho \left(\frac{\partial w}{\partial t} + u \frac{\partial w}{\partial x} + v \frac{\partial w}{\partial y} + w \frac{\partial w}{\partial z} \right) = \rho g_z - \frac{\partial p}{\partial z} + \mu \left(\frac{\partial^2 w}{\partial x^2} + \frac{\partial^2 w}{\partial y^2} + \frac{\partial^2 w}{\partial z^2} \right) \quad (5.14)$$

where u , v and w are the water film velocity in x , y and z directions respectively. Also, ρ , g and μ are the water density (kg/m^3), the acceleration of gravity (m/s^2) and the water viscosity (kg/m.s) respectively. Considering the above specified assumption and integrating the above-mentioned equations, the Navier-Stokes equations can be reduced to Equations (5.15) and (5.16), as follows.

$$0 = \rho g_x + \mu \frac{\partial^2 u}{\partial y^2} \quad (5.15)$$

$$0 = \rho g_y + \frac{\partial p}{\partial y} \quad (5.16)$$

where the gravity g is only in the x -direction, then:

$$\frac{\partial^2 u}{\partial y^2} = -\frac{\rho g}{\mu} \quad (5.17)$$

The single and double integral of Equation (5.17) yields:

$$\frac{\partial u}{\partial y} = -\frac{\rho g}{\mu} y + c_1 \quad (5.18)$$

$$u = -\frac{\rho g y^2}{\mu 2} + c_1 y + c_2 \quad (5.19)$$

Considering two boundary conditions, the zero-shear stress condition at the liquid free surface and the zero-water film velocity at $y=h$, the velocity profile can be obtained as:

$$u = \frac{\rho g}{\mu} \left(hy - \frac{y^2}{2} \right) \quad (5.20)$$

The volume flow rate over an ice-covered insulator can be calculated as:

$$Q = \int_0^h u b dy = \int_0^h \frac{\rho g}{\mu} \left(hy - \frac{y^2}{2} \right) b dy = \frac{\rho g W h^3}{\mu 3} \quad (5.21)$$

where W is the surface width in the z -direction. Thus, the water film thickness can be determined as follows:

$$h = \left[\frac{3\mu Q}{\rho g W} \right]^{1/3} \quad (5.22)$$

The variation of water film thickness based on Equation (5.22) is depicted in Figure 5.5.

Water film thickness during flashover occurrence is 0.36 mm.

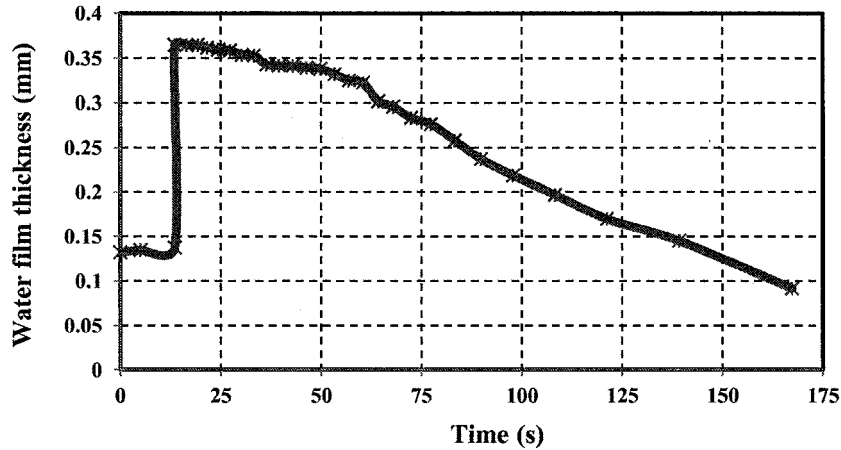


Figure 5.5. Water film thickness.

Based on Equation (5.9), the equivalent surface conductivity is equal to the product of the equivalent water film conductivity and its equivalent thickness. Based on this concept and the results obtained from experiments, the relationships between the equivalent surface conductivity, γ_e and the freezing water conductivity, σ_w under AC and DC voltages are as follows:

$$\gamma_e(\mu\text{s}) = 0.081\sigma_w \left(\frac{\mu\text{s}}{\text{cm}}\right) + 2.8 \quad \text{for AC voltage} \quad (5.23)$$

$$\gamma_e(\mu\text{s}) = 0.096\sigma_w \left(\frac{\mu\text{s}}{\text{cm}}\right) + 3.3 \quad \text{for DC+ voltage} \quad (5.24)$$

$$\gamma_e(\mu\text{s}) = 0.074\sigma_w \left(\frac{\mu\text{s}}{\text{cm}}\right) + 2.9 \quad \text{for DC- voltage} \quad (5.25)$$

Under DC+ conditions, the sensitivity of γ_e to σ_w is hardly greater than that under AC conditions. This is perhaps due to the fact that the heating effect of DC+ arcs is stronger than that of AC arcs [133].

5.3.2.2. Variation of water film thickness along the ice-covered insulator

To the best of our knowledge, less fundamental work has been done on the determination of the electrical surface conductivity dynamics along ice-covered insulators. Hence, the information related to the variation of water film thickness and surface conductivity along the insulator is helpful to further our knowledge on the process of arc propagation over ice surfaces.

There are not sufficient scientific contributions showing the non-uniformity of the voltage, leakage current, and temperature distribution along an iced-covered insulator surface. The first step towards studying and understanding these issues is to investigate the distribution of water thickness and its conductivity along an ice-covered insulator. It will therefore be assumed that the water film has a conical frustum shape instead of a cylindrical shape with the same volume. Figure 5.6 illustrates the geometry of an iced-covered insulator with uniform and non-uniform water films.

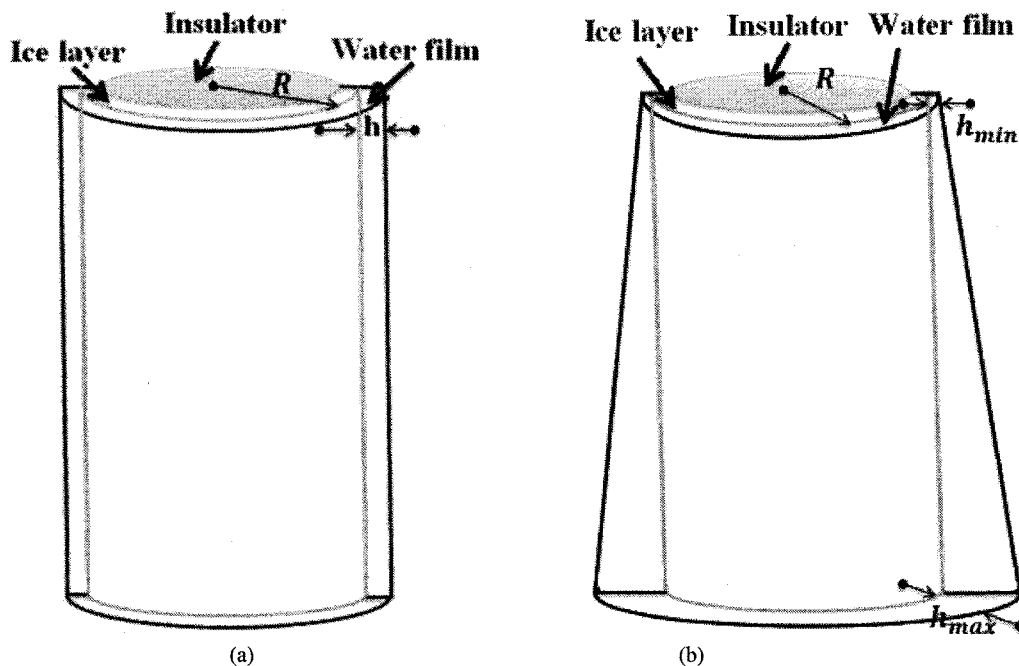


Figure 5.6. Water film on ice-covered insulator, (a): uniform water film, (b): non-uniform water film.

Based on the above mentioned assumptions, the following simplified mathematical relationship was derived to provide the thickness of a non-uniform water film along the insulator.

$$h_{\max}^2 + (3R + h_{\min})h_{\max} + (3Rh_{\min} + h_{\min}^2 - 3h^2 - 6Rh) = 0 \quad (5.26)$$

where h , h_{\max} , h_{\min} and R are uniform water film thickness, maximum water film thickness, minimum water film thickness and ice-covered insulator radius respectively. According to laboratory observations, the maximum water film conductivity at the upper part of the insulator is considered at the first stage of the water film collection from the ice surface before flashover occurrence. The measured values of h_{\min} under DC+, DC- and AC are 0.173 mm, 0.168 mm and 0.177 mm, respectively. The value of h_{\max} is calculated using Equation (5.26). Using two measurement points at the top and bottom of the insulator, the relations related to the variation of water film thickness and conductivity along insulator can be written as follows:

$$h(\text{mm}) = 0.0022L(\text{cm}) + 0.177 \quad \text{for AC} \quad (5.27)$$

$$h(\text{mm}) = 0.0022L(\text{cm}) + 0.173 \quad \text{for DC+} \quad (5.28)$$

$$h(\text{mm}) = 0.0023L(\text{cm}) + 0.168 \quad \text{for DC-} \quad (5.29)$$

In the same way, the variation in water film conductivity, σ_{film} , along the insulator was calculated based on Equation (5.9) as follows, (in the case of a freezing water conductivity of 80 $\mu\text{s/cm}$):

$$\sigma_{\text{film}} = \frac{9.28}{0.0022L(\text{cm})+0.177} \quad \text{for AC} \quad (5.30)$$

$$\sigma_{\text{film}} = \frac{10.98}{0.0022L(\text{cm})+0.173} \quad \text{for DC+} \quad (5.31)$$

$$\sigma_{\text{film}} = \frac{8.82}{0.0023L(\text{cm})+0.168} \quad \text{for DC-} \quad (5.32)$$

Recently, FEM methods have been based on approximate data of natural ice behavior without accounting for flashover conditions [92], [93]. Therefore, considerations of water film thickness and conductivity could be helpful in simulating real boundary conditions for ice-covered insulators.

5.3.3. Propagation criterion and arc velocity

Based on Hampton's investigations - in the case of a cylindrical configuration with practically constant resistance per unit length - an arc will propagate if the voltage gradient (kV/m) along the cylinder (water column in Hampton tests), E_{ice} , is higher than the voltage gradient in the arc column E_{arc} [15]:

$$E_{\text{arc}} < E_{\text{ice}} \quad (5.33)$$

The arc voltage gradient E_{arc} is given by [115]:

$$E_{\text{arc}} = AI^{-n} \quad (5.34)$$

where arc constants are $A = 208.9$, $n = 0.449$ for DC+ and $A = 84.6$, $n = 0.772$ for DC- [31].

E_{ice} , as a constant field, can be deduced simply by:

$$E_{\text{ice}} = \frac{R_{\text{ice}}I_{\text{arc}}}{L_f - x} \quad (5.35)$$

To determine the arc propagation velocity (m/s), a relation proportional to the discharge current, was established [154].

$$v(t) = \frac{I_{\text{arc}}(t)}{q_L} \quad (5.36)$$

where q_L is the average charge per unit length (C/m), considered constant for practical purposes [154].

$$q_L = \frac{1}{x} \int_0^t I_{\text{arc}}(t) \quad (5.37)$$

5.4. Two –arc model of flashover

Experimental investigations have shown that, in the case of post type insulators longer than 1 m, there usually were two or three arcs on the insulators in series with the residual ice layer [72]. For each of these arcs, there is one point on the ice layer where the current lines are concentrated. When this happens, flashover on an ice-covered post-type insulator should be described by the multi-arcs model. When two arcs form, as considered in this work, the phenomenon can be described by the model depicted in Figure 5.7a. In calculating the residual resistance, one should consider the current concentration at the two arc roots. This model can be equivalently split into two parts, as shown in Figure 5.7b. Based on the proposed simplified equivalent electric circuit (Figure 5.8), the equations introduced above may be modified and expressed as follows, considering that x_1 and x_2 are the lengths of the local arcs.

$$L_{\text{arc}}(x_1) = \frac{\mu_0}{2\pi} \left[0.25 + \ln \left(D_f / r \right) \right] \quad (5.38)$$

$$L_{\text{arc}}(x_2) = \frac{\mu_0}{2\pi} \left[0.25 + \ln \left(\frac{D_f}{r} \right) \right] \quad (5.39)$$

$$\frac{1}{r_{\text{arc}}(x_1)} \frac{dr_{\text{arc}}(x_1)}{dt} = \frac{1}{\tau} \left(1 - \frac{r_{\text{arc}}(x_1) I_{\text{arc}}^2}{P_0} \right) \quad (5.40)$$

$$\frac{1}{r_{\text{arc}}(x_2)} \frac{dr_{\text{arc}}(x_2)}{dt} = \frac{1}{\tau} \left(1 - \frac{r_{\text{arc}}(x_2) I_{\text{arc}}^2}{P_0} \right) \quad (5.41)$$

$$R_{\text{ice}}(x_1) = \frac{1}{2\pi\gamma_e} \left[\frac{\pi(L_1 - x_1)}{a} + \ln \left(\frac{a}{2\pi r} \right) \right] \quad (5.42)$$

$$R_{\text{ice}}(x_2) = \frac{1}{2\pi\gamma_e} \left[\frac{\pi(L_2 - x_2)}{a} + \ln \left(\frac{a}{2\pi r} \right) \right] \quad (5.43)$$

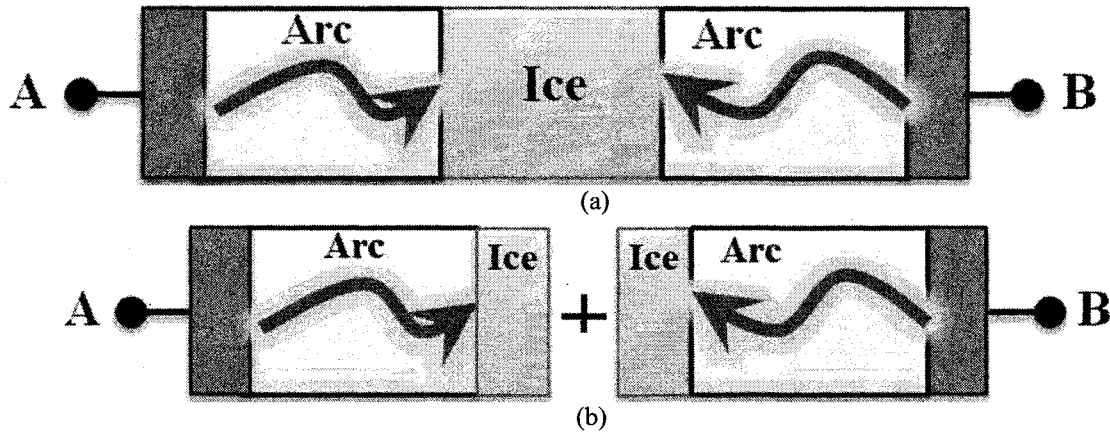


Figure 5.7. (a): two arcs model, (b): equivalent model for two arcs.

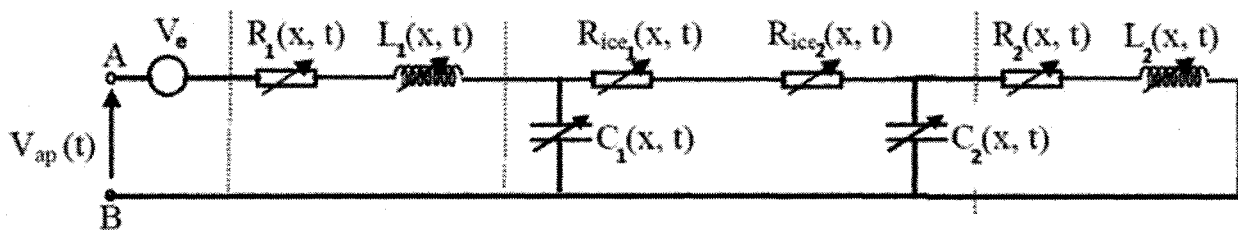


Figure 5.8. A simplified equivalent electric circuit.

In order to simplify the model, the capacitor C is neglected and all remaining components form a series circuit. Therefore, the equivalent resistance and inductance per unit length of arc channel can be written as follows:

$$R_{ice}(x) = R_{ice}(x_1) + R_{ice}(x_2) = \frac{1}{2\pi\gamma_e} \left[\frac{\pi(L-x)}{a} + 2 \ln \left(\frac{a}{2\pi r} \right) \right] \quad (5.44)$$

$$L_{arc}(x) = L_{arc}(x_2) + L_{arc}(x_1) = \frac{\mu_0}{\pi} \left[0.25 + \ln \left(D_f/r \right) \right] \quad (5.45)$$

5.5. General description of the proposed dynamic model

Figure 5.9 shows a simplified flowchart of the self-consistent time-dependent mathematical model proposed to predict DC and AC flashover. The input data are as follows: insulator geometry, ice layer characteristics and/or properties, applied voltage, and some initial values. The discharge time base is divided into steps dt (lower than the arc time constant) starting from $t = 0$.

At each time step, the critical conditions for continued propagation of the discharge are tested and, if they are satisfactory, the discharge continues to progress up to the final jump stage. Otherwise the arc extinguishes and flashover cannot take place. At this time, a new step is considered by increasing the applied voltage. The simulation is restarted again with initialization of the input data. At the time, when the two arc roots meet together - which corresponds to the case when the length of arc 1 plus that of arc 2 equals the arc distance of the insulator which can be expressed by Equation 5.46 - flashover will take place:

$$x_1 + x_2 \geq L \quad (5.46)$$

Under AC voltage, this moment happens at the peak value of the last quarter cycle ($T/4$, T being the period) [124] and so, velocity is adjusted to achieve a complete flashover at this time. Before this moment, while the surface conductivity is less than its critical value, the length of arc is considered constant and the current variation is due to the surface conductivity change, as well as to the arc resistance. Then, under the calculated value of flashover voltage, the simulation is repeated to calculate the parameters in the last stage. For each iteration, arc resistance and length are initialized.

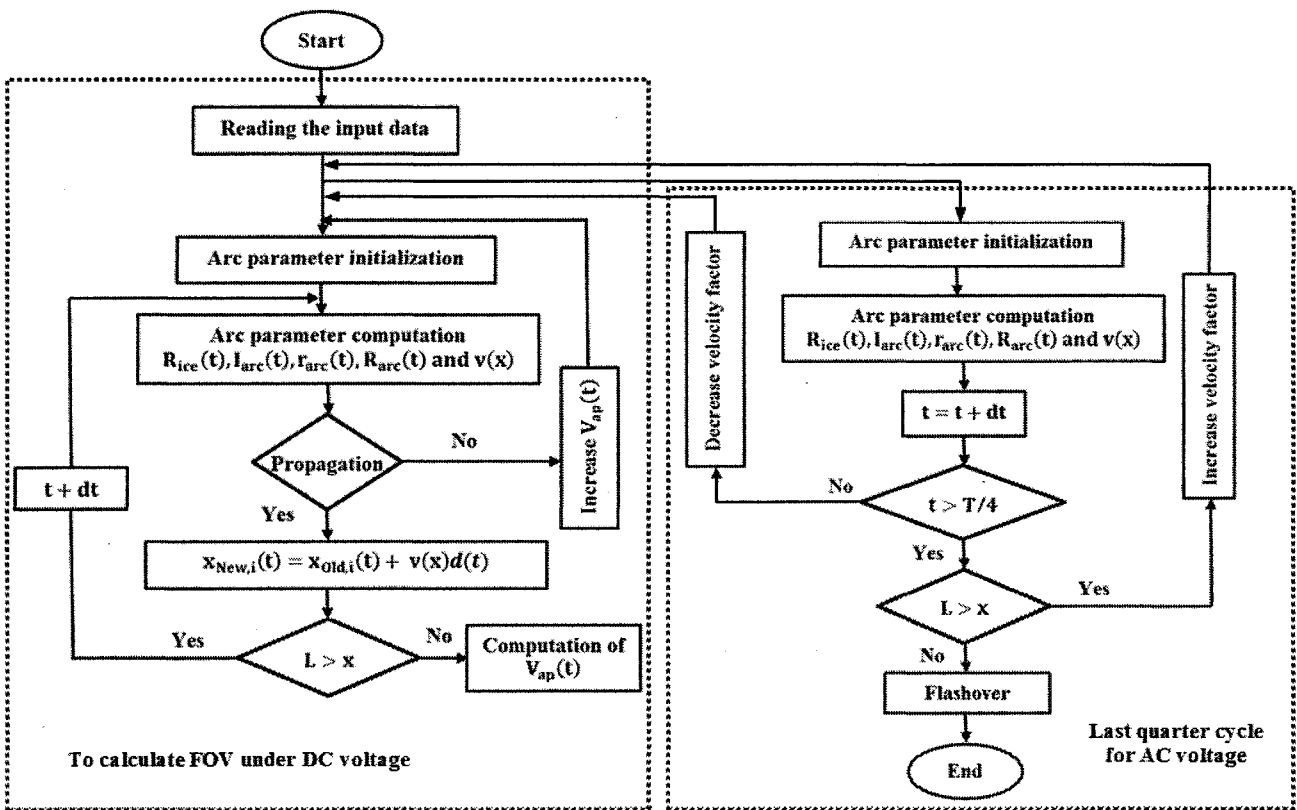


Figure 5.9. General flowchart of AC and DC modeling.

5.6. Conclusion

A self-consistent dynamic two-arc model allowing predicting the behavior of AC and DC arcs on ice-covered post insulators was proposed in this chapter. Based on an electrical equivalent circuit, a number of relationships were used or proposed to determine different variables involved in the arc phenomenon. The surface conductivity at the time of flashover was determined using a novel method based on fluid mechanics and Navier-Stokes equations as well as the measurement of the water film conductivity and flow rate of an ice-covered post insulator. This model makes it possible to determine not only the minimum flashover voltage (V_{MF}) but also some characteristics of the discharge, including temporal evolution of leakage current, arc characteristics and icing severity of the insulator. The model takes into account the variation of freezing water conductivity, insulator geometry, the ice layer characteristics, the applied voltage polarities and some fundamental concepts of air gap formation. This model may constitute a powerful tool for the selection of EHV and UHV insulators subjected to ice accretion.

CHAPTER 6

MODEL VALIDATION AND NUMERICAL SIMULATIONS

CHAPTER 6

MODEL VALIDATION AND NUMERICAL SIMULATIONS

6.1. Introduction

Flashover on an ice-covered insulator starts with the initiation of an arc which propagates along the ice surface. This is a situation similar to the flashover of a polluted insulator. Obenaus's model was developed to describe flashover under DC conditions [108]. Rizk added suitable criteria to adapt the model for AC flashover [151]. Laboratory investigations have shown that the Obenaus's model coupled with re-ignition conditions has proved to be accurate and adaptable to a wide range of ice surface flashover situations. A two-arc dynamic model, based on the Obenaus's concept, was elaborated to predict the behavior of AC and DC flashover on ice-covered post-type insulators in Chapter 5. In this chapter, the results predicted by the proposed model will be validated against experimental ones obtained using ice-covered post insulators, considering different lengths and freezing water conductivities under AC and DC voltages. In addition, in order to interpret the experimental results, the potential and electric-field distributions around an ice-covered post insulator, during a melting period, were determined under different air gap configurations using a Finite Element Method (FEM).

6.2. Validation of the equivalent surface conductivity mathematical model

The current AC and DC dynamic models were established based on the equivalent surface conductivity proposed by Zhang *et al.* [31]. Indeed, this empirical relation fitted the experimental data with a standard error of γ_e varying between ± 1 to ± 16 μs . Therefore, an inevitable discrepancy between simulated values and measured values is observed. Hence, in order to develop the current models, the equivalent surface conductivity obtained from the proposed method presented in Chapter 5 was applied. To verify the validity of this method, simulation results were compared to experimental ones obtained from a systematic study, including the influences of voltage type and polarity, freezing water conductivity, and insulator arc distance on minimum flashover voltage and leakage current.

Figures 6.1 to 6.4 illustrate the single-arc model performance when predicting leakage current as it occurs a few moments before complete flashover on an ice-covered post insulator, under DC and AC. When flashover occurred, leakage current increased up to several mA in a very short period and then suddenly increased rapidly. The results show that there is good agreement between the computed and measured leakage currents. This difference is probably due to either the random variation of some parameters such as arc propagation trajectory, complexity of ice flashover mechanism, or to some simplifications made in the modeling of the arc channel parameters. Moreover, under AC voltage, the frequency difference between simulated and measured AC leakage currents might be due to the data sampling frequency by the LabviewTM measurement system.

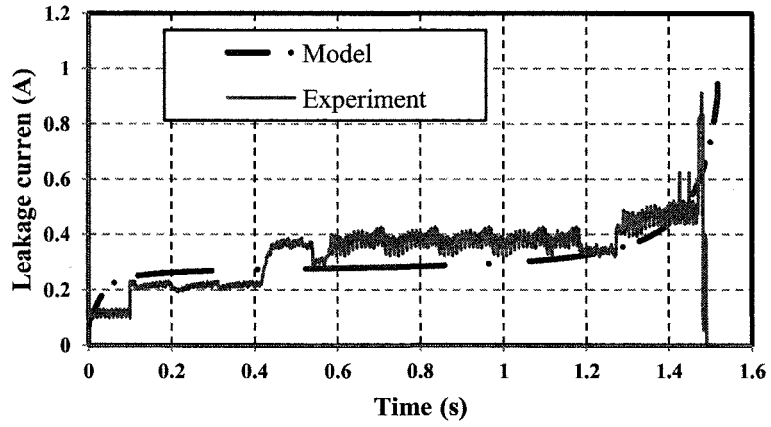


Figure 6.1. Comparison of the measured and computed leakage current of the positive arc with dry arc distance of 173 cm.

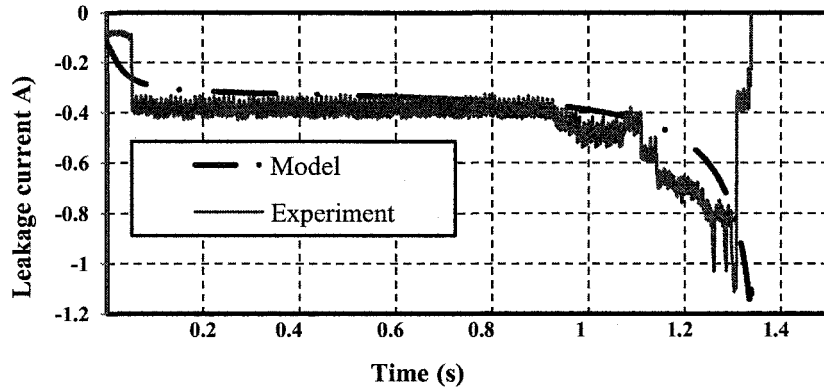


Figure 6.2. Comparison of the measured and computed leakage current of the negative arc with dry arc distance of 173 cm.

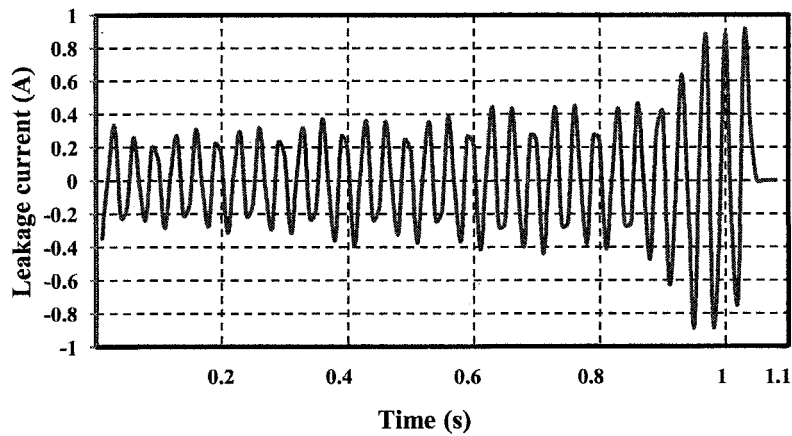


Figure 6.3. Measured leakage current of AC arc with dry arc distance of 173 cm.

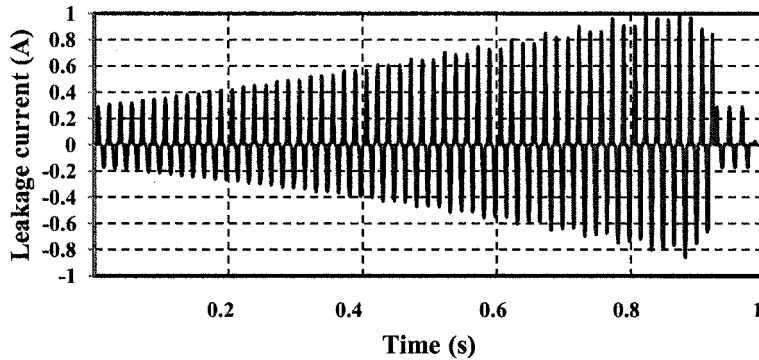


Figure 6.4. Simulated leakage current of AC arc with dry arc distance of 173 cm.

Figures 6.5 and 6.6 show the minimum flashover voltage values obtained by the single-arc dynamic model compared to experimental values from related to configurations 1 and 3, under DC+ and DC- voltages respectively. Two values of freezing water conductivity were considered, namely $80 \mu\text{S}/\text{cm}$ and $150 \mu\text{S}/\text{cm}$. The minimum flashover voltage decreased with increasing freezing water conductivity. From these results, it may be observed that there is a good degree of agreement between the minimum flashover voltage calculated from the model and the experimental ones. This may be due to the difference between the upper and lower arc velocities, as the model is based on the mean velocity of the arc.

The DC+ flashover voltage is predicted to be a median of 20% higher than the DC- level with the mathematical model, which compares well with the experimental values. This renders calculation of the DC- flashover voltage more important for engineering applications.

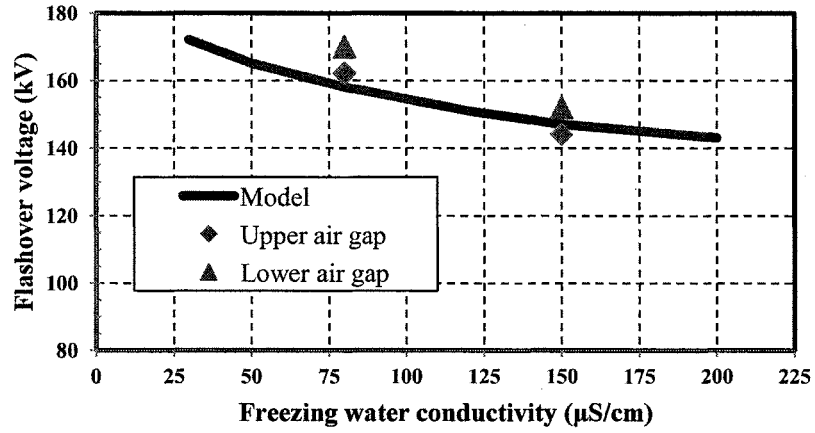


Figure 6.5. V_{MF} for different freezing water conductivities under DC+ with dry arc distance of 173 cm.

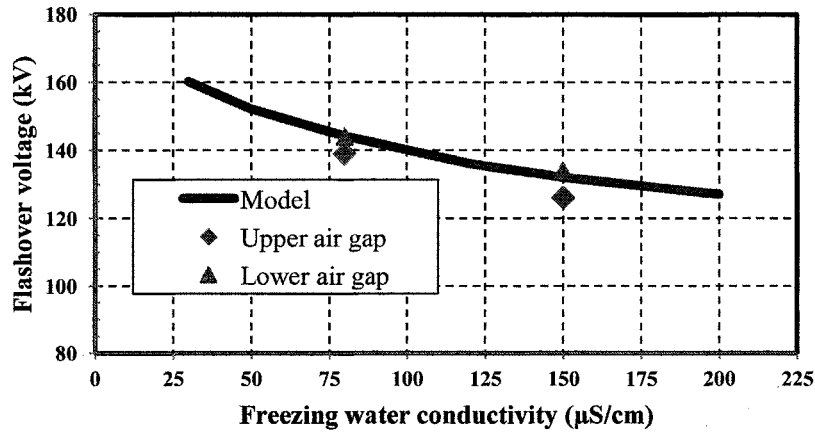


Figure 6.6. V_{MF} for different freezing water conductivities under DC- with dry arc distance of 173 cm.

Figure 6.7 shows the minimum flashover voltage values obtained by the one-arc dynamic model, compared to the values obtained from experiments under AC voltage. The minimum flashover voltage declines with increasing freezing water conductivity. Since the experiments under AC voltage were carried out for two air gap positions, (consequently two arc formations), there is an error in the computed flashover voltage based on the single arc model.

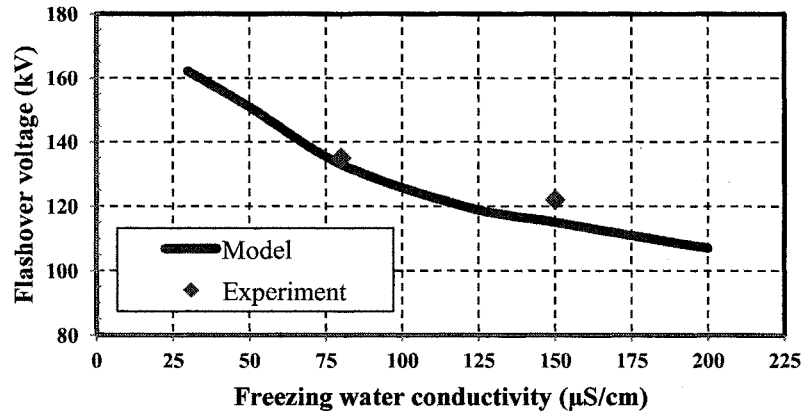


Figure 6.7. V_{MF} for different freezing water conductivities under AC with dry arc distance of 173 cm.

The experimental results were taken from [33] where a 103 cm post insulator was tested under uniform wet-grown ice. The simulated results of the variation in the minimum flashover voltage obtained with the proposed equivalent surface conductivity are not only in good agreement with the experimental results, but also with the results obtained by Tavakoli *et al.* [33] with their dynamic model (Figure 6.8).

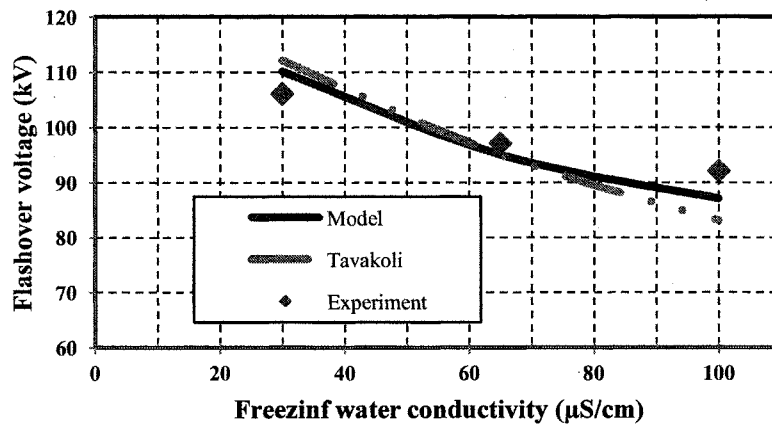


Figure 6.8. Calculated and experimental flashover voltages for different freezing water conductivities with dry arc distance of 103 cm.

6.3. Validation of the proposed two-arc model

Under EHV and UHV, long insulators such as post insulators with arc length/distance greater than 1 m are used. Under these conditions, voltage distribution is highly non-uniform, particularly after the appearance of icicles. Therefore, more than one air gap may be formed, causing a multi-arc initiation. In this case, it is required to expand the currently available single-arc model to a two-arc model for predicting the flashover voltage of ice-covered EHV and UHV insulators. To verify the validity of the proposed mathematical models, simulation results were compared to minimum flashover voltages and leakage currents recorded from experiments.

6.3.1. Validation of the DC two-arc model

In order to validate the simulation results from the proposed model depicted by the flowchart given in Figure 5.9, the experimental results of a two-air gap configuration under different freezing water conductivities were used. Figures 6.9 and 6.10 depict the comparison between computed values of the instantaneous arc propagation current, by the two-arc dynamic model, and those measured experimentally for both voltage types (DC+ and DC-).

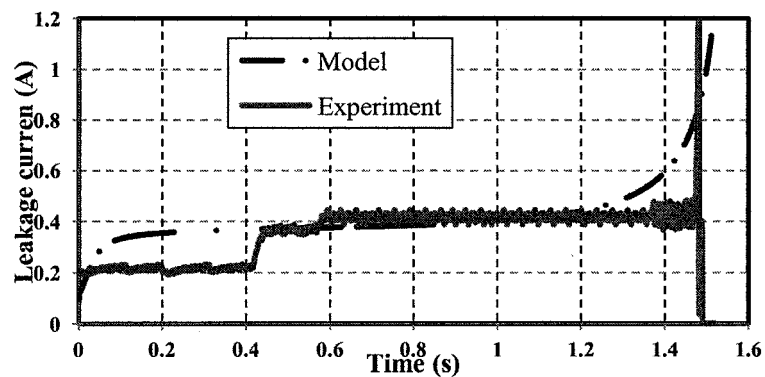


Figure 6.9. Comparison of the measured and computed leakage current under DC+ by two-arc model.

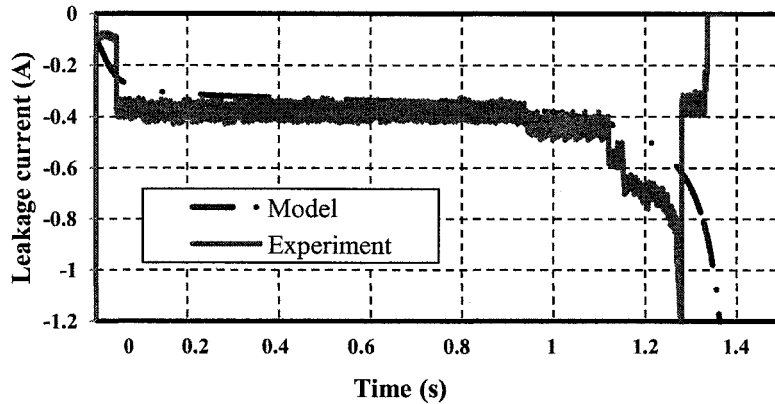


Figure 6.10. Comparison of the measured and computed leakage current under DC- by two-arc model.

It can be observed that the present model predicts leakage currents that agree satisfactorily with the experimental ones.

Figures 6.11 and 6.12 shows flashover voltages calculated by the two-arc dynamic model and the corresponding minimum flashover results for the ice-covered post insulators as a function of freezing water conductivity, under DC+ and DC- respectively. From these results, it may be observed that there is good agreement between the flashover voltages calculated from the developed model and the experimental results, with a maximum error of 5%.

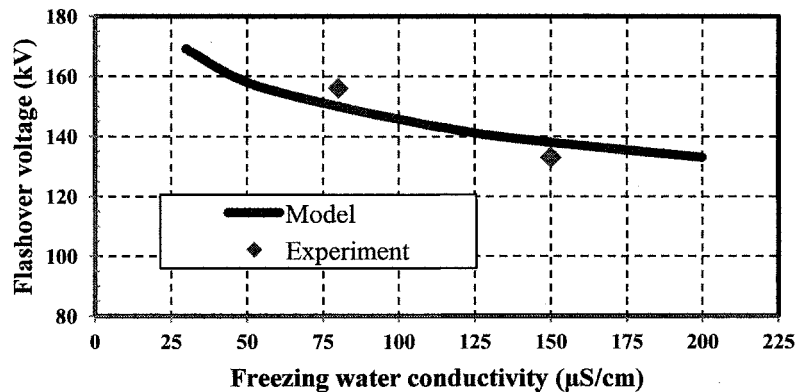


Figure 6.11. V_{MF} for different freezing water conductivities under DC+ with dry arc distance of 173 cm.

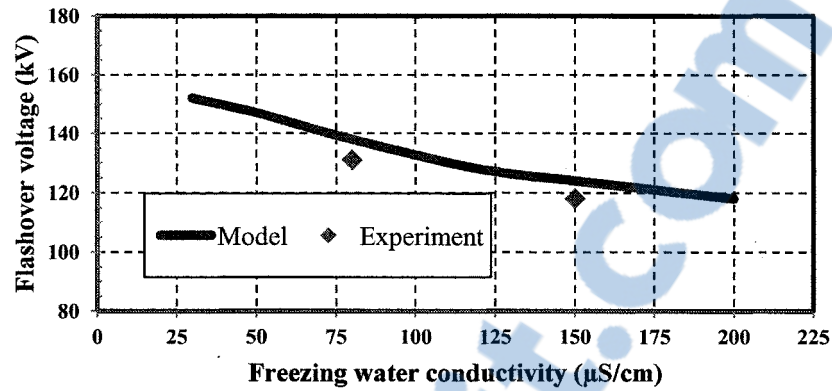


Figure 6.12. V_{MF} for different freezing water conductivities under DC- with dry arc distance of 173 cm.

6.3.2. Validation of the AC two-arc model

Figures 6.13 and 6.14 compare the minimum flashover voltage values, V_{MF} , obtained by the model, with those of the experiments. The error in the calculation is probably related to the assumption of a constant value for P_o in Equation (5.5), since this parameter showed a considerable variation related to variations in insulator lengths, and freezing water conductivities.

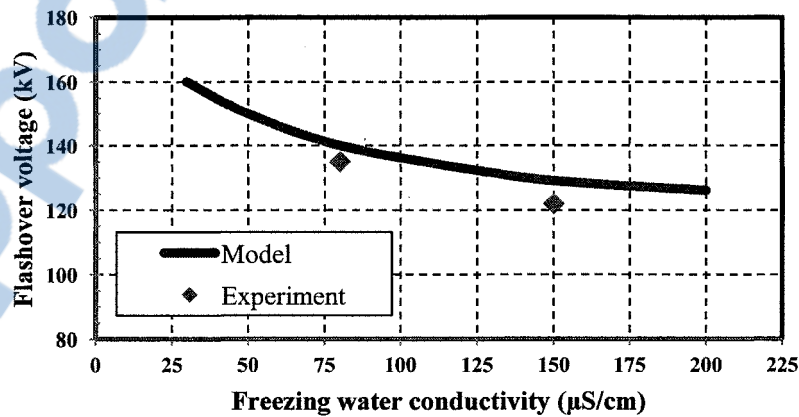


Figure 6.13. V_{MF} for different freezing water conductivities under AC with dry arc distance of 173 cm.

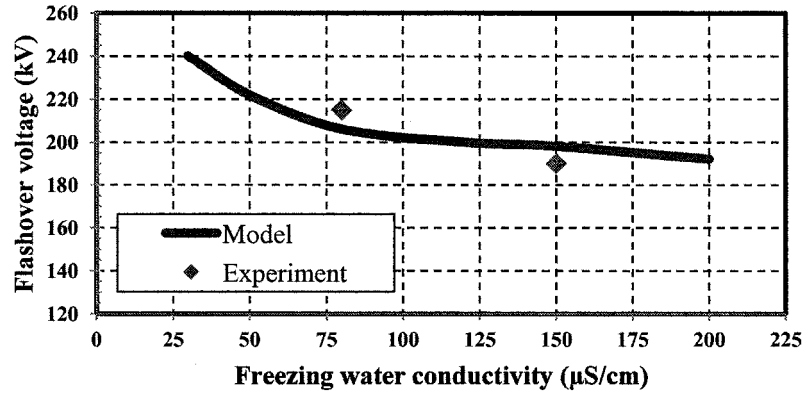


Figure 6.14. V_{MF} for different freezing water conductivities under AC with dry arc distance of 275 cm.

Figure 6.15 and 6.16 show the influence of dry arc distance on the minimum flashover voltage of a post insulator, uniformly covered with wet-grown ice. The experimental and simulation results compare well, thus validating the proposed two-arc model. It may be seen that the V_{MF} presents a slight non-linear increase with increasing arc distance.

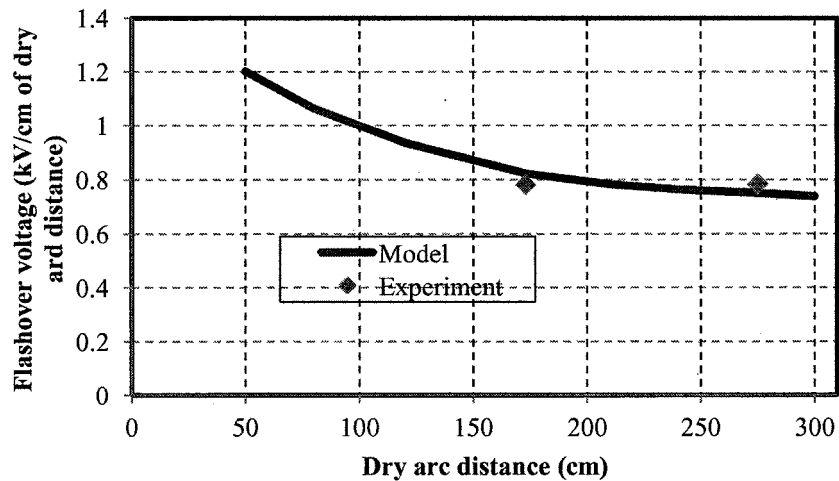


Figure 6.15. The calculated and experimental results for different dry arc distance under AC with $\sigma=80 \mu\text{S/cm}$.

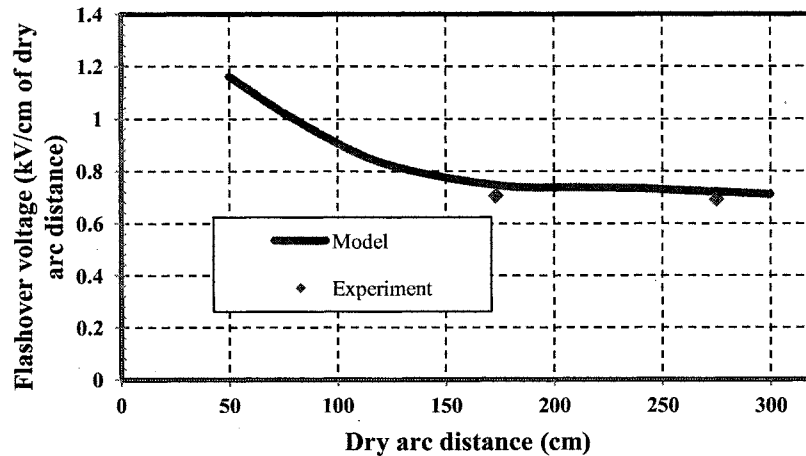


Figure 6.16. The calculated and experimental results for different dry arc distance under AC with $\sigma=150 \mu\text{S/cm}$.

6.4. Numerical simulations of potential and electric-field distributions along an ice-covered post insulator

Creating a water film on an ice surface can be achieved by increasing the ambient temperature or by thermal exchanges involving the stabilized arc burning on the ice surface. The high conductivity of a water film can cause a considerable voltage drop along air gaps [73] and, consequently, cause the formation of electrical arcs leading to flashover. Therefore, air gap position has an obvious effect on the flashover performance of ice-covered insulators.

In order to explain the experimental results, the electrical potential distributions along the three tested configurations under AC and DC voltages were numerically simulated. For this purpose, the commercial multi-physics software COMSOL was used. To reduce the characteristic complexity of the modeling, it was assumed that half of the insulator string surface was uniformly covered with ice, and also the water film forms along the ice surface with uniform thickness and conductivity. The simulation parameters are presented in Table 6.1. The



conductivities of the bulk ice, porcelain and air are ignored in the numerical simulations as they are not significant when compared to those of a water film on an ice surface.

Table 6. 1. Simulation parameters [155].

	Porcelain	Ice	Air	Water film
Relative permittivity	6	75	1	81
Conductivity (S/m)	0	0	0	0.013
Thickness (mm)	-	15	-	0.15

6.4.1. Potential distribution along the insulator under DC voltage

Figure 6.17 shows the distribution of equipotential lines for each simulated configuration under DC service voltage. The results related to the potential and electric field distributions obtained for the different ice configurations are presented in Figures 6.18 and 6.19 respectively. The simulation results indicate the presence of a highly conductive water film at the ice surface, leading to a high equipotential line concentration in the air gaps, especially for those close to the HV electrode, where a significant voltage drop is observed.

To investigate the effect of air gap positions and of the number of air gaps on the potential and the electric-field distributions, the voltage drop along the different air gaps - as observed during the melting regime - was calculated. The simulation was performed under a voltage gradient of 75 kV/m of arc distance. Equation (6.1) gives the breakdown voltage as a function of air-gap length, varying from 2 to 20 cm, as obtained in [92]:

$$V_b(\text{kV}) = 3.96 \times (\text{cm}) + 7.49 \quad (6.1)$$

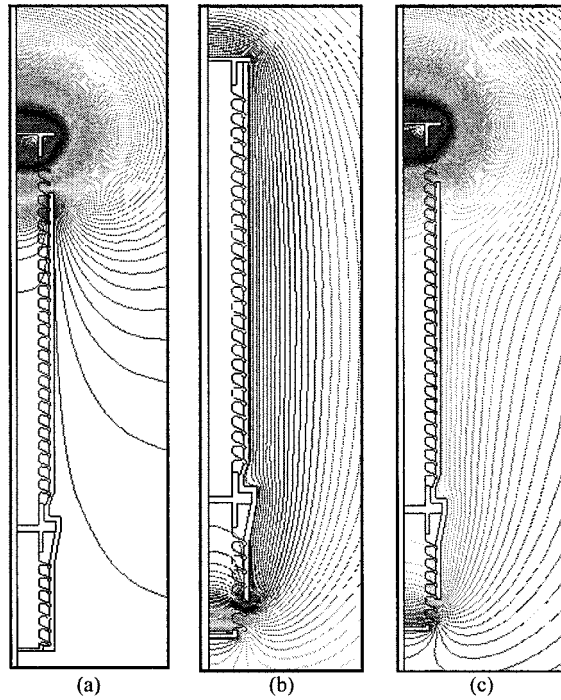


Figure 6.17. Equipotential lines distributions for a wet ice- covered insulator: a) upper air gap, b) lower air gap, c) lower and upper air gaps.

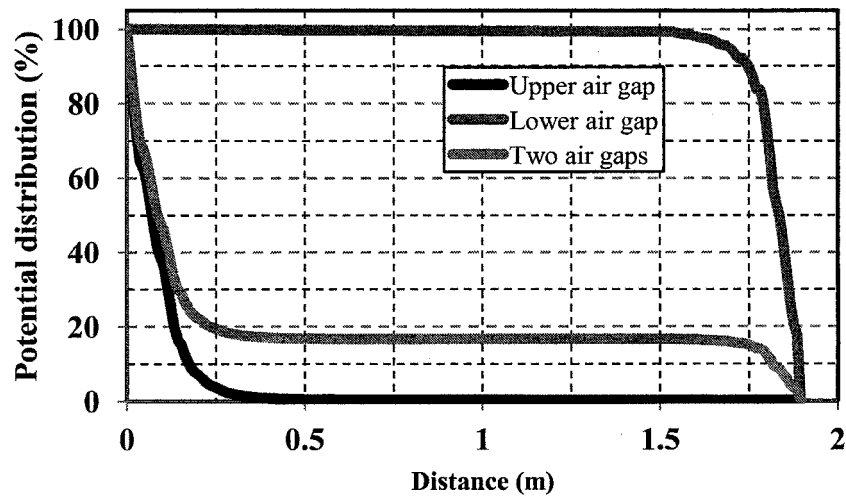


Figure 6.18. Potential distributions under DC voltage.

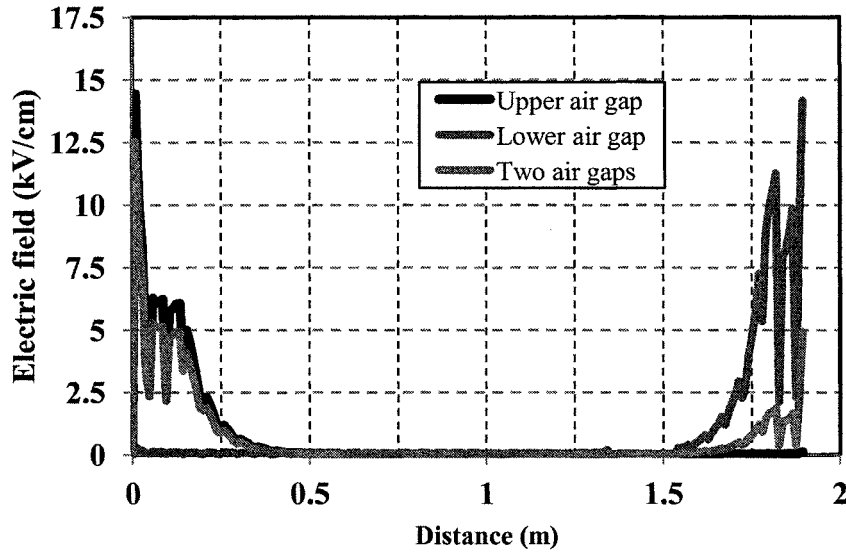


Figure 6.19. Electric field distributions under DC voltage.

The value obtained for V_b (48% of applied voltage) compared to the voltage drop values, as shown in Figure 6.18, confirms the presence of a partial arc along upper air gap in configurations 1-dc and 3-dc as well as lower air gap in configuration 2-dc. Therefore, the voltage drop is always greater along the air gap close to the HV electrode. This is due to the fact that, with an ice-free insulator, the potential distribution is not linear and presents a significant voltage drop along the first sheds close to the HV electrode. Hence, the breakdown voltage at the upper air gap occurs sooner than at the lower one. Under certain conditions, the partial arc will increase the extent of the water film on the insulator surface, which may cause the partial arc to spread over the ice surface and lead to flashover if the critical conditions are reached under lower voltage.

6.4.2. Potential and electric-field distributions along the insulator under AC voltage

In this numerical study, the effect of the number of air gaps on potential distribution along the ice-covered insulator under AC voltage was investigated. To achieve this goal, the three configurations of air gap location presented in Chapter 4 are considered. The distribution of equipotential lines for each simulated configuration is shown in Figure 6.20. Figures 6.21 and 6.22 show the simulation results of the potential and electric field distributions along the ice-covered insulator under the aforementioned configurations, respectively.

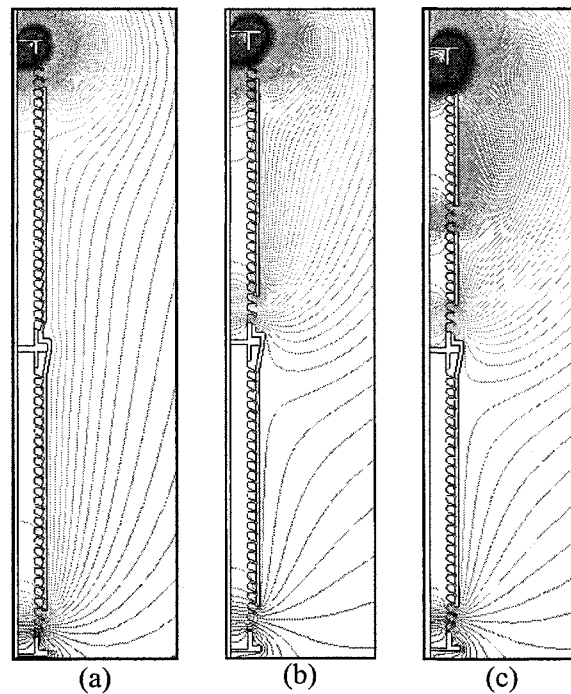


Figure 6.20. Equipotential lines distributions for a wet ice- covered insulator: a) 2 air gaps, b) 3 air gaps, c) 4 air gaps.

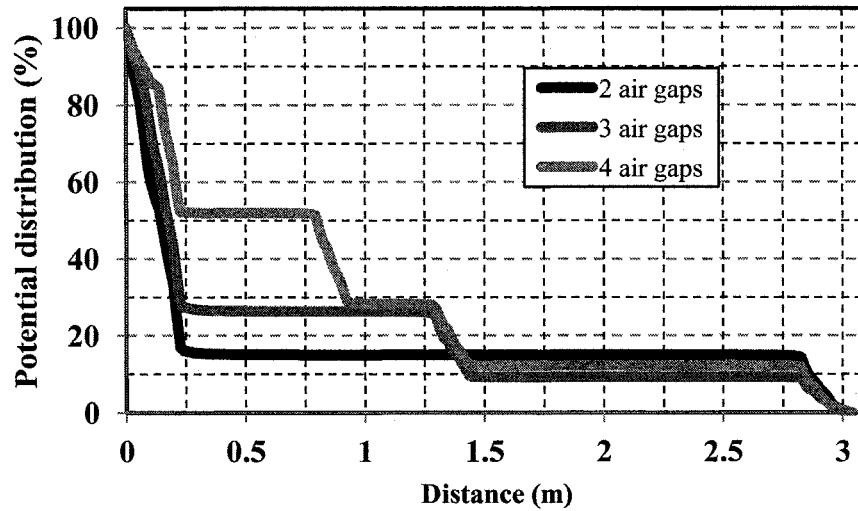


Figure 6.21. Potential distributions under AC voltage.

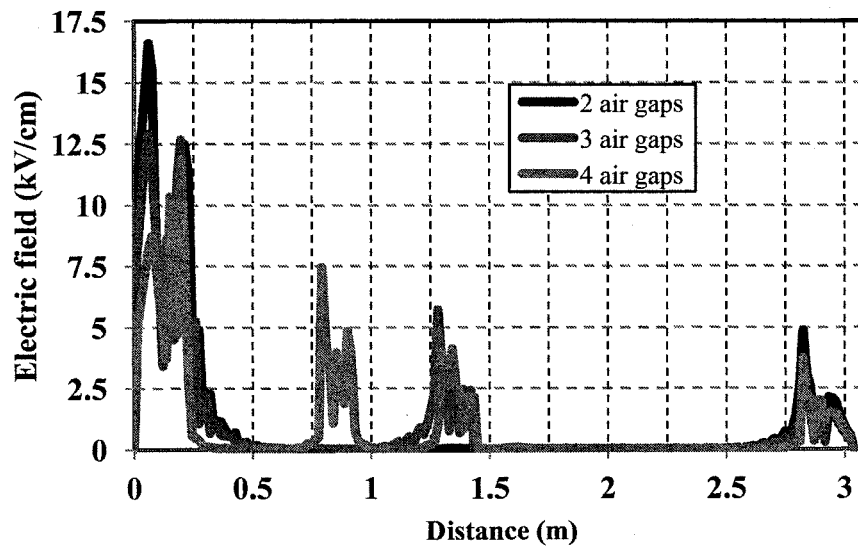


Figure 6.22. Electrical field distributions under AC voltage.

For each ice accretion, the total applied voltage, set at 200 kVrms, is almost distributed along the air gaps. This is due to the presence of the highly conductive water film at the ice

surface. Moreover, the simulation results confirm that the number of air gaps has a significant effect on the potential distribution along the ice-covered station insulator.

To verify the effect of the number of air gaps on the partial arc formation, the voltage drops are computed and summarized in Table 6.2. At first glance, the simulation results reported in Table 6.2 confirmed the fact that the presence of the water film at the ice surface considerably increases the voltage drop along the air gaps, which demonstrates the critical nature of the melting regime. Furthermore, since the air gap close to the HV electrode has the higher voltage drop, the voltage drop distribution is non-uniform. As shown in Table 6.2, it appears that the voltage drop along the upper air gap, close to the HV electrode, for all configurations increases above V_b (31.5% of applied voltage), which indicates that a partial arc can be initiated. The appearance of the partial arc along the upper air gap close to the HV electrode leads to a redistribution of the potential along the insulator. The voltage drop; V_{arc} along an arc with length X can thus be calculated using the following equation [93].

$$V_{arc}(kV) = 3.282 x(cm) \quad (6.2)$$

In this context, the partial arc across the upper air gap was taken into account in the numerical simulations in order to reevaluate the potential redistribution along the other air gaps. This redistribution of potential along the ice-covered insulator leads to partial arc appearance along the second air gap from the top of the insulator, for all configurations.

Table 6.2. Voltage drop along air gaps.

Configuration number	1-ac		2-ac			3-ac			
Air gap number	1	2	1	2	3	1	2	3	4
Voltage drop (%)	83.3	14.5	72.0	16.8	9.4	47.0	23.2	16.7	12.1

This redistribution suggests that about 75.5%, 52% and 35.5% of the applied voltage dropped along air gap 2 for configurations 1-ac, 2-ac and 3-ac respectively; which is higher than the breakdown voltage of the air gap. Therefore, the occurrence of a partial arc across the first air gap leads to the appearance of another partial arc across the second air gap for all configurations. In this case, a new redistribution of potential may be presented for configurations 2-ac and 3-ac, based on Equation (6.1). In the case of configuration 2-ac, an increase of about 28.5 % in applied voltage was noted along the third air gap after the occurrence of a partial arc across second air gap (Table 6.3). In this condition, the voltage drop across the third air gap from the top is higher than the breakdown voltage. Thus, third partial arc appears along this third air gap. On the other hand, for configuration 3-ac, the voltage drop across the third air gap as well as the last air gap, close to the grounded electrode, is lower than the corresponding breakdown voltage. Hence, in the case of configuration 3-ac, higher applied voltage is needed to initially breakdown the third air gap and possibly the last air gap. This explains why the highest V_{MF} value is obtained for this four-air-gap configuration.

Table 6.3. Voltage drop along air gaps after the formation of a partial arc along second air gap.

Configuration number	1-ac		2-ac			3-ac			
Air gap number	1	2	1	2	3	1	2	3	4
Voltage drop for redistribution 1 (%)	23.0	75.5	23.0	52.0	24.0	23.0	35.5	23.3	17.0
Voltage drop for redistribution 2 (%)	-	-	23.0	23.0	52.5	23.0	23.0	30.0	22.0

6.5. Conclusion

The two-arc model presented in Chapter 5 was compared to the experimental results of ice-covered EHV insulators obtained previously. As an application, this model was used to study the effects of some parameters on the minimum flashover voltage under different voltage types and polarities. The V_{MF} decreases with an increase in freezing water conductivity and increases with an increase in insulator dry arc distance. There was good agreement between the measured and calculated values of minimum flashover voltage and leakage current. The improved model appears to be a powerful tool for the design of outdoor insulators in cold climate regions.

Furthermore, axisymmetric numerical simulations using the Finite Element Method (FEM) to compute the potential distribution along the insulator and determine the partial arc appearance onset along each air gap were performed in this chapter. The simulation results show that the number and position of air gaps have substantial effects on the minimum flashover voltage of ice-covered insulators. In the three-air-gap configurations tested under DC voltage, the V_{MF} shows the lowest value when two air gaps appear at the top and bottom of the insulator. Also, it has the lowest value with configuration 2-ac when three air gaps were created at the top, bottom and middle of the insulator under AC voltage. Numerical simulations can be helpful in selecting the best booster sheds (BS) configuration under icing conditions.

CHAPTER 7

**CONCLUSIONS AND
RECOMMENDATIONS**

CHAPTER 7

CONCLUSIONS AND RECOMMENDATIONS

7.1. Concluding Remarks

A number of experiments based on different air gap positions were carried out under AC and DC voltages to examine the flashover performance of EHV insulators covered with ice. Also, a two-arc dynamic model was developed for predicting the AC and DC minimum flashover voltage of ice-covered insulators. Based on the results obtained from the present study, the following conclusions can be drawn.

- 1) Arc propagation over an ice surface was studied experimentally using high-speed video camera techniques. The key findings of the analysis are summarized below:
 - a) Photos taken from arc propagation over an ice surface showed three arc paths, in parallel, including the bulk ice, the water film layer and the air along the water film surface. Due to higher conductivity of water film compared to that of bulk ice and air, the major part of an arc propagates through water film surface.
 - b) The arc propagation process is completed in three stages. During the first stage, the arc length remains shorter than 40% of the total insulator length, the average arc velocity is low and voltage type as well as freezing water conductivity may not affect the propagation velocity. In the second stage, the arc length expands from 40% to 80% of the

insulator length while the arc propagation velocity increases rapidly. At the final stage, flashover is complete and the arc reaches its maximum velocity.

- c) The effect of freezing water conductivity, which governs surface conductivity, on the arc velocities under DC and AC voltages were investigated. As water conductivity is increased, more energy is injected into the arc channel, which accelerates the arc propagation. Thus, it could be concluded that the higher the water conductivity, the higher the arc velocity. Moreover, these results revealed that arc velocity under DC- is higher than DC+ and AC.
 - d) The critical arc length for flashover occurrence was measured and found to fall within 60-80% of the total length of the insulator, independently of the initial air gap length and position. This parameter can be considered as one of flashover criteria for arc modeling.
- 2) The number and position of air gaps have some obvious effects on the minimum flashover voltage of ice-covered insulators. In the three air-gap configurations tested in this study under AC and DC voltages, the minimum flashover voltage of the post insulator under icing conditions was examined.
- a) In the three air-gap configurations tested under DC, the V_{MF} showed the lowest value when two air gaps appeared at the top and bottom of the insulator. In fact, in the case of configuration 3-dc (one air gap at the top and one air gap at the bottom of the insulator), the local arcs have longer initial lengths and could get their critical lengths earlier than configurations 1-dc (air gap at the top of the insulator) and 2-dc (air gap at the bottom of the insulator). This could explain why the V_{MF} is higher for configurations 1-dc and 2-dc than for configuration 3-dc.

- b) In the three air-gap configurations tested under AC, the V_{MF} showed the highest value with the configuration including four air-gaps. Compared to configuration 1-ac (two air gaps), the local arc in the case of three air gaps, has a longer initial length and reaches its critical length sooner. Therefore, the V_{MF} is lower in the case of a configuration containing three air gaps rather than two air gaps. On the other hand, for configuration 3-ac (four air gaps), the voltage drops across third and last air gaps (at the bottom end of the insulator) are lower than the corresponding breakdown voltage. Hence, a higher applied voltage was required for configuration 3-ac in order to breakdown the third and last air gaps. Therefore, configuration 3-ac has the highest minimum flashover voltage.
- c) The results obtained are of great importance as they can help in improving the electrical performance of large insulators under icing conditions. This can be achieved by controlling the number of air gaps through the installation of booster sheds and corona rings on insulators.
- 3) Experimental results showed that the value of the minimum flashover and maximum withstand voltages obtained under DC+ are higher than those gotten under DC- and AC for different air gap configurations. The effect of polarity on the minimum flashover and maximum withstand voltages under these conditions is within 15-25% according to freezing water conductivity and insulator length. The polarity effect on the V_{MF} of an ice-covered insulator is likely due to different propagation mechanisms of the partial arcs under each polarity.

- a) Since arc propagation velocity under DC- is higher than that of DC+ and AC, arcs can reach their critical length for the final jump leading to flashover earlier. Therefore, flashover happens at a lower voltage level under DC- than under DC+ and AC.
 - b) Because of the branched foot of the positive arc, the discharge current penetrates the ice surface at several contact points. Therefore, the current constrictions cause added electrical resistances, which lead to additional voltage drops and increases the V_{MF} under positive polarity.
- 4) The effect of two main parameters; namely freezing water conductivity and insulator length on V_{MF} , was investigated. A higher freezing conductivity resulted in a lower minimum flashover voltage. Also, the minimum flashover voltage increased slightly non-linearly with an increase in the insulator length.
 - 5) The simulation results carried out with FEM-based software (COMSOL) showed that the high permittivity of ice, compared to that of air and porcelain, leads to a high equipotential line concentration across the air gaps, particularly for those close to the HV electrode. During a melting period, almost 98% of the applied voltage is distributed along the air gaps, regardless of their number and position.
 - 6) Under icing conditions, when the insulator is covered with a wet-grown glaze ice, the voltage distribution along the insulator is uneven. The simulation results showed that the presence of air gaps can improve voltage distribution resulting in an enhancement of the flashover performance of the ice-covered insulator.
 - 7) The formation of a partial arc across an air gap leads to a redistribution of voltage along an ice-covered insulator. Therefore, the presence of a partial arc along an air gap leads to the appearance of a partial arc along another air gap. Due to the fact that the number of

partial arcs is dependent upon the presence of air gaps, the flashover performance of an insulator covered with ice varies with the position and number of air gaps.

- 8) To compute the accurate value of ice resistance, a novel approach was proposed to establish a linear relationship between the equivalent surface conductivity and the freezing water conductivity of an ice-covered post insulator during flashover. This method was based on a number of measurements, carried out to determine the water film thickness and its conductivity as well as the development of mathematical models, taking into account the water film flow rate through the ice surface.
- 9) Due to the non-uniformity of the voltage, the leakage current and the temperature distribution along an iced-covered insulator, the formation of a water film on its ice surface was assumed non-uniform. Considering a conical frustum shape for the water film, the variation of its thickness and its conductivity along the insulator were calculated. Additionally, considerations of water film thickness and conductivity could be helpful in simulating real boundary conditions for ice-covered insulators.
- 10) Based on the experimental results, two-arc dynamic models, under DC and AC, were developed for predicting flashover parameters of ice-covered EHV insulators. The minimum flashover voltage values predicted by the model respond in an inherently cohesive manner to the variation of the main parameters such as the freezing water conductivity, the insulator length and voltage type. Higher insulator lengths and lower freezing water conductivities result in higher minimum flashover voltage. Good agreement was also observed between the flashover voltage calculated from the improved two-arc model and those obtained experimentally on EHV insulators.

11) The improved model is also a good basis for the development of multi-arc models and a powerful tool for the design and selection of EHV insulators subjected to ice accretion. Further studies concerning arc resistance measurements as a function of its temperature are needed to improve the present model for estimating arc parameters with higher accuracy.

7.2. Recommendations for future work

- 1) Due to the lack of DC flashover results on long insulators, a primary recommendation might involve re-adjusting the proposed model by carrying out several DC flashover tests on long post insulators under icing conditions.
- 2) Since long insulators are used for ultra-high voltage network, more than two arcs resulting from created air gaps can appear along insulators, leading to flashover. Hence, it is recommended to establish a multi-arc model to predict flashover behavior of ice-covered insulators precisely.
- 3) Experimental results show that air gaps have significant influences on flashover performance of ice-covered insulators. Hence, it is suggested to consider other air gap positions to achieve an optimized air gap configuration for each given insulator length. This might be helpful in selecting booster sheds positions.
- 4) In order to improve the flashover voltage of insulators under icing conditions, the assessment of flashover performance of insulators using existing alternatives, such as installation of booster sheds and corona rings along insulators under DC voltage, is recommended.

- 5) To complete the current model, the determination of the relationship between arc conductivity and arc temperature under icing conditions is suggested. In addition, to improve the equations related to the variation of water film thickness and its conductivity, measuring arc temperatures propagating through ice-covered insulators is recommended.

REFERENCES

- [1] M. Kawai, "AC Flashover tests at project UHV on ice-coated insulators," *IEEE Trans. Power App. Syst.*, vol. PAS-89, no. 8, pp. 1800–1804, Nov. 1970.
- [2] H. M. Schneider, "Artificial ice tests on transmission line insulators – A progress report," *IEEE/PES Summer Meeting, San Francisco, USA*, no. A75-491-1, pp. 347–353, 1975.
- [3] E. A. Cherney, "Flashover performance of artificially contaminated and iced long-rod transmission line insulators," *IEEE Trans. Power App. Syst.*, vol. PAS-99, no. 1, pp. 46–52, 1980.
- [4] M. D. Charneski, G. L. Gaibrois, and B. F. Whitney, "Flashover tests of artificially iced insulators," *IEEE Trans. Power App. Syst.*, vol. PAS-101, no. 8, pp. 2429–2433, Aug. 1982.
- [5] J. F. Drapeau and M. Farzaneh, "Ice accumulation characteristics on Hydro-Quebec H.V insulators," *6th Int. Workshop on the Atmospheric Icing of Structures, Budapest, Hungary*, pp. 225–230, 1993.
- [6] A. Meier and W.M. Niggli, "The influence of snow and ice deposits on supertension transmission line insulator strings with special reference to high altitude operations," *IEEE Conf. Publ. 44, London, England*, pp. 386–395, 1968.
- [7] Z. Vuckovic and Z. Zdravkovic, "Effect of polluted snow and ice accretion on high voltage transmission line insulators," *Proc. 5th Int. Workshop Atmospheric Icing Structures, Tokyo, Japan*, paper B4-3, 1990.
- [8] S. M. Fikke, J. E. Hanssen, and L. Rolfseng, "Long range transported pollutants and conductivity of atmospheric ice on insulators," *IEEE Trans. Power Delivery*, vol. 8, no. 3, pp. 1311–1321, Jul. 1993.
- [9] D. Wu and R. Hartings, "Correlation between the AC withstand voltage and insulator lengths under icing tests," *Proc. 9th Int. Workshop Atmospheric Icing Structures, Chester, U.K.*, p.6, 2000.
- [10] T. Fujimura, K. Naito, Y. Hasegawa, and T. Kawaguchi, "Performance of insulators covered with snow or ice," *IEEE Trans. Power App. Syst.*, vol. PAS-98, no. 5, pp. 1621–1631, 1979.
- [11] H. Matsuda, H. Komuro, and K. Takasu, "Withstand voltage characteristics of insulator strings covered with snow or ice," *IEEE Trans. Power Delivery*, vol. 6, no. 3, pp. 1243–1250, 1991.
- [12] L. Shu, C. Sun, J. Zhang, and L. Gu, "AC flashover performance on iced and polluted insulators for high altitude regions," *Proc. 7th Int. Symp. High Voltage Eng., Dresden, Germany*, pp. 303–306, 1991.
- [13] M. Farzaneh and J. Kiernicki, "AC and DC flashover performance of ice-covered insulators during a de-icing period," *Proc. of 5th Int. Workshop on the Atmospheric Icing of Structures, Tokyo, Japan*, Paper B-48, pp. 1–4, 1990.
- [14] M. Farzaneh, C. T. Baker, A. Bernstorff, K. Brown, W. a. Chisholm, C. de Turreil, J. F. Drapeau, S. Fikke, J. M. George, E. Gndt, T. Grisham, I. Gutman, R. Hartings, R. Kremer, G. Powell, L. Rolfseng, T. Rozek, D. L. Ruff, D. Shaffner, V. Sklenicka, R. Sundararajan, and J. Yu, "Insulator icing test methods and procedures a position paper prepared by the ieeee task force on insulator icing test methods," *IEEE Trans. Power Delivery*, vol. 18, no. 4, pp. 1503–1515, Oct. 2003.

- [15] B. F. Hampton, "Flashover mechanism of polluted insulation," *Proc. IEE*, vol. 111, no. 5, pp. 985–990, 1964.
- [16] S. Hesketh, "General criterion for the prediction of pollution flashover," *Proc. IEE*, vol. 114, no. 4, pp. 531–532, 1967.
- [17] J.S.T. Looms, "Insulators for high voltage," IEE Power Engineering Series 7, London, 1990.
- [18] M. Farzaneh and J.F. Drapeau, "AC flashover performance of insulators covered with artificial ice," *IEEE Trans. Power Delivery*, vol. 10, no. 2, pp. 1038–1051, 1995.
- [19] M. Farzaneh, "Ice accretion on high-voltage conductors and insulators and related phenomena," *Phil. Trans. Roy. Soc.*, vol. 358, no. 1776, pp. 2971–3005, 2000.
- [20] CIGRE Task Force 33.04.09, "Influence of ice and snow on the flashover performance of outdoor insulators, part I: Effects of Ice," *Electra*, vol. 187, pp. 91–111, 1999.
- [21] M. Farzaneh, J. T. Burnham, T. Carreira, E. Cherney, W. A. Chisholm, R. Christman, R. Cole, J. Cortinas, C. De Tourreil, J. F. Drapeau, S. Fikke, R. Gorur, T. Grisham, I. Gutman, J. Kuffel, A. Phillips, G. Powell, L. Rolfse, M. Roy, T. Rozek, D. L. Ruff, A. Schwalm, V. Sklenicka, G. Stewart, R. Sundararajan, M. Szeto, R. Tay, and J. Zhang, "Selection of station insulators with respect to ice and snow — Part I: technical context and environmental exposure," A position paper prepared by the IEEE Task Force on icing performance of line insulators, *IEEE Trans. Power Delivery*, vol. 20, no. 1, pp. 264–270, 2005.
- [22] M. Farzaneh and J. Kiernicki, "Flashover problems caused by ice build-up on insulators," *IEEE Electr. Insul. Mag.*, vol. 11, no. 2, pp. 5–17, 1995.
- [23] M. Farzaneh and I. Fofana, "Experimental study and analysis of corona discharge parameters on an ice surface," *J. Phys. D: Appl. Phys.*, vol. 37, no. 5, pp. 721–729, Mar. 2004.
- [24] M. Farzaneh and W.A. Chisholm, "Insulators for icing and polluted environments," IEEE Press series on Power Engineering, IEEE/John Wiley, New York, p. 680, 2009.
- [25] M. Farzaneh and O. T. Melo, "Properties and effect of freezing and winter fog on outline insulators," *J. Cold Regions Sci. Techn.*, vol. 19, no. 1, pp. 33–46, 1990.
- [26] M. Farzaneh, J. Zhang, and X. Chen, "Modeling of the AC arc discharge on ice surfaces," *IEEE Trans. Power Delivery*, vol. 12, no. 1, pp. 325–338, 1997.
- [27] I. Ndiaye, "Approche physique du développement de streamers positifs sur une surface de glace," Ph.D. dissertation, UQAC, 2007.
- [28] S. Farokhi, "Mechanisms of arc propagation over an ice surface," Ph.D. dissertation, UQAC, 2010.
- [29] M. Farzaneh and J. Kiernicki, "Flashover performance of IEEE standard insulators under ice conditions," *IEEE Trans. Power Delivery*, vol. 12, no. 4, pp. 1602–1613, 1997.
- [30] M. Farzaneh, J. Kiernicki, R. Chaarani, J. F. Drapeau, and R. Martin, "Influence of wet-grown ice on the AC flashover performance of ice covered insulators," *Proc. of 9th Int. Symp. on High Voltage Eng.*, Austria, no. 3176, pp. 1–4, 1995.

- [31] M. Farzaneh and J. Zhang, "Modeling of DC arc discharge on ice surfaces," *IEE Proceedings Gen. Trans. Dist.*, vol. 147, no. 2, pp. 81–86, 2000.
- [32] M. Farzaneh, I. Fofana, C. Tavakoli, and X. Chen, "Dynamic modeling of DC arc discharge on ice surfaces," *IEEE Trans. Dielectr. Electr. Insul.*, vol. 10, no. 3, pp. 463–474, 2003.
- [33] C. Tavakoli, M. Farzaneh, I. Fofana, and A. Beroual, "Dynamics and modeling of AC arc on surface of ice," *IEEE Trans. Dielectr. Electr. Insul.*, vol. 13, no. 6, pp. 1278–1285, Dec. 2006.
- [34] IEEE std 1783, "IEEE Guide for test methods and procedures to evaluate the electrical performance of insulators in freezing conditions," 2009.
- [35] R. W. Fox and A. T. McDonald, "Introduction to fluid mechanics," in in Fourth Edition, John Wiley and Sons, Inc., 1992.
- [36] M. Farzaneh and J. Zhang, "A Multi-arc model for predicting AC critical flashover voltage of ice-covered insulators," *IEEE Trans. Dielectr. Electr. Insul.*, vol. 14, no. 6, pp. 1401–1409, Dec. 2007.
- [37] I. Imai and Ichiro, "Studies on ice accretion," *Researches on Snow and Ice*, no. 1, pp. 35–44, 1953.
- [38] H. Oguchi et al., "Icing on electric wires," *Researches on snow and ice*, *Researches on Snow and Ice*, no. 1, pp. 45–49, 1953.
- [39] D. Kuroiwa, "Icing and snow accretion," *Monograph Series of Research, Institute of Applied Electricity, Japan*, pp. 1–30, 1958.
- [40] D. Kuroiwa, "Icing and snow accretion on electric wires," *U.S Army Cold Regions Researches and Engineering Laboratory, Research Report 123*, pp. 1–10, 1965.
- [41] M. Farzaneh and J. Kiernicki, "Flashover performance of ice-covered insulators," *Canadian J. Elec. Comp. Eng.*, vol. 22, no. 3, pp. 95–109, 1997.
- [42] M. Farzaneh and J. Zhang, "Behavior of DC arc discharge on ice surfaces," *Proc.8th Int. Workshop on the Atmospheric Icing of Structures, Iceland*, pp. 193–197, 1998.
- [43] M. Farzaneh, J. Kiernicki, and J. F. Drapeau, "Ice accretion on energized line insulators," *Int. J. Offshore Polar Eng.*, vol. 2, no. 3, pp. 228–233, 1992.
- [44] M. Faraday, "Experimental researches in chemistry and physics," *Royal Institution Discourse*, Taylor and Francis, New York, p. 496, 1859.
- [45] H. Gelin and R. Stubbs, "Ice electrets," *J. Chem. Phys.*, vol. 42, no. 3, pp. 967–971, 1965.
- [46] C. Jaccard, "Four-point method for measuring the volume and surface conductivities of a thin sample," *Z. Angew. Math. Phys.*, vol. 17, no. 6, pp. 657–663, 1966.
- [47] P.R. Camp, W. Kiszenick, and D. Arnold, "Electrical conduction in ice," *New York, Plenum Press*, pp. 450–470, 1969.
- [48] N. Maeno and H. Nishimura, "The electrical properties of ice surfaces," *J. Glaciol.*, vol. 21, no. 85, pp. 193–205, 1978.

- [49] J. M. Caranti and A. J. Illingworth, "Frequency dependence of the surface conductivity of ice," *J. Phys. Chem.*, vol. 87, no. 21, pp. 4078–4083, 1983.
- [50] V. F. Petrenko and R. W. Whitworth, "Physics of ice," Oxford University Press, USA, p. 373, 1999.
- [51] N.H. Fletcher, "The surface of ice," in *Physics and Chemistry of Ice*, Royal Society of Canada, Ottawa, pp. 132–36, 1973.
- [52] I. Golecki and C. Jaccard, "Intrinsic surface disorder in ice near the melting point," *J. Phys. C: Solid State Phys.*, vol. 11, no. 20, pp. 4229–4237, 1978.
- [53] D. Beaglehole and D. Nason, "Transition layer on the surface on ice," *Surface science*, vol. 96, no. 3, pp. 357–363, 1980.
- [54] H. Dosch, A. Lied, and J. Bilgram, "Disruption of the hydrogen-bonding network at the surface of Ih ice near surface premelting," *Surface science*, vol. 336, no. 1, pp. 43–50, 1996.
- [55] Y. Furukawa and H. Nada, "Anisotropy in molecular-scaled Growth kinetics at ice-water interfaces," *J. Phys. Chem. B*, vol. 101, no. 32, pp. 6163–6167, 1997.
- [56] B. Pittenger, S. Fain, M. Cochran, J. Donev, B. Robertson, A. Szuchmacher, and R. Overney, "Premelting at ice-solid interfaces studied via velocity-dependent indentation with force microscope tips," *Phys. Rev. B*, vol. 63, no. 13, p. 134102 (1–15), Mar. 2001.
- [57] H. Bluhm, D. F. Ogletree, and C. S. Fadley, "The premelting of ice studied with photoelectron," *J. Phys.: Condens. Matter*, vol. 14, no. 8, pp. 227–233, 2002.
- [58] V. Sadtchenko and G. E. Ewing, "Interfacial melting of thin ice films: An infrared study," *J. Chem. Phys.*, vol. 116, no. 11, pp. 4686–4697, 2002.
- [59] P. G. Buchan, "Electrical conductivity of insulator surface ices," *Research Report of Ontario Hydro*, no. 89–31-K, pp. 1–17, 1989.
- [60] H. T. Bui, L. C. Phan, C. Huraux, and J. Pissolato, "HVDC flashover on the surface of conductive ice," *IEEE Int.Symp. Elec. Insu.*, Montreal, Canada, no. 84CH1964–6, pp. 85–88, 1984.
- [61] N. Sugawara, S. Ito, and H. Nakauchi, "AC surface flashover voltage of ice depending on soluble ions," *Proceedings of Int. Sym.Elec. Insu. Mate.*, pp. 433–436, 1998.
- [62] M. Farzaneh, J. Zhang, and X. Chen, "A laboratory study of leakage current and surface conductivity of ice samples," *IEEE Conf. Electr. Insul. Dielectr. Phenomena (CEIDP)*, pp. 631–638, 1994.
- [63] M. Farzaneh, X. Chen, and J. Zhang, "A study of surface conductivity and flashover voltage of ice samples formed under various freezing conditions," *Int. J. Offshore Polar Eng.*, vol. 6, no. 4, pp. 298–303, 1996.
- [64] J. Zhang, M. Farzaneh, and X. Chen, "Variation of ice surface conductivity during flashover," *IEEE Conf. Electr. Insul. Dielectr. Phenomena (CEIDP)*, no. 1995, pp. 479–483.
- [65] M. Farzaneh, X. Chen, and J. Zhang, "The influence of applied voltage on the surface conductivity of atmospheric ice deposited on insulating surfaces," *Proceedings of IEEE Int. Symp. Electr. Insul.*, pp. 16–19, 1996.

- [66] M. Farzaneh and W. A. Chisholm, "Effects of ice and snow on the electrical performance of power network insulators," in Chapter 7, *Atmospheric Icing of Power Networks Atmospheric Icing of Power Networks*, 2008, pp. 269–325.
- [67] M. Farzaneh, C. Volat, and A. Gakwaya, "Electric field modelling around an ice-covered insulator using boundary element method," *Proceedings of IEEE Int. Symp. Electr. Insul., CA, USA*, pp. 349–355, 2000.
- [68] C. Volat, M. Farzaneh, and A. Gakwaya, "Dynamic variations of potential and electric field distributions around an ice-covered insulator during ice accretion," *Proc. 10th Int. Workshop Atmospheric Icing Structures, Czech Republic*, pp. 85–90, 2002.
- [69] C. Volat, "Modélisation physique et numérique par la méthode des éléments inis de frontière de la distribution du potentiel et du chyamp électrique le long d'un isolateur standard de poste 735 kV recouvert de Glace," Ph.D. Dissertation, University of Quebec in Chicoutimi, 2002.
- [70] D. Bueckert, "Ice storm damage tallied," *Report of Canada News on Ice Storm '98*, 1998.
- [71] M. Farzaneh and J. L. Laforte, "Effect of voltage polarity on icicles grown on line insulators," *Int. J. Offshore Polar Eng.*, vol. 2, no. 4, pp. 298–302, 1992.
- [72] J. Farzaneh-Dehkordi, "Experimental study and mathematical modeling of flashover of EHV insulators covered with ice," M.Sc. Dissertation, University of Quebec in Chicoutimi, 2004.
- [73] S. Taheri, M. Farzaneh, and I. Fofana, "Influence of air gaps on the DC withstand voltage of ice-covered UHV insulators," *IEEE Conf. Electr. Insul. Dielectr. Phenomena (CEIDP)*, pp. 745–748, Oct. 2012.
- [74] L. C. Phan and H. Matsuo, "Minimum flashover voltage of iced insulators," *IEEE Trans. Dielectr. Electr. Insul.*, vol. EI-18, no. 6, pp. 605–618, 1983.
- [75] N. Sugawara, K. Takayama, K. Hokari, K. Yoshida, and S. Ito, "Withstand voltage and flashover performance of iced insulators depending on the density of accreted," *Proc. 6th Int. Workshop Atmospheric Icing Structures, Budapest, Hungary*, pp. 231–235, 1993.
- [76] L. Shu, L. Gu, and C. Sun, "A study of minimum flashover voltage of ice-covered suspension insulators," *Proc. 7th Int. Symp. High Voltage Eng., Chicoutimi, Canada*, pp. 87–92, 1996.
- [77] S. Taheri, M. Farzaneh, C. Potvin, and I. Fofana, "DC Flashover performance of insulators under icing conditions," *Proc. 14th Int. Workshop Atmospheric Icing Structures, Chongqing, China*, paper C2_3_ID1186, 2011.
- [78] A. M. Rahal and C. Huraux, "Flashover mechanism of high voltage insulators," *IEEE Trans. Power App. Syst.*, vol. PAS-98, no. 6, pp. 2223–2231, 1979.
- [79] K. Kannus and V. Verkkonen, "Effect of coating on the dielectric strength on high voltage insulators," *Proc. 4th Int. Workshop Atmospheric Icing Structures, Paris, France*, pp. 296–300, 1998.
- [80] W. A. Chisholm et al., "The cold-fog test," *IEEE Trans. Power Delivery*, vol. 11, no. 4, pp. 1874–1880, 1996.
- [81] X. Jiang, L. Chen, Z. Zhang, C. Sun, and J. Hu, "Equivalence of influence of pollution simulating methods on DC flashover stress of ice-covered insulators," *IEEE Trans. Power Delivery*, vol. 25, no. 4, pp. 2113–2120, Oct. 2010.

- [82] X. Jiang, Y. Chao, Z. Zhang, J. Hu, and L. Shu, "DC flashover performance and effect of sheds configuration on polluted and ice-covered composite insulators at low atmospheric pressure," *IEEE Trans. Dielectr. Electr. Insul.*, vol. 18, no. 1, pp. 97–105, Feb. 2011.
- [83] H. Su, Z. Jia, Z. Sun, Z. Guan, and L. Li, "Field and laboratory tests of insulator flashovers under conditions of light ice accumulation and contamination," *IEEE Trans. Dielectr. Electr. Insul.*, vol. 19, no. 5, pp. 1681–1689, Oct. 2012.
- [84] Y. Liu, S. Gao, D. Huang, T. Yao, X. Wu, Y. Hu, and W. Cai, "Icing flashover characteristics and discharge process of 500 kV AC transmission line suspension insulator strings," *IEEE Trans. Dielectr. Electr. Insul.*, vol. 17, no. 2, pp. 434–442, Apr. 2010.
- [85] Y. Sabri, "Static modelling of AC flashover on contaminated insulators covered with ice using intelligent identification methods," Ph.D. Dissertation, University of Quebec in Chicoutimi, 2009.
- [86] C. Tavakoli, "Dynamic modeling of AC arc development on ice surfaces," Ph.D. Dissertation, University of Quebec in Chicoutimi, 2004.
- [87] Y. Li, "Study of the influence of altitude on the characteristics of the electrical arc on polluted ice surface," Ph.D. Dissertation, University of Quebec in Chicoutimi, 2002.
- [88] K. Kannus, K. Lahti, and K. Nousiainen, "Comparisons between experiments and calculations of the electrical behavior of ice-covered high voltage insulators," *Proc. 8th Int. Workshop Atmospheric Icing Structures*, Iceland, pp. 325–331, 1998.
- [89] F. Su and Y. Jia, "Icing on Insulator String of HV Transmission Lines and Its Harmfulness," *Proc. 3th Int. Offshore and Polar Eng. Conf.*, Singapore, vol. 2, pp. 655–658, 1993.
- [90] M. Hara and C. Phan, "A study of the leakage current of H.V insulators under glaze and rime," *Can. Electr. Eng. J.*, vol. 3, no. 3, pp. 15–22, 1978.
- [91] I. Fofana, M. Farzaneh, H. Hemmatjou, and C. Volat, "Study of discharge in air from the tip of an icicle," *IEEE Trans. Dielectr. Electr. Insul.*, vol. 15, no. 3, pp. 730–740, Jun. 2008.
- [92] C. Volat and M. Farzaneh, "Three-dimensional modeling of potential and electric-field distributions along an EHV ceramic post insulator covered with ice — Part I: simulations of a melting period," *IEEE Trans. Power Delivery*, vol. 20, no. 3, pp. 2006–2013, 2005.
- [93] C. Volat and M. Farzaneh, "Three-dimensional modeling of potential and electric-field distributions along an EHV ceramic post insulator covered with ice — Part II: Effect of air gaps and partial arcs," *IEEE Trans. Power Delivery*, vol. 20, no. 3, pp. 2014–2021, 2005.
- [94] M. Farzaneh, C. Volat, and J. Zhang, "Role of air gaps on AC withstand voltage of an ice-covered insulator string," *IEEE Trans. Dielectr. Electr. Insul.*, vol. 13, no. 6, pp. 1350–1357, Dec. 2006.
- [95] M. Farzaneh, J. Zhang, and R. Chaarani, "Effects of air gaps on the flashover of ice-covered insulators," *Proc. 14th Int. Sym. High-Voltage Eng. (ISH)*, Beijing, Chine, pp. 1–6, 2005.
- [96] R. Chaarani, "Étude de l'influence des caractéristiques des isolateurs sur leurs performances électriques dans des conditions de givrage," Ph.D. Dissertation, University of Quebec in Chicoutimi, 2003.

- [97] H. Akkal, C. Volat, and M. Farzaneh, "Improving electrical performance of ehv post station insulators under severe icing conditions using modified grading rings," *IEEE Trans. Dielectr. Electr. Insul.*, vol. 20, no. 1, pp. 221–228, Feb. 2013.
- [98] W. McDermid and T. Black, "Experience with preventing external flashovers in HVDC converter stations," *Conference Record of the 2008 IEEE International Symposium on Electrical Insulation*, pp. 81–84, Jun. 2008.
- [99] D. Wu, K. A. Halsan, and S. M. Fikke, "Artificial ice tests for long insulator strings," *Proc. 7th Int. Symp. High Voltage Eng., Chicoutimi, Canada*, pp. 67–71, 1996.
- [100] M. Farzaneh, J. Zhang, and C. Volat, "Effect of insulator diameter on AC flashover voltage of an ice-covered insulator string," *IEEE Trans. Dielectr. Electr. Insul.*, vol. 13, no. 2, pp. 264–271, 2006.
- [101] Y. Watanabe, "Flashover tests of insulators covered with ice or snow," *IEEE Trans. Power App. Syst.*, vol. PAS-97, no. 5, pp. 1788–1794, 1978.
- [102] P. E. Renner, H. L. Hill, and O. Ratz, "Effect of icing on DC insulation strength," *Proc. IEEE summer power meeting and EHV Conf., Los Angeles, USA*, pp. 1201–1206, 1970.
- [103] M. Farzaneh, J. Zhang, and Y. Li, "Effects of low air pressure on ac and dc arc propagation on ice surface," *IEEE Trans. Dielectr. Electr. Insul.*, vol. 12, no. 1, pp. 60–71, Feb. 2005.
- [104] Y. Li, M. Farzaneh, and J. Zhang, "Effects of voltage type and polarity on flashover performances at low atmospheric pressure on an ice surface," *Proc. 8th Int. Offshore and Polar Eng. Con., Montreal, Canada*, vol. 11, pp. 543–546, 1998.
- [105] M. Farzaneh, Y. Li, and J. Zhang, "Effects of altitude on AC flashover on ice surfaces," *Proc. 10th Int. Symp. High-Voltage Eng. (ISH), Montreal, Canada*, pp. 73–76, 1997.
- [106] L. Shu, M. Farzaneh, Y. Li, and C. Sun, "AC flashover performance of polluted insulators covered with artificial ice at," *IEEE Conf. Electr. Insul. Dielectr. Phenomena (CEIDP)*, pp. 609–612, 2001.
- [107] J. Hu, C. Sun, X. Jiang, Z. Zhang, and L. Shu, "Flashover performance of pre-contaminated and ice-covered composite insulators to be used in 1000 kV UHV AC transmission lines," *IEEE Trans. Dielectr. Electr. Insul.*, vol. 14, no. 6, pp. 1347–1356, Dec. 2007.
- [108] F. Obenaus, "Fremdschichtüberschlag und Kriechweglänge," *Deutsche Elektrotechnik*, vol. 4, pp. 135 – 136, 1958.
- [109] G. Neumarker, "Verschmutzungszustand und Kriechweg," *Monatsber. D. Deut. Akad. Wiss., Berlin*, vol. 1, pp. 352–359, 1959.
- [110] L. L. Alston and S. Zoledziowski, "Growth of discharges on polluted insulation," *Proceedings of IEE*, vol. 110, no. 7, pp. 1260–1266, 1963.
- [111] P. Claverie, "Predetermination of the behaviour of polluted insulators," *IEEE Trans. Power App. Syst.*, vol. PAS-90, no. 4, pp. 1902–1908, 1971.
- [112] P. Claverie and Y. Pocheron, "How to choose insulators for polluted areas," *IEEE Trans. Power App. Syst.*, vol. PAS-92, no. 3, pp. 1121–1131, 1972.

- [113] F. A. M. Rizk, "A criterion for AC flashover of polluted insulators," Proceedings of IEEE Power Engineering Society Winter Power Meeting, New York, USA, no. 71CP135-PWR, p. 135, 1971.
- [114] R. Wilkins, "Flashover voltage of high-voltage insulators with uniform surface-pollution films," Proc. IEE, vol. 116, no. 3, pp. 457–465, 1969.
- [115] F. A. M. Rizk, "Mathematical models for pollution flashover," Electra, vol. 78, pp. 71–03, 1981.
- [116] S. M. Fikke, "Possible effects of contaminated ice on insulator strength," Proc. 5th Int. Workshop Atmospheric Icing Structures, Tokyo, Japan, Paper No. B4-2-(1), 1990.
- [117] M. Farzaneh, "Effect of ice thickness and voltage polarity on the flashover voltage on ice covered high voltage insulators," Proc. 7th Int. Symp. High Voltage Eng., Dresden, Germany, vol. 4, pp. 203–206, 1991.
- [118] M. Farzaneh, J. Zhang, S. Brettschneider, and A. M. Miri, "DC Flashover performance of ice-covered insulators," Proc. 10th Int. Symp. High-Voltage Eng. (ISH), Montreal, Canada, vol. 3, pp. 77–80, 1997.
- [119] J. Zhang and M. Farzaneh, "Computation of AC critical flashover voltage of insulators covered with ice," Proc. Int. Conf. Power Syst. Tech., Beijing, China, vol. 1, pp. 524–528, 1998.
- [120] J. Zhang and M. Farzaneh, "Propagation of AC and DC arcs on ice surfaces," IEEE Trans. Dielectr. Electr. Insul., vol. 7, no. 2, pp. 269–276, Apr. 2000.
- [121] X. Chen, "Modeling of electrical arc on ice surfaces," Ph.D. Dissertation, UQAC-École Polytechnique de Montréal, 1999.
- [122] J. Zhang and M. Farzaneh, "Modeling of flashover on ice-covered insulators with multi air gaps," Proc. IEEE PES Trans. Dist. Conf., Dallas, USA, pp. 109–114, 2006.
- [123] O. Mayr, "Beitrag zur théorie der statischen und der dynamischen lichtbogens," Archiv fur Elektrotechnik, vol. 37, pp. 588–608, 1943.
- [124] I. Fofana, C. Tavakoli, and M. Farzaneh, "Dynamic modeling of AC iced insulator flashover characteristics," Proc. IEEE Power Tech, Bologna, Italy, vol. 2, 2003.
- [125] I. Fofana and M. Farzaneh, "Application of dynamic model to flashover of ice-covered insulators," IEEE Trans. Dielectr. Electr. Insul., vol. 14, no. 6, pp. 1410–1417, Dec. 2007.
- [126] I. Fofana, M. Farzaneh, C. Tavakoli, and A. Beroual, "Dynamic modeling of flashover process on insulator under atmospheric icing conditions," IEEE Conf. Electr. Insul. Dielectr. Phenomena (CEIDP), pp. 605–608, 2001.
- [127] I. Fofana and M. Farzaneh, "Process of discharge initiation and arc development on an ice-covered insulator," Proc. IEEE PES Trans. Dist. Conf., Dallas, USA, pp. 601–606, 2001.
- [128] C. Volat, M. Farzaneh, and N. Mhaguen, "Improved FEM models of one- and two-arcs to predict AC critical flashover voltage of ice-covered insulators," IEEE Trans. Dielectr. Electr. Insul., vol. 18, no. 2, pp. 393–400, Apr. 2011.
- [129] Q. Yang, W. Sima, C. Sun, L. Shu, and Q. Hu, "Modeling of DC flashover on ice-covered HV insulators based on dynamic electric field analysis," IEEE Trans. Dielectr. Electr. Insul., vol. 14, no. 6, pp. 1418–1426, Dec. 2007.

- [130] Q. Yang, S. W, C. Sun, K. Wu, and J. Li, "A new AC flashover model of ice-covered HV insulators based on numerical electric field analysis," *IET Gener. Transm. Distrib.*, vol. 2, no. 4, pp. 600–609, 2008.
- [131] R. Wilkins, "Arc propagation along an electrolyte surface," *Proc. IEE*, vol. 118, no. 12, pp. 1886–1892, 1971.
- [132] M. F. Hoyaux, "Arc physics," *Srpinger-Verlag New York inc*, 1968.
- [133] M. Ishii and H. Ohashi, "Polarity effect in dc withstand voltages of contaminated surfaces," *IEEE Trans. Electr. Insul.*, vol. 23, no. 6, pp. 1033–1042, 1988.
- [134] T. Matsumoto, M. Ishii, and T. Kawamura, "Optoelectronic measurement of partial arcs on a contaminated surface," *IEEE Trans. Electr. Insul.*, vol. EI-19, no. 6, pp. 543–549, 1984.
- [135] D. C. Jolly, "Contamination flashover theory and insulator design," *J. of the Franklin Inst.*, vol. 294, no. 6, pp. 483–500, 1972.
- [136] A. Nekahi and M. Farzaneh, "Excitation temperature determination of an arc formed over an ice surface using optical emission spectroscopy," *IEEE Trans. Dielectr. Electr. Insul.*, vol. 18, no. 6, pp. 1829–1834, Dec. 2011.
- [137] A. Nekahi and M. Farzaneh, "Rotational temperature measurement of an arc formed over an ice surface," *IEEE Trans. Dielectr. Electr. Insul.*, vol. 18, no. 3, pp. 755–759, Jun. 2011.
- [138] A. Nekahi, "Spectroscopic investigation of an arc over an ice surface," Ph.D. Dissertation, University of Quebec in Chicoutimi, 2011.
- [139] S. Farokhi, M. Farzaneh, and I. Fofana, "The effect of polarity on dc arc development over an ice surface," *J. Phys. D: Appl. Phys.*, vol. 43, no. 18, p. 185202, May 2010.
- [140] S. Farokhi, M. Farzaneh, and I. Fofana, "Experimental investigation of the process of Arc propagation over an ice surface," *IEEE Trans. Dielectr. Electr. Insul.*, vol. 17, no. 2, pp. 458–464, Apr. 2010.
- [141] D. Jolly and C. Poole, "Flashover of contaminated insulators with cylindrical symmetry under DC conditions," *IEEE Trans. Electr. Insul.*, vol. EI-14, no. 2, pp. 77–84, Apr. 1979.
- [142] I. G. Kesaev, "Cathode processes in the mercury arc," *American Institute of Physics*, vol. 8, no. 4, p. 70, 1965.
- [143] A. Pillai and R. Hackam, "Effect of DC pre-stress on AC and DC surface flashover of solid insulators in vacuum," *IEEE Trans. Electr. Insul.*, vol. EI-18, no. 3, pp. 292–300, Jun. 1983.
- [144] S. Farokhi, M. Farzaneh, and I. Fofana, "Study of ultraviolet emission and visible discharge along an ice surface," *IEEE Conf. Electr. Insul. Dielectr. Phenomena (CEIDP)*, pp. 654–657, Oct. 2008.
- [145] L. Shu, Y. Shang, X. Jiang, Q. Hu, Q. Yuan, J. Hu, Z. Zhang, S. Zhang, and T. Li, "Comparison between AC and DC flashover performance and discharge process of ice-covered insulators under the conditions of low air pressure and pollution," *IET Generation, Transmission & Distribution*, vol. 6, no. 9, p. 884, 2012.
- [146] X. Jiang, S. Wang, Z. Zhang, S. Xie, and Y. Wang, "Study on AC flashover performance and discharge process of polluted and iced IEC standard suspension insulator string," *IEEE Transactions on Power Delivery*, vol. 22, no. 1, pp. 472–480, Jan. 2007.

- [147] M. Farzaneh, J. Zhang, and X. Chen, "DC Characteristics of local arc on ice surfaces," *Atmospheric Research*, vol. 46, no. 2, pp. 49–56, 1998.
- [148] I. Fofana and A. Beroual, "A predictive model of the positive discharge in long air gaps under pure and oscillating impulse shapes," *J. Phys. D: Appl. Phys.*, vol. 30, no. 11, pp. 1653–1667, 1997.
- [149] J. M. Meek and J. D. Graggs, "Electrical breakdown of gases," John Wiley and Sons, New York, p. 878, 1978.
- [150] R. Sundararajan and R. S. Gorur, "Dynamic arc modeling of pollution flashover of insulators under DC voltage," *IEEE Trans. Electr. Insul.*, vol. 28, no. 2, pp. 209–218, 1993.
- [151] F. A. M. Rizk and D. H. Nguyen, "Digital simulation of source-insulator interaction in HVDC pollution tests," *IEEE Trans. Power Delivery*, vol. 3, no. 1, pp. 405–410, 1988.
- [152] N. Dhahbi-Megrache, "Modélisation dynamique des décharges sur les surfaces d'isolateurs pollués sous différentes formes de tension: élaboration d'un critère analytique de propagation," Ph.D. Dissertation, Ecole Central de Lyon, France, 1998.
- [153] I. Fofana and A. Beroual, "Predischage models of dielectric liquids," *Japanese J. Appl. Phys*, vol. 37, no. 5A, pp. 2540–7, 1998.
- [154] Renardières Group, "Positive discharge in long air gaps at les renardières," *Electra*, no. 53, pp. 31–153, 1977.
- [155] C. Volat and M. Farzaneh, "A simple axisymmetric model for calculation of potential distribution along ice-covered post station insulators during a melting period," *IEEE Conf. Electr. Insul. Dielectr. Phenomena (CEIDP)*, pp. 232–235, 2008.